RP TU Rheinland-Pfälzische Technische Universität Kaiserslautern Landau

Mitochondrial import is under surveillance of cytosolic factors: specific roles of TOMM34 and Ubc8

vom Fachbereich Biologie

der Rheinland-Pfälzischen Technischen Universität Kaiserslautern-Landau

zur Verleihung des akademischen Grades Dr. rer. nat. genehmigte

Dissertation

von

Saskia Rödl, M.Sc., geb. in Speyer

Mündliche Prüfung: 06.11.2024

Dekan:	Prof. Dr. Stefan Kins
Promotionskommissionsvorsitzender:	Prof. Dr. Tanja Maritzen
Berichterstattende:	Prof. Dr. Johannes M. Herrmann
	Prof. Dr. Ekkehard Neuhaus

D 386

EIDESSTATTLICHE ERKLÄRUNG

Hiermit erkläre ich wahrheitsgemäß, dass ich die hier vorliegende Dissertation selbstständig, ohne unzulässige Hilfe Dritter verfasst und keine anderen als die angegebenen Quellen und Hilfsmittel verwendet habe. Die aus anderen Quellen übernommenen Daten und Konzepte sind unter Angabe der Quelle gekennzeichnet.

Zur Erstellung der vorliegenden Arbeit habe ich keine entgeltliche Hilfe von Vermittlungs- und Beratungsdiensten in Anspruch genommen.

Diese Arbeit, und auch keine Teile hiervon, wurden weder im In- noch im Ausland bereits als Prüfungsarbeit für eine wissenschaftliche Prüfung eingereicht und ich habe mich zuvor noch keiner Doktorprüfung unterzogen. Ich erkläre, dass ich weder die gleiche noch eine andere Abhandlung bei einem anderen Fachbereich oder einer anderen Universität als Dissertation eingereicht habe.

Die Bestimmungen der Promotionsordnung des Fachbereiches Biologie der Rheinland-Pfälzischen Technischen Universität Kaiserslautern-Landau sind mir bekannt. Im Besonderen weiß ich, dass ich vor Vollzug der Promotion zur Führung des Doktortitels nicht berechtigt bin.

Saskia Rödl

Kaiserslautern, 29.08.2024

DARLEGUNG DES EIGENANTEILS

Die Messung aller massenspektrometrischer Daten (Abbildung 16B, C, Abbildung 17A, Abbildung 21B, C, Abbildung 22A, Abbildung 24A, Abbildung S5, Abbildung S8) sowie die statistische Auswertung der SILAC-Messung (Abbildung 21B, C, Abbildung 22A) wurden von Markus Räschle (Center for MS Analytics, RPTU Kaiserlautern-Landau) durchgeführt. Die statistische Auswertung der Immunopräzipitations-Messung (Abbildung 16B, C, Abbildung 17A, Figure S5) wurde von Annika Nutz durchgeführt. Die Abbildung der Enrichment scores (Abbildung 22B) wurde von Carina Fendahl erstellt. Der genetische Screen (Abbildung19B, Abbildung S7A) wurde von Katja Hansen durchgeführt. Die Abbildungen 24D, E und 25A-D zeigen Daten von Fabian den Brave und Thomas Becker (Institut für Biochemie und Molekularbiologie, Universität Bonn). Die Klonierung der Plasmide für den IQ-Compete Assay, sowie die Experimente hierzu (Abbildung 13B-D, Abbildung S3B-F, Abbildung S4) wurden von Yasmin Hoffman im Rahmen ihrer von mir betreuten Masterarbeit durchgeführt. Alle übrigen in dieser Arbeit gezeigten Originaldaten wurden von mir generiert.

Die vorliegende Einschätzung über die erbrachte Leistung von Dritten wurde mit den genannten Personen einvernehmlich abgestimmt.

Saskia Rödl

Kaiserslautern, den 29.08.2024

Prof. Dr. Johannes M. Herrmann

Kaiserslautern, den 29.08.2024

DARLEGUNG ALLER BENUTZTEN HILFSMITTEL UND HILFESTELLUNGEN

Zur Erstellung dieser Arbeit wurde das Microsoft Office 365 Softwarepaket (Word und Excel) genutzt. Das Literaturverzeichnis und Literaturverweise wurden mittels Zotero erstellt. Alle statistischen Analysen und Auswertungen erfolgten mittels Microsoft Excel, Perseus oder R Studio. Die gezeigten Abbildungen wurden mithilfe der Corel Technical Suite 2020 erstellt. Proteinstrukturen wurden mit dem UCSF Chimera Tool, phylogenetische Bäume mit dem MUSCLE Multiple Sequence Alignment Tool und Sequenz Alignments mit dem Clustal Omega multiple sequence alignment Tool visualisiert. Mikroskopische Aufnahmen wurden mit den Softwarepaketen Fiji und Leica LasX analysiert. Zur Quantifizierung aller Western Blot und Import Experimente wurden die Softwares ImageQuant und Fiji genutzt. ChatGPT und DeepL wurden für die Formulierungsoptimierung einzelner Sätze eingesetzt.

Saskia Rödl

Kaiserslautern, den 29.08.2024

LIST OF PUBLICATIONS

2024 **Rödl S.**, Hoffman Y., Jung F. *et al*. A priority code in presequences: mitochondrial targeting signals assign specific import characteristics to precursor proteins. (submitted)

2024 Jung F., **Rödl S.**, Herrmann J.M., Mühlhaus T. Analysis and prediction of internal mitochondrial targeting signals. (submitted)

2023 Lenhard S., Gerlich S., Khan A., **Rödl S.** *et al*. The Orf9b protein of SARS-CoV-2 modulates mitochondrial protein biogenesis. J Cell Biol. 2023 Oct 2;222(10):e202303002. doi: 10.1083/jcb.202303002

2023 **Rödl S.**, Herrmann J.M. The role of the proteasome in mitochondrial protein quality control. IUBMB Life. 2023 Oct;75(10):868-879. doi: 10.1002/iub.2734

2023 **Rödl S.**, den Brave F., Räschle M. *et al*. The metabolite-controlled ubiquitin conjugase Ubc8 promotes mitochondrial protein import. Life Science Alliance. 2023 Jan;6(1):e202201526. doi: 10.26508/lsa.202201526

SUMMARY

Mitochondrial precursor proteins need to master a complex journey from the cytosol to their final destination within mitochondria. Several hundreds of proteins are simultaneously targeted to and imported into mitochondria by a vast variety of import pathways. To ensure their proper biogenesis, mitochondria closely collaborate with numerous cytosolic factors involving components of the chaperone network and the ubiquitin-proteasome system (UPS). This study aimed to uncover novel mechanisms by which cells monitor proper mitochondrial biogenesis.

On the one hand, I elucidated in how far the great versatility of N-terminal presequences contribute to the orderly process of protein import. By fusing several presequences of variable lengths to the model protein DHFR, I generated a test set of precursors which only differ in their targeting sequence. *In vitro* imports and IQ-Compete, a novel assay specifically established for this study, revealed considerable differences in the import efficiencies of these precursors *in vitro* and *in vivo*. Investigating the presequences of Oxa1 and Atp5 as representatives of the test set, I found that either denaturation and preincubation, respectively, or deletion of the receptors Tom70/71 only diminished the import efficiency of the Oxa1 presequence. Furthermore, using immunoprecipitation experiments, I identified the cytosolic co-chaperone and tetratricopeptide repeat (TPR) protein TOMM34 to bind to the presequence of Oxa1 but not to that of Atp5 in reticulocyte lysate from rabbits. Since the mammalian protein TOMM34 is not present in yeast, I investigated whether a yeast TPR co-chaperone might be similarly involved in mitochondrial biogenesis instead. I was able to show that the depletion of the co-chaperone Cns1 resulted in reduced protein levels of the two mitochondrial proteins Oxa1 and Mam33, hinting towards previously unknown role of Cns1 in mitochondrial biogenesis.

On the other hand, I revealed novel insights into the surveillance of mitochondrial protein import by specific UPS components. A genetic screen in yeast suggests the ubiquitin conjugase Ubc8 to play a role in efficient precursor biogenesis. I could verify this finding by detecting elevated precursor levels in a Ubc8 deletion mutant. Using dynamic SILAC mass spectrometry, I demonstrated that the loss of Ubc8 broadly affects mitochondrial protein levels. *In vitro* imports allowed me to attribute these observations to impaired import efficiencies into mitochondria isolated from Δ*ubc8* cells. By employing proteomic analyses, I found the receptor Tom22 to be the most diminished component among all proteins of the import machineries in

Δ*ubc8*. In line with this, blue native PAGE experiments revealed strongly diminished levels of the receptor Tom22 being assembled into the TOM complex upon the deletion of Ubc8.

Taken together, my findings reveal new aspects of the complex interplay of mitochondria with the cytosolic chaperone network and the UPS to enable proper mitochondrial biogenesis. Some presequences specifically recruit the cytosolic co-chaperone TOMM34 which enables highly efficient import via Tom70. Additionally, the ubiquitin conjugase Ubc8 promotes effective assembly of the receptor Tom22 into a fully functional TOM complex and thereby maintains efficient protein import.

ZUSAMMENFASSUNG

Mitochondriale Präproteine müssen eine komplexe Reise vom Zytosol bis zu ihrem endgültigen Zielort in den Mitochondrien meistern. Mehrere hundert Proteine werden gleichzeitig zu den Mitochondrien transportiert und über eine große Vielzahl an Importwegen importiert. Um ihre ordnungsmäßige Biogenese sicherzustellen, kollaborieren Mitochondrien eng mit zahlreichen zytosolischen Komponenten, einschließlich Komponenten des Chaperon-Netzwerkes und des Ubiquitin-Proteasom-Systems (UPS). Ziel dieser Arbeit war es, neue Mechanismen zu enthüllen, durch welche die Zellen die ordnungsgemäß ablaufende mitochondriale Biogenese überwachen.

Einerseits habe ich aufgeklärt, inwieweit die große Vielfalt von N-terminalen Präsequenzen zu dem geordneten Ablauf des Proteinimports beitragen. Durch die Fusion von mehreren Präsequenzen verschiedener Längen mit dem Modellprotein DHFR habe ich ein Testset an Präproteinen generiert, welche sich lediglich durch ihre Zielquenzen unterscheiden. *In vitro* Imports und IQ-Compete, ein neuartiger Assay, welcher speziell für diese Studie entwickelt wurde, zeigten große Unterschiede in den Importeffizienzen dieser Präproteine *in vitro* als auch *in vivo*. Bei der Untersuchung der Präsequenzen von Oxa1 und Atp5 als Vertreter des Testsets fand ich heraus, dass die Denaturierung bzw. Vorinkubation der Präproteine oder die Deletion der Rezeptoren Tom70/71 nur die Importeffizienz der Oxa1-Präsequenz verringerten. Des Weiteren konnte ich mit Hilfe von Immunopräzipitationsexperimenten nachweisen, dass das zytosolische Co-Chaperon und Tetratricopeptid-repeat (TPR) Protein TOMM34 im Retikulozytenlysat aus Kaninchen an die Präsequenz von Oxa1, jedoch nicht an die von Atp5, bindet. Jedoch ist das Säugetierprotein TOMM34 nicht in Hefe vorhanden. Stattdessen konnte ich zeigen, dass die Abreicherung des Co-Chaperons Cns1 aus Hefe zu reduzierten Proteinmengen der beiden mitochondrialen Proteine Oxa1 und Mam33 führt, was auf eine bisher unbekannte Rolle von Cns1 in der mitochondrialen Biogenese hindeutet.

Andererseits habe ich neuartige Erkenntnisse über die Überwachung des mitochondrialen Imports durch spezifische UPS Komponenten gewinnen können. Ein genetischer Screen in Hefe hat darauf hingewiesen, dass die Ubiquitin-Konjugase Ubc8 eine Rolle in der effizienten Präprotein-Biogenese spielt. Ich konnte diese Entdeckung durch die Detektion erhöhter Präproteinmengen in einer Ubc8-Deletionsmutante verifizieren. Mit Hilfe von dynamischer SILAC-Massenspektrometrie konnte ich nachweisen, dass der Verlust von Ubc8 die mitochondrialen Proteinmengen stark beeinflusst. Mittels *in vitro* Imports konnte ich diese

Beobachtungen auf eine beeinträchtigte Importeffizienz in Mitochondrien, welche aus Δ*ubc8* Zellen isoliert wurden, zurückführen. Mit Hilfe von Proteomanalysen fand ich heraus, dass der Rezeptor Tom22 die am stärksten verringerte Komponente aller Proteine der Import-Maschinerie in Δ*ubc8* ist. In Übereinstimmung hiermit zeigten Blau-nativ-PAGE-Experimente, dass aufgrund der Deletion von Ubc8 deutlich verminderte Mengen des Rezeptors Tom22 in den TOM-Komplex eingebaut werden.

Zusammenfassend offenbaren meine Ergebnisse neue Aspekte des komplexen Zusammenspiels von Mitochondrien mit dem zytosolischen Chaperon-Netzwerk und dem UPS, um eine korrekte mitochondriale Biogenese zu ermöglichen. Manche Präsequenzen rekrutieren spezifisch das zytosolische Co-Chaperon TOMM34, welches einen hocheffizienten Import über Tom70 ermöglicht. Zusätzlich fördert die Ubiquitin-Konjugase Ubc8 den effektiven Einbau des Rezeptors Tom22 in einen voll funktionsfähigen TOM-Komplex und sorgt so für einen effizienten Proteinimport.

TABLE OF CONTENTS

1. INTRODUCTION

1.1. Mitochondrial biogenesis

Mitochondria are essential organelles of eukaryotic cells that fulfill a great variety of functions. The organelle exhibits a characteristic, double-membrane-bounded structure which allows the separation into different sub-compartments. The outer membrane (OM) separates the organelle from its cellular environment. The inner membrane (IM) forms internal ridges, so called cristae, and surrounds the interior of the organelle which is termed matrix. The interspace between the IM and OM is called intermembrane space (IMS) [1]. Each sub-compartment contains its specific spectrum of proteins which is required for their respective functions. Mitochondrial biogenesis strongly relies on the expression of nuclear encoded proteins. In yeast only eight of the 900-1000 mitochondrial proteins are encoded on the mitochondrial genome, whereas in humans only 13 of the approximately 1500 are encoded this way [2,3]. All other proteins are synthesized on cytosolic ribosomes and imported into mitochondria. While most mitochondrial proteins are imported post-translationally, a co-translational import mode has been suggested for a small number of proteins, most of which were hydrophobic IM proteins [4–6]. About 60% of all nuclear-encoded mitochondrial proteins are targeted to the matrix using an N-terminal mitochondrial targeting sequence (MTS or presequence). However proteins located in other compartments of the organelle employ a huge diversity of other mitochondrial targeting sequences (Figure 1) [7]. In the cytosol, precursors are stabilized by chaperones of the heat shock protein (Hsp) 70 and Hsp90 protein families together with their co-chaperones and ushered to the mitochondrial surface receptors for subsequent import [8]. Parts of this paragraph were adopted from my review [9].

1.1.1. Mitochondrial targeting sequences – there is more than just one signpost

Based on the complex structure of mitochondria, multiple import routes are utilized to sort proteins into the different compartments of the organelle. Precursor proteins employ a great diversity of targeting sequences to ensure proper targeting to the organelle, import via their specific import route, and correct insertion into a membrane if necessary [7]. Targeting sequences can be found at the C- or N-terminus of proteins but they can also be located within the protein sequence (Figure 1).

Most matrix proteins own N-terminal MTSs whose lengths typically range from about 10 to 80 amino acid residues but presequences with less than 10 to more than 100 amino acids are also

known [10,11]. Presequences mainly consist of positively charged (lysine and arginine), hydrophobic (leucine, isoleucine, valine, and alanine) and hydroxylated (serine and threonine) residues. One key feature is the strong tendency to form an amphipathic α-helix with one hydrophobic (Φ) and one positively charged (+) side [12]. Once the protein reaches the mitochondrial matrix, the matrix processing peptidase (MPP) cleaves off the presequence, initiating folding of the matured protein [13]. Subsequent degradation of the presequence peptides is mediated by mitochondrial metalloproteases [14,15]. Unlike most N-terminal MTS-containing proteins, a few matrix proteins, including Hsp10, do not undergo proteolytic processing by MPP but rather retain the presequence as part of the mature protein [16]. Some matrix proteins additionally contain internal mitochondrial targeting sequences (iMTSs), which are located within the protein sequence and exhibit similar structural characteristics to presequences [17]. Whereas presequences are sufficient for protein import [18], iMTSs are not sufficient but strongly support protein import by keeping precursors in an import-competent state [17,19]. In some cases, MPP additionally cleaves downstream of an internal targeting sequence to generate two individual proteins [20].

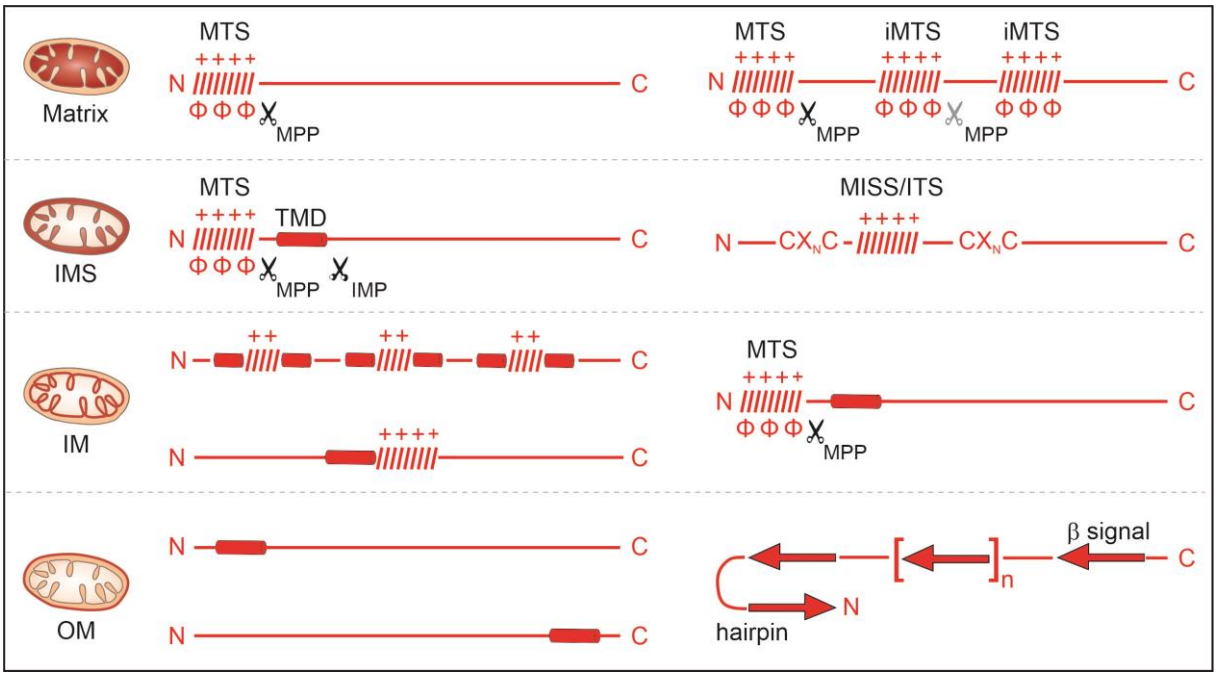

Figure 1: Precursors carry a huge diversity of mitochondrial targeting sequences for proper targeting to the different mitochondrial subcompartments. Depending on the localization of mitochondrial proteins within the organelle, precursors employ a huge diversity of mitochondrial targeting sequences. Typical features of the targeting sequences can be assigned to proteins of the matrix, the intermembrane space (IMS), the inner membrane (IM) or the outer membrane (OM), respectively. However, overlaps between the groups are possible. For detailed description see text. MTS = mitochondrial targeting sequence, iMTS = internal mitochondrial targeting sequence, MPP = matrix processing peptidase, TMD = transmembrane domain, IMP = inner membrane protease, ITS = intermembrane space targeting signal, MISS = mitochondrial intermembrane space sorting, + = positively charged residues, Φ = hydrophobic residues.

As Figure 1 illustrates, multiple other targeting sequences direct proteins to the IMS, the IM and OM. Depending on their size, IMS proteins make use of two different kinds of targeting sequences. Larger proteins typically contain bipartite sequences which consist of an N-terminal MTS that is followed by a transmembrane domain (TMD) that functions as a hydrophobic sorting sequence [21]. MPP as well as the inner membrane protease (IMP) cleave off both targeting sequences to release a soluble protein into the IMS [22,23]. In contrast, smaller IMS proteins often use internal cysteine-rich mitochondrial intermembrane space sorting (MISS) signals, also called intermembrane space targeting signals (ITSs). MISS/ITS signals consist of short twin CXnC (CX_3C or CX_9C, C= cysteine) motives which are linked by an amphipathic helix [24,25].

Regarding the targeting sequences of IM proteins, three different classes have been identified. First, the highly abundant protein family of metabolite carriers lack cleavable presequences but rather contain hydrophobic internal targeting sequences. In most cases, carriers contain three targeting modules, each comprising a pair of TMDs which are connected by a helical loop [26,27]. Second, some monotopic proteins of the IM contain internal targeting sequences comprising a TMD followed by a positively charged region that is hypothesized to mimic an MTS [28]. As a third group, some IM proteins carry N-terminal presequences followed by a TMD. This so-called "stop-transfer-signal" arrests the precursor in the import machinery during import and MPP cleavage enables lateral release of the protein into the IM [21,29].

Signal-anchored (SA)- or tail-anchored (TA) proteins of the OM contain TMDs in their N- or C-terminal region, which target and anchor these proteins into the lipid bilayer. Lasty, β-barrel proteins of the OM employ a so-called β-signal in their most C-terminal β-strand. Alignments predict PoxGxxHyxHy (Po = polar, G = glycine, Hy = hydrophobic) as a conserved β-signal sequence [30]. The hydrophobicity of the most C-terminal β-strand and the formation of a β-hairpin is additionally required for the proper targeting of β–barrel proteins [31].

1.1.2. The great versatility of mitochondrial import pathways

Depending on the localization of the protein within mitochondria, precursors make use of various import pathways. Each pathway is characterized by the involvement of specific import components including chaperones, receptors, translocases, and more, which all together enable proper protein sorting (Figure 2) [7].

Proteins with an N-terminal presequences use the TOM-TIM23 import pathway to be translocated into the matrix or to be integrated into the inner membrane. The translocase of the

outer membrane (TOM) complex forms the main entry gate into mitochondria for a huge majority of mitochondrial proteins and mediates translocation across the OM. On the mitochondrial surface, presequences first get recognized by Tom20 and Tom22, two receptors of the TOM complex. Here, highly specific binding is achieved by distinct recognition of the amphipathic characteristics of presequences. Whereas Tom20 mainly binds the hydrophobic side of the amphipathic α-helix, Tom22 exhibits binding sites for the positively charged region [32]. Subsequently, the pore-forming β-barrel protein Tom40 facilitates translocation across the OM. Only recently it has been shown that a conserved polar glutamine-rich patch in the Tom40 channel is crucial for the interaction with the precursors [33]. Structural analysis of TOM identified distinct pathways through Tom40, specific for its great variety of client precursors, which enable organized translocation [34]. Tim23, a subunit of the TIM23 complex, was believed to form pore-like channels to thread proteins through the IM. However, there is recent evidence for precursors being translocated across the IM at the Tim17 bilayer interface [33,35,36]. In addition, the non-essential protein Mgr2 has been shown to seal the lateral opening of Tim17, thereby protecting the precursor as well as the hydrophobic patch of Tim17 from the lipid bilayer. However, Mgr2 is only loosely associated with TIM23 which enables lateral release of IM proteins into the membrane, if required [37]. Furthermore, the membrane potential across the IM ($\Delta\psi$) as well as the ATP-driven presequence translocase-associated motor (PAM) energetically assist in translocating precursors across the IM [38]. In the matrix, MPP clips of the MTS and the protein is folded into its respective three-dimensional structure [13].

Proteins of the IMS typically use the disulfide relay pathway, which is also called MIA (mitochondrial intermembrane space assembly) pathway. In this case, the precursors use the TOM complex to enter mitochondria before the cysteine-rich motifs of these proteins get recognized by the IM-anchored IMS protein Mia40. Due to the formation of mixed disulfide bonds, Mia 40 promotes oxidative folding of its substrates [39].

The highly abundant metabolite carrier proteins are sorted into the IM by the TOM-TIM22 import route. The internal, highly hydrophobic targeting modules are recognized by Tom70, the third receptor of the TOM complex. To prevent toxicity of the hydrophobic precursors, Tom70 contains chaperone binding sites and closely collaborates with cytosolic chaperones [8,19]. After translocation through the Tom40 pore, chaperones of the IMS, composed of small Tim proteins, bind to the precursors and transfer them to the TIM22 complex. Tim22 subsequently mediates insertion into the IM [40].

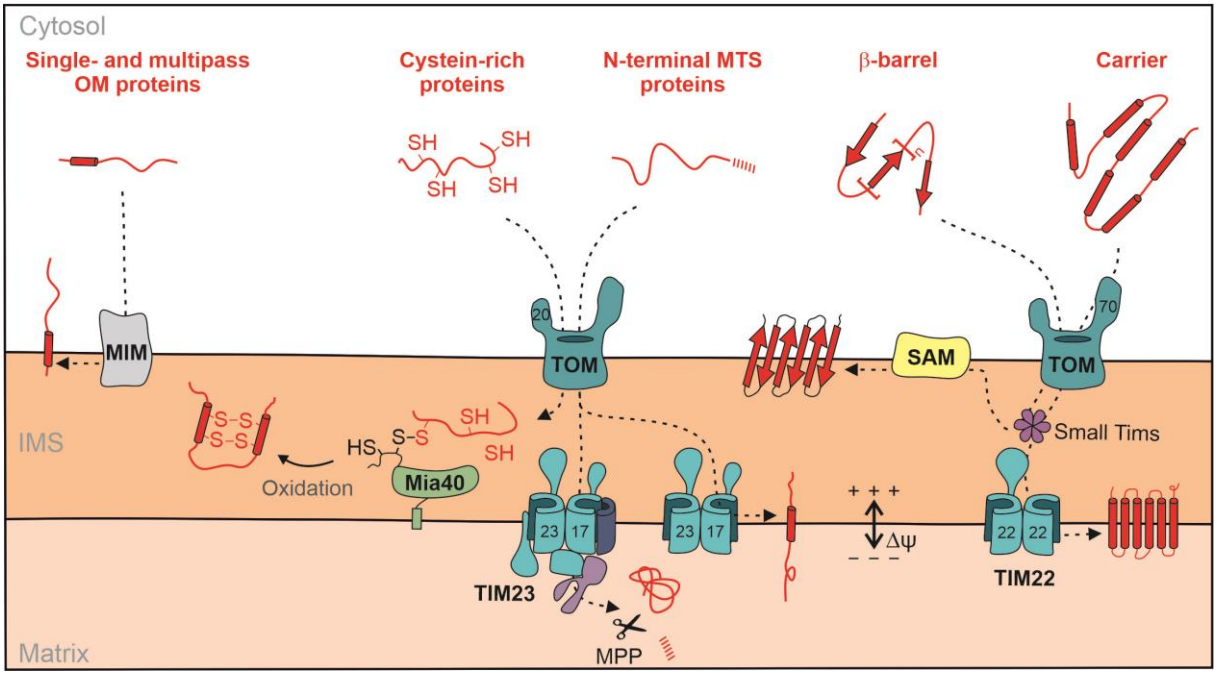

Figure 2: Precursor proteins use different import pathways for protein sorting into mitochondria. MTS-containing proteins of the matrix or the inner membrane (IM) use the TOM-TIM23 import route. Intermembrane space (IMS) proteins employ cysteine-rich motifs which are crucial for recognition by the disulfide relay pathway (MIA pathway). Members of the metabolite carrier family use the TOM-TIM22 import pathway in order to be inserted into the IM. β-barrels are inserted into the outer membrane (OM) with the help of the SAM complex. The MIM complex inserts single- and multispanning OM proteins in a TOM-independent manner. IMS = intermembrane space, SAM = sorting and assembly machinery, MIM = mitochondrial import (complex).

Pore-forming β-barrel proteins are destined for incorporation into the OM. Firstly, the TOM receptors Tom20 and Tom70 recognize the β-signals and -hairpin structures of these proteins. Tom40, being a β-barrel protein itself, subsequently mediates translocation across the OM. In the IMS, β-barrels are bound by chaperones consisting of small Tim proteins [41] and guided to the sorting and assembly machinery (SAM). The core-component and β-barrel protein Sam50 finally facilitates insertion into the OM [42–44].

The last group of mitochondrial proteins are single- or multispanning α-helical proteins located in the OM. The details about the import pathways of these proteins are only partially reveled so far. The mitochondrial import (MIM) complex has been shown to be mainly involved in the import of α-helical proteins [45,46], however, the utilized import routes appear to be rather diverse and not restricted to the sole involvement of MIM. Especially multi-spanning proteins are imported via MIM in a Tom70-dependent manner [45,47]. In contrast, single-spanning proteins are imported by free MIM complexes. Lastly, portions of MIM interact with SAM for import and early assembly of the small Tom proteins [48].

1.2. The chaperone network and its role in mitochondrial biogenesis

Chaperones are major components within the protein homeostasis (proteostasis) network. This network comprises a variety of means which ensure the preservation of all proteins in their physiological conformation and quantity range. It comprises three functionally distinct pathways which tightly cooperate with each other: protein synthesis, folding and degradation.

Chaperones assist in a multitude of processes including folding and assembly of newly synthesized proteins as well as protein refolding and disaggregation. By recognizing hydrophobic stretches, chaperones can bind to a great variety of substrates. However, chaperones do not only recognize hydrophobic patches within cytosolic un- or misfolded proteins, but they also bind to hydrophobic residues of mitochondrial precursor proteins. Approximately 40 years ago, *in vivo* and *in vitro* analyses already demonstrated that components of the Hsp70 protein family play a role in promoting protein import into mitochondria [49,50]. Hsp70 chaperones consist of an N-terminal ATPase domain, a substrate binding domain and a C-terminal domain which assists in trapping the substrate in the substrate binding domain [51,52]. The binding specificity of Hsp70s has been extensively studied using synthetic peptides with random sequences. Hsp70 chaperones preferentially bind to peptides containing clusters of hydrophobic and positively charged but few or no acidic amino acid residues. In contrast, negatively charged peptides are bound with very low affinity [53–56]. Peptide sequences strongly resembling mitochondrial presequences bind to Ssa1, a major cytosolic Hsp70 chaperone in yeast, and stimulate its ATPase activity. Here, the amphiphilicity of the presequences strongly influences the binding affinity to Ssa1 [57]. Another major group of chaperones are the Hsp90s. Members of this group exhibit an N-terminal ATP binding domain, a middle domain which interacts with Hsp70s as well as many substrate proteins, and a C-terminal domain which is involved in the characteristic homodimer formation of Hsp90s [58]. Hsp90s act downstream of Hsp70s, however, chaperones of both superfamilies functionally collaborate in their activities. In yeast, Ssa1 directly interacts with the Hsp90 chaperone Hsp82. This interaction as well as other processes, including regulation of the chaperone activity and substrate binding, is strongly supported by a multitude of co-chaperones [59–61]. Although Hsp70s and Hsp90s exhibit very different overall structures, both classes share conserved EEVD motives located at the C-terminus of many members of these protein families. This EEVD motif functions as a major binding site for co-chaperones containing a tetratricopeptide repeat (TPR) domain [62]. TPR motifs are comprised of 34 amino acid residue repeats which form helix-turn-helix structures and are often arranged into arrays of three to 16

consecutive motifs within a protein [63,64]. Although the overall resulting super helix structure enables binding to a multitude of ligands exhibiting different amino acid sequences and secondary structures, the ligand binding by TPR proteins is typically very specific. Commonly, TPR proteins bind to rather short peptide sequences comprising five amino acid residues, however they can also recognize longer sequences [65]. The MEEVD motif of Hsp90 was one of the first sequence identified to be recognized by TPR proteins [66,67]. The conserved amino acid residues in TPR domains interacting with the EEVD motifs of chaperones are called carboxylate clamp. To date, several TPR-containing co-chaperones have been identified which link Hsp70s and Hsp90s and thereby promote mitochondrial protein import. These include Sti1/HOP (Hsp70-Hsp90 organizing protein) and TOMM34 [68,69]. In addition, the TOM receptor Tom70 also contains TPR domains for chaperone binding and therefore functions as a co-chaperone on the surface of mitochondria during mitochondrial biogenesis [19]. Chaperone functionality is additionally supported by other types of co-chaperones, including J-domain containing co-chaperones, nucleotide exchange factors and more. Overall, chaperones in conjunction with their co-chaperones play important roles in mitochondrial biogenesis by preventing cytosolic aggregation of hydrophobic precursor proteins and by promoting import.

1.3. Protein degradation by the ubiquitin-proteasome system

Under physiological conditions, but even more pronounced under stress or changing environmental conditions, the abundance of thousands of proteins needs to be tightly monitored and controlled. Large-scale analyses revealed selective degradation of numerous proteins by the ubiquitin-proteasome system (UPS) in *Saccharomyces cerevisiae* (*S. cerevisiae*) [70]. The average half-life of all analyzed proteins was found to be approximately 43 minutes. However, particularly unstable proteins with half-lives of less than 4 minutes were identified in addition. This indicates that the UPS plays a key role in regulating the protein abundance of these proteins. Since proteins with short half-lives often function as regulators of cellular processes, the UPS is not only involved in protein quality control and the maintenance of proteostasis, but also assumes regulatory functions within a cell.

1.3.1. The ubiquitin-proteasome system

Proteins destined for proteasomal degradation are marked with polyubiquitin chains which are recognized by the 26S proteasome. The covalent attachment of ubiquitin (Ub) molecules to substrate proteins is mediated by a fine-tuned enzyme cascade including E1, E2 and E3 proteins (Figure 3).

The cascade exhibits a hierarchical ordering with one E1, 13 E2 and 60-100 E3 proteins in yeast [71]. Ub-conjugation is initialized by the ubiquitin-activating enzyme (E1, Uba1 in yeast [72]), which promotes the activation of Ub. In this step, ATP hydrolysis catalyzes the formation of a high-energy thioester bond between the E1 and the Ub molecule. AMP and an inorganic pyrophosphate are released. In a subsequent step, Ub is transferred to a ubiquitin-conjugating enzyme (E2, Ubc1-13 in yeast [71]). Lastly, the Ub-bound E2 binds a ubiquitin-ligase (E3) that specifically interacts with substrate proteins and therefore mediates substrate selectivity.

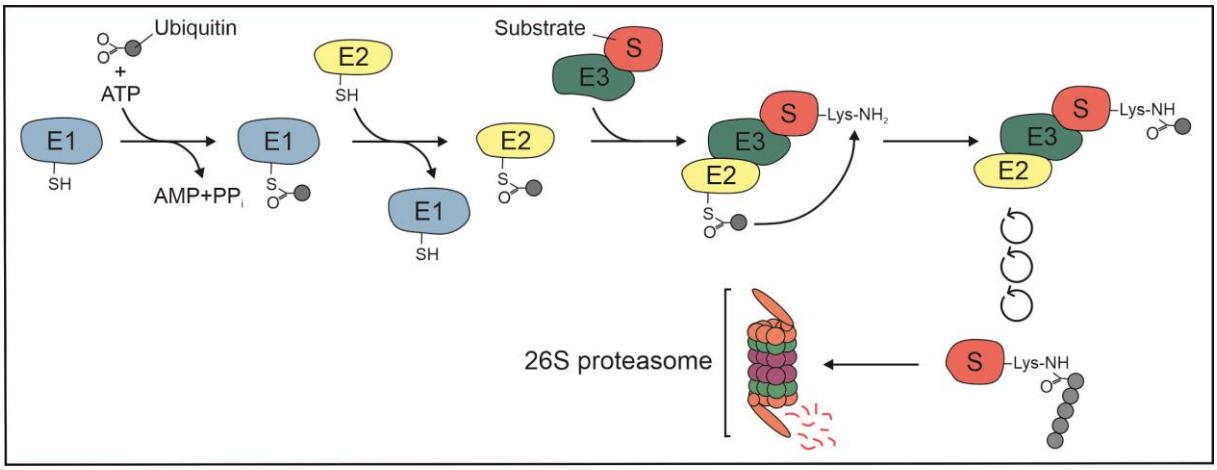

Figure 3: A cascade of E1, E2 and E3 proteins attaches polyubiquitin chains to proteins as a signal for proteasomal degradation. Ubiquitin-activating enzymes (E1s) activate ubiquitin (Ub) in an ATP hydrolysis-dependent step. Activated ubiquitin is transferred to a ubiquitin-conjugating enzyme (E2) which interacts with a ubiquitin ligase (E3). E3s additionally bind substrate proteins to which the Ub molecule is attached via a lysine residue. Multiple iterations of this enzyme cascade allow the formation of polyubiquitin chains that mark proteins, besides others, for proteasomal degradation. The 26S proteasome deubiquitinates, unfolds and proteolytically cleaves the substrate.

The Ub molecule is, most commonly, transferred to a lysine residue of the substrate protein. Ub can either be directly transferred from the E2 to the substrate (RING ligases) or is transferred first to the E3 protein itself as an intermediate step (HECT- or RBR-ligases). Due to multiple iterations of this cascade polyubiquitin chains are formed. Ub itself contains seven lysine residues (K6, K11, K27, K29, K33, K48, K63) which allow numerous variations of Ub linkages [73]. Polyubiquitin chains comprising linkages via K48 were found to mainly mark proteins for proteasomal degradation [74]. The regulatory particle of the 26S proteasome recognizes protein-attached polyubiquitin chains, deubiquitinates and unfolds the substrate protein prior to the proteolytic cleavage by the proteasomal core subunit [75]. Polyubiquitin chains containing linkages via other lysine residues, as well as mono- or multiubiquitination, convey signals for many other cellular processes including signal transduction, DNA damage repair, transcription and cell cycle regulation [76]. Ubiquitination is a reversible reaction. Deubiquitinases (DUBs) catalyze the removal of single Ub molecules, thereby increasing the variability of linkage topologies. Released Ub may be reactivated through E1 proteins.

In some cases, ubiquitinated proteins need to be extracted from membranes or complexes to be degraded by the UPS. In such cases, proteasomal degradation is often supported by AAA+ proteins. The AAA+ ATPase Cdc48 acts as an unfoldase in the cytosol and binds to UBX (ubiquitin regulatory X) domain-containing co-factors and others for its proper functionality [77,78].

1.3.2. The role of the UPS in mitochondrial biogenesis

The UPS plays a crucial role in the surveillance of mitochondrial proteins. The cytosolic proteasome is heavily involved in the so-called mitochondria-associated degradation (MAD), which comprises the degradation of many mature and newly synthesized mitochondrial proteins by the UPS.

The degradation of mitochondrial OM proteins strongly depends on their extraction from the lipid bilayer. The underlying degradation mechanism was extensively studied using the identified substrate proteins Fzo1, Msp1, Tom70 and Mdm34 [79]. The E3 proteins Mdm30 and Rsp5 mediate ubiquitination of these proteins and promote their proteasomal degradation (Figure 4A) [80]. At least for Fzo1, the two functionally distinct DUBs Ubp2 and Ubp12 control and adjust the ubiquitin chains thereby regulating the stability of Fzo1 [81]. The Cdc48 adaptor protein Doa1 recognizes ubiquitinated OM proteins and recruits Cdc48 together with its co-factors Ufd1 and Npl4 for subsequent protein unfolding and extraction [79].

Apart from OM proteins, also proteins of the IMS are controlled by the UPS. This requires their Tom40-mediated retrotranslocation across the OM (Figure 4B). Reduction of the disulfide bonds of IMS proteins induces their transport across the OM into the cytosol, at least *in vitro*. Details about the retrotranslocation process and the factors involved in the ubiquitination of IMS proteins remain elusive. However, the cytosolic UPS is assumed to prevent the accumulation of defective proteins in the IMS.

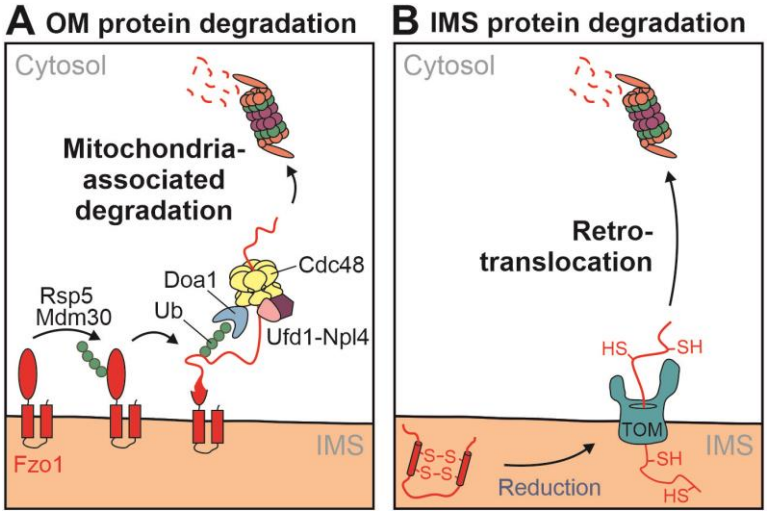

Figure 4: Mitochondria-associated degradation (MAD) facilitates proteasomal degradation of mitochondrial proteins. (A) Degradation of outer membrane (OM) proteins. The ubiquitin ligases Mdm30 and Rsp5 are involved in the ubiquitination of Fzo1 and thereby mark the protein for proteasomal degradation. Doa1 bridges the Cdc48-Ufd1-Npl4 complex to the attached polyubiquitin chain. This enables the unfolding and extraction of Fzo1 followed by proteasomal degradation in the cytosol. **(B)** Degradation of IMS proteins. In a process called retrotranslocation, misfolded or partially reduced IMS proteins can be released into the cytosol via the TOM complex. In the cytosol, these proteins get degraded by the proteasome. IMS = intermembrane space. This figure and the figure legend were modified from my review [9].

Furthermore, the UPS plays a major role in the protein quality control during mitochondrial biogenesis. Firstly, non-imported precursors are monitored by the UPS (Figure 5A). Under physiological, non-stressed conditions, the UPS already depletes fractions of mitochondrial precursor proteins from the cytosol [82]. When mitochondrial protein import is impaired, nascent precursors are directed for proteasomal degradation to prevent their accumulation in the cytosol [83]. Under these conditions, the capacity of the entire UPS is strongly increased [84,85]. Interestingly, the stability of precursors in the cytosol differs considerably, indicating that specific signals regulate the individual turnover rates. Furthermore, mitochondrial precursors are degraded on the surface of the endoplasmic reticulum (ER) by ER-associated degradation (ERAD) or in the nucleus [86,87].

Secondly, the UPS extracts mis-localized TA proteins destined for the ER from the mitochondrial OM (Figure 5B) and vice versa. TA proteins contain a TMD whose features, including hydrophobicity and charge, are responsible for the specific targeting of these proteins to mitochondria, the ER, or peroxisomes, respectively [88]. Nevertheless, TA proteins can mis-localize to the membranes of the wrong organelle. On the mitochondrial surface, the hexameric AAA+ ATPase Msp1 recognizes and extracts TA proteins of the ER [89]. After retargeting to the ER surface, the proteins are either inserted into the ER membrane or degraded by the ERAD machinery. The TA proteins are ubiquitinated by the E2 proteins Ubc6 and Ubc7 in conjunction with the E3 protein Doa10 [90]. Cdc48, together with its cofactors Npl4 and Ufd1, subsequently extracts the ubiquitinated TA proteins from the ER membrane promoting their proteasomal

degradation. Like Msp1, the recently discovered ATPase Spf1 clears the ER membrane from mis-localized mitochondrial proteins [91,92]. Whether these proteins can be retargeted to mitochondria remains elusive.

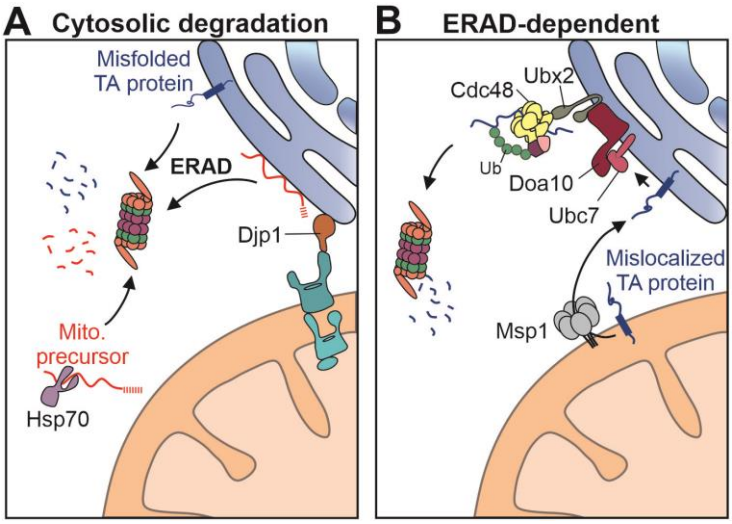

Figure 5: Quality control of non-imported and mis-localized proteins. (A) Cytosolic precursor degradation. The proteasome controls the cytosolic number of mitochondrial precursors by the selective degradation of non-imported proteins. Precursors that associate with the ER surface get removed in an ER-associated degradation (ERAD)-dependent manner. **(B)** ERAD-dependent degradation. The AAA-ATPase Msp1 extracts mis-localized tail-anchored (TA) proteins of the ER from the mitochondrial outer membrane. These proteins are retargeted to the ER where they are either inserted into the membrane or degraded in a Doa10- and Cdc48-dependent manner. This figure and the figure legend were modified from my review [9].

Furthermore, the UPS monitors the mitochondrial import channels by clearing stalled import intermediates. To avoid clogging of the import pores, the TOM complex is continuously monitored by the mitochondrial protein translocation-associated degradation (mitoTAD) pathway (Figure 6A). The membrane protein Ubx2 serves as central factor of this monitoring process. It recruits the extractor protein Cdc48 together with its co-factors to cleanse proteins from the TOM complex. Ubx2 recruitment to mitochondria is enabled by its direct binding to the OM receptor Tom70 [93].

Pth2 and Dsk2 are core factors of an alternative, mitoTAD-independent, mechanism for the constitutive degradation of stalled import intermediates. They were recently identified in a high-resolution complexome profiling study which analyzed protein associations in the mitochondrial proteome as interactors of the TOM complex [94]. Pth2 is a peptidyl-tRNA hydrolase of the OM that constitutively interacts with the TOM complex. Pth2 binds to Dsk2, which targets polyubiquitinated proteins to the proteasome [95,96]. Ubiquitination of stalled import intermediates is catalyzed by the E3 protein Rsp5. The DUB Ubp16 counteracts Rsp5-mediated ubiquitin attachment on the mitochondrial surface [94,97].

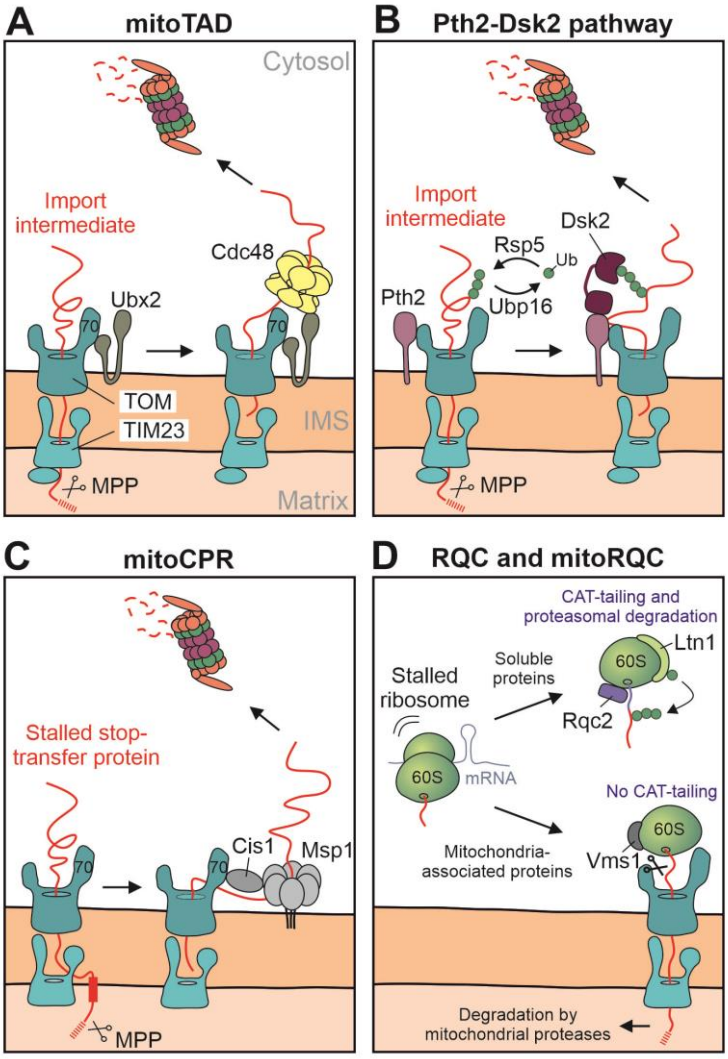

Figure 6: Stalled import intermediates and stalled nascent chains are under surveillance of the UPS. (A) mitoTAD. Ubx2 continuously monitors the TOM complex and extracts stalled import intermediates in a Cdc48-dependent manner. **(B)** Pth2-Dsk2 pathway. Pth2 and Dsk2 are part of another mechanism that continuously clears the TOM complex from stalled import intermediates. The E3 protein Rsp5 mediates ubiquitination of arrested precursors and Pth2-associated Dsk2 facilitates their transfer to the proteasome. **(C)** mitoCPR**.** Mitochondrial stress conditions induce the expression of Cis1 which connects the extractor protein Msp1 to the TOM receptor Tom70. Msp1 extracts stalling-prone inner membrane proteins with N-terminal stop-transfer sequences. **(D)** mitoRQC. Vms1 prevents CAT-tailing of stalled nascent polypeptides and thereby clears the TOM complex from attached ribosome-nascent chain complexes and prevents aggregation of CAT-tailed proteins within mitochondria. This figure and the figure legend were modified from my review [9].

Whereas mitoTAD and the Pth2-Dsk2 pathway are permanently monitoring the TOM complex, the mitochondrial compromised protein import response (mitoCPR) is only activated upon mitochondrial protein import stress (Figure 6C). Adverse conditions, such as $\Delta\psi$ reduction or overexpression of stop-transfer proteins which clog the import machinery, initiate mitoCPR by induction of the stress-responsive protein Cis1 [98]. Cis1 connects the AAA+ ATPase Msp1 to the TOM complex via Tom70. Subsequently, Msp1 extracts the stalled import intermediates and passes them on to the proteasome for degradation [99].

Lastly, in case of stalled ribosomes, the mitochondrial ribosomal quality control (mitoRQC) removes nascent polypeptides from the TOM complex (Figure 6D). The Cdc48-binding protein Vms1 (for VCP/Cdc48-associated mitochondrial stress-responsive) is a peptidyl-tRNA hydrolase that associates with stalled ribosomes on the mitochondrial surface. Binding of Vms1 prevents the addition of so-called CAT-tails (for Carboxy-terminal Alanine and Threonine tails [100]) to the nascent polypeptides and thereby limits the release of aggregation-prone CAT-tailed polypeptides into mitochondria [101,102]. Imported aberrant polypeptides are cleared by intramitochondrial proteases. Parts of the paragraph 1.3.2 were adopted from my review [9].

1.3.3. The role of the UPS in the metabolic remodelling of yeast cells

The abundance of many proteins strongly depends on the prevailing metabolic condition. For example, changes from fermentation to respiration and vice versa are associated with a complex remodeling of the proteome which is the consequence of altered protein synthesis and protein degradation [2]. The glucose-induced degradation deficient (GID) pathway describes one of the UPS-mediated responses being activated upon the switch from respiratory to fermentative growth conditions. This response is also called catabolite degradation. In this regard, the glucose-induced degradation of the gluconeogenic enzymes Fbp1, Pck1, Mdh2 and Icl1 has been extensively studied. The E2 protein Ubc8/Gid3 in collaboration with the GID complex, a cytosolic E3 protein complex, promotes rapid ubiquitination and degradation of these proteins upon glucose addition [103,104]. Selective substrate recognition is mediated by the two substrate-binding subunits Gid4/Vid24 and Gid10 [105,106]. The substrate specificities of Gid4 and Gid10 overlap, however, they are not identical. Whereas all other Gid proteins are constitutively expressed, the expression of the two substrate-binding proteins is induced upon altered growth conditions. Synthesis of Gid4 is induced by the addition of glucose, hence Gid4 functions as the main regulator of the GID pathway. In contrast, Gid10 is induced upon osmotic stress and starvation. Gid4 recognizes its classical substrate proteins in a process called N-end rule pathway, which describes the recognition of N-terminal proline residues at position 1 and 2 of the substrate sequence [107]. However, recently it was shown that substrate recognition might not be restricted to substrates of the N-end rule pathway but that Gid4 and Gid10 bind a more diverse set of N-terminal sequences [108]. Glucose-induced degradation via the GID pathway in conjunction with prior inactivation of the enzymes prevent excessive energy consumption by futile cycles [109]. Parts of the paragraph 1.3.3 were adopted from my review [9].

2. AIM

The previous sections clearly illustrate the high complexity of mitochondrial biogenesis. Precursor proteins are imported by numerous import pathways which in turn comprise a great variety of import components. For correct targeting to and localization within mitochondria, precursors make use of a vast diversity of targeting sequences. Furthermore, mitochondria closely collaborate with the cytosolic UPS and the chaperone network to ensure their proper biogenesis. The aim of this thesis is to elucidate novel aspects how cells modulate mitochondrial biogenesis.

Precursor proteins themselves, especially their presequences, have a major impact on their import behavior. Targeting sequences directing precursor proteins to the mitochondrial surface were discovered long time ago [18,110]. Although presequences are extremely variable, they share common sequence and structural characteristics. In this thesis, I investigated the fundamental reason why N-terminal presequences facilitate protein import with strongly varying efficiencies. By fusing different presequences to the model protein DHFR, I generated a test set of precursor proteins which only differ in their N-terminal targeting sequences. I employed numerous *in vitro* assays and mass spectrometry to reveal the underlying reasons which are responsible for the strong variations in the import efficiencies. Additionally, in collaboration with Yasmin Hoffman, I investigated the import behavior of the test precursors in living yeast cells by applying IQ-Compete (for Import and De-Quenching Competition), a novel assay specifically established for this study by Yasmin ([111]).

As mentioned before, mitochondrial biogenesis is additionally monitored by numerous factors sustaining cytosolic proteostasis, with components of the UPS being one of them [9]. In a recent study, a genetic screen in yeast revealed the cytosolic ubiquitin conjugase Ubc8 to be crucial for the depletion of precursor proteins from the cytosol [86]. It is known, that Ubc8, in collaboration with the GID-complex, is responsible for the selective, glucose-induced degradation of some metabolic enzymes [103,104]. However, to which extent Ubc8 modulates mitochondrial precursor levels and thereby enables proper mitochondrial biogenesis is unknown to date. To address this question, I verified the findings of the previous genetic screen and further analyzed to what degree Ubc8 plays a role in the biogenesis of precursor proteins. I conducted *in vitro* and *in vivo* assays along with mass spectrometry to examine the underlying consequences of an Ubc8 deletion focusing on mitochondrial alterations.

3. RESULTS

Most figures shown in this section are either adopted or modified from my publications [111,112]. People who contributed to this study are mentioned in the relevant sections.

Most matrix proteins contain N-terminal presequences, which facilitate import by binding to the TOM receptor Tom20 and by subsequently promoting translocation through the TOM and TIM machineries (Figure 7). Precursor proteins, especially their targeting sequences, as well as the proper functionality of the import machinery, have a great impact on the import ability and import behavior of mitochondrial proteins.

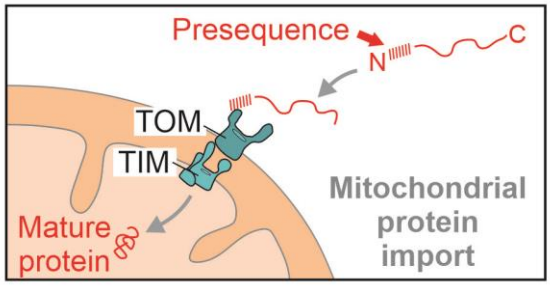

Figure 7: Schematic illustration of the mitochondrial protein import process. Most matrix proteins contain N-terminal presequences for targeting to and import into mitochondria in a Tom20-dependent manner. Modified from [111].

3.1. Presequences provide information about the import efficiency of precursors into isolated mitochondria

In a previous study, the N-terminal presequences of many mitochondrial proteins together with their predicted MPP cleavage sites were identified [10]. It was apparent that the determined presequences considerably differed in length, with most of them being about 20 to 50 amino acid residues long (Figure 8). The common sequence characteristics of MTSs enable rather robust prediction of N-terminal presequences by multiple computational tools, including TargetP [113]. For TargetP, the predicted value ranges from 0 to 1. Scores closer to 1 indicate a stronger prediction for mitochondrial localization. TargetP 1.0 predictions of the previously identified presequences revealed high propensity scores for most of them, irrespective of their length. However, for the predicted scores a certain heterogeneity could be observed.

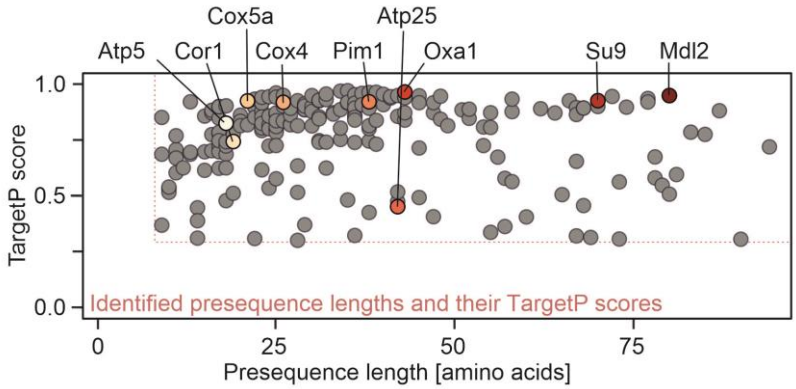

Figure 8: Mitochondrial presequences differ in their sequence length. Diagram showing the length distribution plotted against the corresponding TargetP 1.0 scores [113] of the mitochondrial *S. cerevisiae* presequences published in [10]. Shown are only proteins with TargetP 1.0 scores ≥0.3 and lengths >7 amino acid residues. The presequences included in the test set of this study are labeled. Modified from [111].

The reason as to why the primary sequence and length of MTSs are highly variable between different precursor proteins is unknown. In the following section of this study, the relevance of the existence of various presequences was investigated in further detail. For this purpose, I analyzed a test set of previously characterized presequences (labeled in Figure 8, Figure 9) differing in their respective lengths (from 17 to 80 amino acid residues). A comparison of their primary sequences illustrates the alternating arrangement of positive and hydrophobic amino acid residues that enables the formation of an amphipathic α-helix, a common characteristic feature of presequences [12]. The computed TargetP 1.0 values ranged from approximately 0.9 to 1.0 for most of the sequences, demonstrating consistently high prediction scores for both, short and long presequences.

Protein	TargetP	Sequence	aa
Atp5	0.826	MFNRVFTRSFASSLRAA	17/+3
Cor1	0.744	MLRTVTSKTVSNQFKRSL	18/+4
Cox5a	0.926	MLRNTFTRAGGLSRITSVRF	20/+4
Cox4	0.920	MLSLRQSIRFFKPATRTLCSSRYLL	25/+5
Pim1	0.922	MLRTRTTKTLSTVARTTRAIQYYRSIAKTAAVSQRRF	37/+9
Atp25	0.633	MNKFCLLPFHGKRIGVANIPFTILFKKGPYFLHSHITAVYY	41/+5
Oxa1	0.966	MFKLTSRLVTSRFAASSRLATARTIVLPRPHPSWISFQAKRF	42/+8
Su9	0.927	MASTRVLASRLASQMAASAKVARPAVRVAQVSKRTIQTGSPLQTLKRTQMTSIVNATTRQAFQKRA	66/+12
Mdl2	0.950	MLNGRLPLLRLGICRNMLSRPRLAKLPSIRFRSLVTPSSSQLIPLSRLCLRSPAVGKSLILQSFRCNSSKTVPETSLPS	80/+13/-1

Figure 9: Presequences of the test set used in this study. Shown are the sequences of *S. cerevisiae* presequences and subunit 9 (Su9) of the ATPase of *Neurospora crassa*. The sequences are shown up to the most C-terminal cleavage sites, dependent on the data published in [10]. Positively and negatively charged residues are shown in blue and red, respectively. The TargetP 1.0 values of the proteins and the number of amino acids (aa) and charged residues of the presequences are indicated. Modified from [111].

This test set was used in the following to monitor the import behavior in *in vitro* import experiments. Analysis of the import efficiencies of precursor proteins into isolated yeast mitochondria is a well-established method in this field. In this assay, radiolabeled precursors are synthesized in reticulocyte lysate and then incubated with isolated mitochondria. After different time intervals, the import reaction is stopped, and proteinase K (PK) is added to

degrade all non-imported proteins. Proteins which are not affected by PK treatment, represent the effectively imported proteins. In the matrix, precursors with cleavable presequences are processed by MPP leading to the formation of a mature protein species. For my experiments, I fused the different presequences depicted in Figure 9 to dihydrofolate reductase (DHFR) from mice, a well-characterized protein which has been used for import experiments before and allows easy detection via Autoradiography and Western Blot [114]. Since the mature part of the generated precursors is identical in all the constructs used, this enables me to specifically investigate the relevance and efficiency of the different presequences. For the *in vitro* import experiments, I isolated wild type (WT) mitochondria from cells grown in galactose medium and incubated them with the indicated radiolabeled precursors for 5 and 15 minutes. PK was added and the amount of imported protein, which correlates with the presequence efficiency, was determined. DHFR without a presequence served as a control. As expected, no band was observed for DHFR when PK was added, indicating that firstly, DHFR alone is not imported and secondly, PK degrades all non-imported DHFR (Figure 10A, B). Surprisingly, all tested presequences facilitated the import of DHFR with considerably varying efficiencies. The presequence of Cor1 was only able to import DHFR to very little amounts. This became most apparent during the quantification where nearly no difference between DHFR and Cor1-DHFR was observed. In contrast, the presequences of Cox5a, Atp5, Atp25 and Cox4 were able to import DHFR with low to moderate efficiencies (<50% for the 15 min timepoint relative to Oxa1-DHFR). Thus, I classified them as a group with “low import efficiency”. In addition, I found that the presequences of Pim1, Mdl2, Su9 and Oxa1 were the most efficient presequences included in my test set (>50% for the 15 min timepoint relative to Oxa1-DHFR), so I grouped them together as presequences with “high imported efficiency”. In the following, I will refer to individual members of these two groups as “strong” and “weak” presequences, respectively.

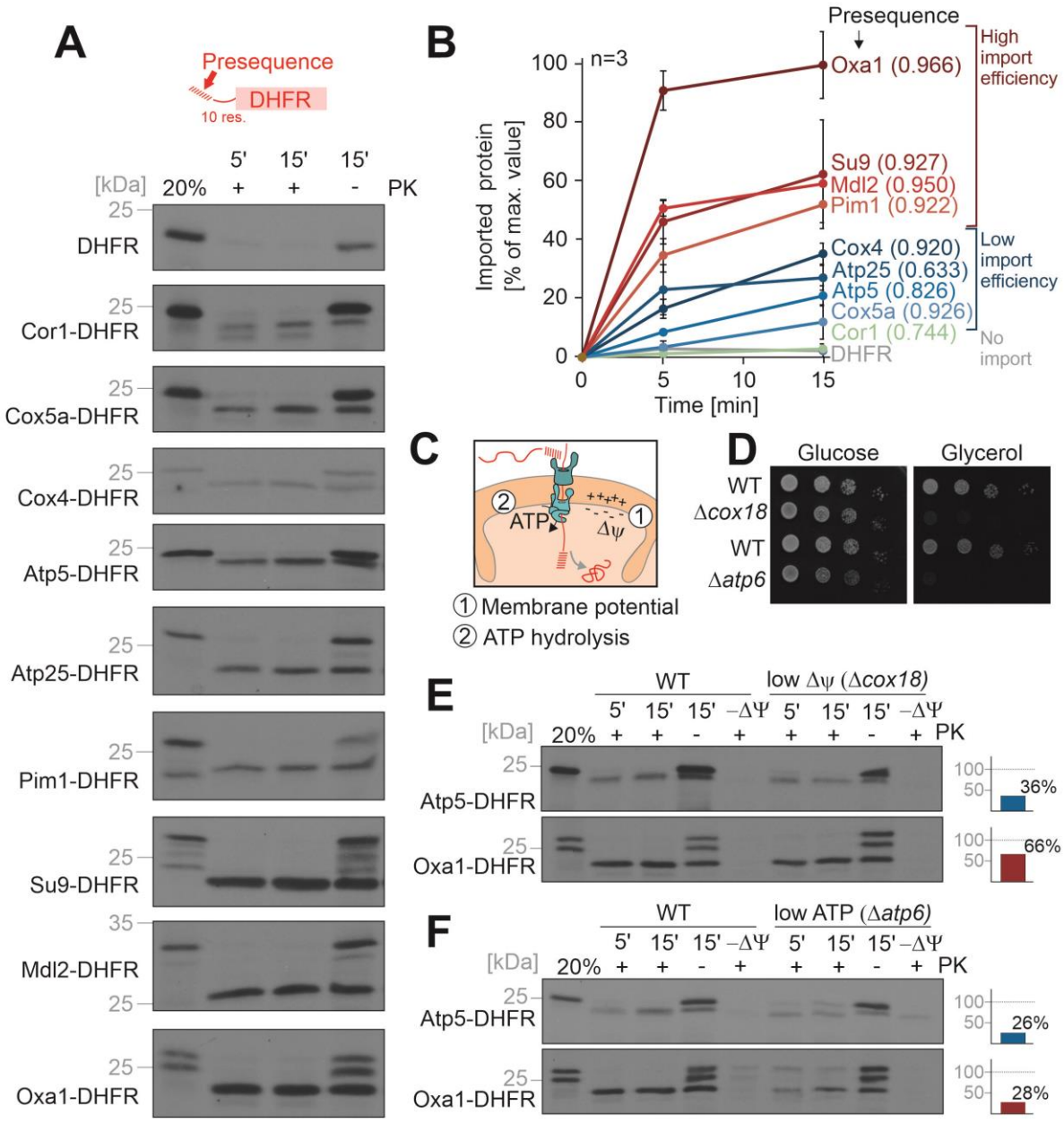

Figure 10: Presequences determine the import efficiency of precursor proteins *in vitro*. (A) The presequences of the indicated proteins including 10 amino acid residues downstream of their MPP cleavage site were fused to DHFR. Radiolabeled precursors were incubated with mitochondria isolated from WT cells grown in galactose medium at 30°C. After 5 and 15 min, the import reactions were stopped, and samples were treated either with or without PK. Proteins were analyzed via Autoradiography. **(B)** Quantification of the +PK samples relative to the - PK samples shown in A. The mean values and standard deviations of three biological replicates (n=3) are displayed (see Figure S1). The numbers behind presequence names represent the predicted TargetP 1.0 scores. **(C)** Schematic overview of the two energy sources that are required for protein import into the matrix. The membrane potential across the inner membrane (Δψ) and ATP hydrolysis in the matrix energize import of matrix proteins. **(D)** The indicated strains were grown in galactose medium, and a ten-fold dilution series was dropped on plates containing either glucose or glycerol as carbon sources. **(E, F)** Radiolabeled precursors were imported into mitochondria isolated from the indicated strains as described for A. For E, ATP, and for F, NADH, were omitted from the import reactions. Diagrams on the right show calculated import efficiencies for 15 min import into the mutant strain relative to import into WT mitochondria. Modified from [111].

Protein import into the matrix relies on the membrane potential across the inner membrane (Δψ) and ATP hydrolysis to energize the mitochondrial Hsp70 in the matrix (Figure 10C). In this context, I investigated whether the impairment of one of these two energizing factors affects

the import of all presequences to the same extent or whether the “weak“ or “strong” presequences are more strongly affected. To do so, I performed *in vitro* imports into mitochondria isolated from Δ*cox18* and Δ*atp6* cells. Cells lacking the cytochrome oxidase assembly protein Cox18 exhibit reduced cytochrome oxidase activity [115] and therefore lower levels of the membrane potential ($\Delta\psi$). Cells lacking Atp6, a subunit of the F_o sector of the ATP synthase, exhibit impaired ATPase activity [116] and therefore diminished ATP levels. I first checked the growth behavior of both mutant strains on fermentative (glucose) and respiratory (glycerol) medium. Δ*cox18* and Δ*atp6*, both were able to grow on glucose but not on glycerol medium (Figure 10D), indicating problems in respiration which is required for proper protein import. In the *in vitro* experiments I found that the import efficiency of all precursors was strongly reduced in Δ*cox18* and Δ*atp6* compared to the WT (Figure 10E, F, Figure S2A, B). However, all proteins were affected to similar degrees.

Based on these results, I concluded, that the differences in presequence efficiencies cannot be explained by different intramitochondrial requirements. Instead, it is more likely that differences upstream of the translocation process, such as targeting or binding to the TOM receptors, may explain the observed variations. Before checking this, I first ensured that my findings about the different import efficiencies are not just artifacts of the *in vitro* import assay, but are also relevant in living cells.

3.2. Presequences determine the import efficiency *in vivo*

To monitor import efficiencies *in vivo*, Yasmin Hoffman, a master's student under my supervision, developed a novel assay based on fluorescence de-quenching [117]. The cloning and experimental data collection regarding this assay was conducted by Yasmin. A detailed description about the individual steps of the development of this assay can be found in her master’s thesis (Cell Biology, RPTU Kaiserslautern-Landau, Supervisor: Johannes M. Herrmann). In brief, we generated a fusion protein consisting of GFP fused to a quencher (Q) peptide and a C-terminal degron (D), resulting in a GFP-quencher-degron (GFP-Q-D) reporter construct. The sequence of CL1 was used as degron [118]. In the linker sequence between the GFP and the Q, we included the cleavage site for a yeast-optimized variant of the *Tabacco Etch virus* protease (uTEV) [119] (Figure S3A). In Figure 11 the fundamental principle of the assay is depicted. In the absence of the uTEV protease, GFP fluorescence is quenched, and the degron facilitates rapid degradation of the reporter construct by the proteasome. However, expression of a cytosolic uTEV protease results in cleavage of the reporter and therefore in strong

fluorescence since GFP is no longer quenched. In our experiments, DHFR was fused N-terminally to the uTEV protease which allows detection of the protein. Due to the later application of the assay in measuring protein import, we named the assay IQ-Compete, which stands for Import and de-Quenching Competition assay.

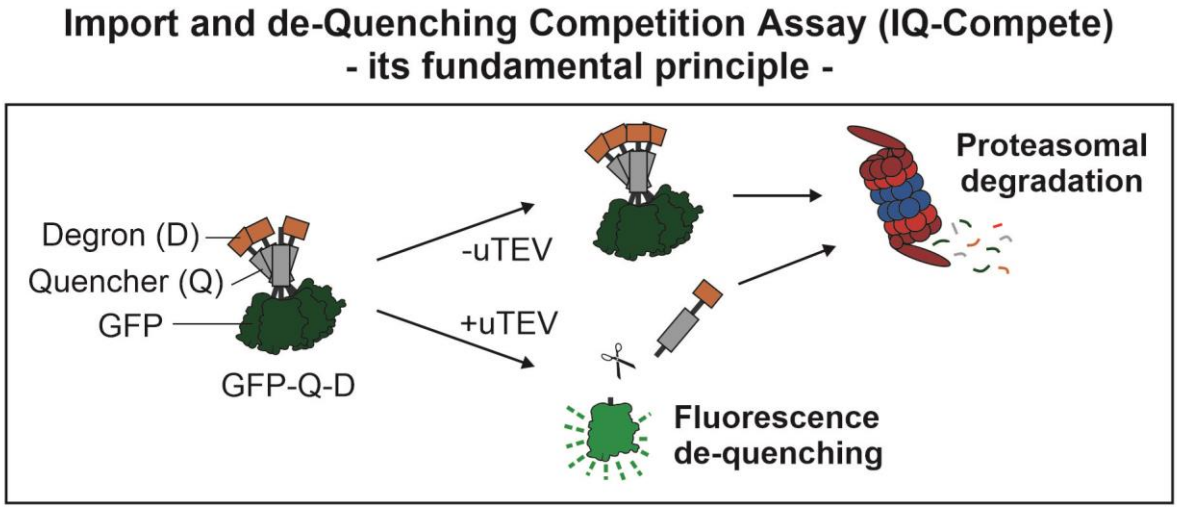

Figure 11: Schematic illustration of the basic principle of the IQ-Compete assay. A reporter construct consisting of GFP fused to a quencher (Q) and a degron (D) gets expressed in yeast cells. A cleavage site for a yeast optimized uTEV protease is inserted between the GFP and the Q peptide. When no uTEV is expressed, GFP fluorescence remains quenched, and the reporter gets degraded by the proteasome. Expression of the protease results in cleavage of the reporter and hence in fluorescence. The GFP-Q-D construct depicted here, was drawn by Annika Egeler. Modified from [111].

However, before the IQ-Compete assay was used to monitor protein import in living yeast cells, we first tested the basic functionality of the assay. For this, we performed a Western blot analysis to verify the expression of the GFP-Q-D reporter and the uTEV protease. We detected strong signals for the expressed uTEV protease and for the cleaved GFP-G-D construct in the corresponding cells (Figure S3B). Futhermore, we performed fluorescence microscopy and flow cytometry. First, we confirmed the fluorescence signals to be well-detectable and measurable using both methods (Figure S3C–F). Second, we showed that in the absence of a uTEV protease, the degron enabled efficient degradation of the reporter construct. Consequently, the background levels were comparably low relative to the signal intensity of WT cells. Third and lastly, we proved that the co-expression of a cytosolic uTEV protease with the GFP-Q-D reporter led to strong fluorescence, with an intensity similar to the one of WT cells expressing GFP.

In summary, the results demonstrated the successful development of a novel assay which can be used to monitor the presence or absence of the uTEV protease in the cytosol of yeast cells.

Next, we applied this assay to check, if the presequences of our test set also determine the import efficiency of precursor proteins *in vivo*. To do so, we integrated the GFP-G-D reporter

and the uTEV protease into the genome of WT cells. This time, the uTEV protease was fused to the C-terminus of the different presequences and DHFR. Hypothetically, the amount of the protease present in the cytosol should directly correlate with the "strength" of the presequence (Figure 12; Figure 13A). This means, for presequences which facilitate highly efficient import, the fused protease should be imported quickly, resulting in (very) low protease levels in the cytosol. Hence, the GFP-Q-D construct should remain uncleaved and subsequently undergoes degradation by the proteasome. Consequently, the GFP should remain quenched and no fluorescence should be detectable (Figure 12, upper panel). In contrast, when presequences with lower import efficiency are fused to the uTEV protease, the cytosolic levels of the protease should increase. Depending on the levels of the cytosolic protease, the corresponding amount of the GFP-Q-D reporter gets cleaved and fluorescence signals, with import-dependent intensities, should be measurable (Figure 12, lower panel). The import of the protease into mitochondria and fluorescence de-quenching by non-imported protease in the cytosol therefore compete.

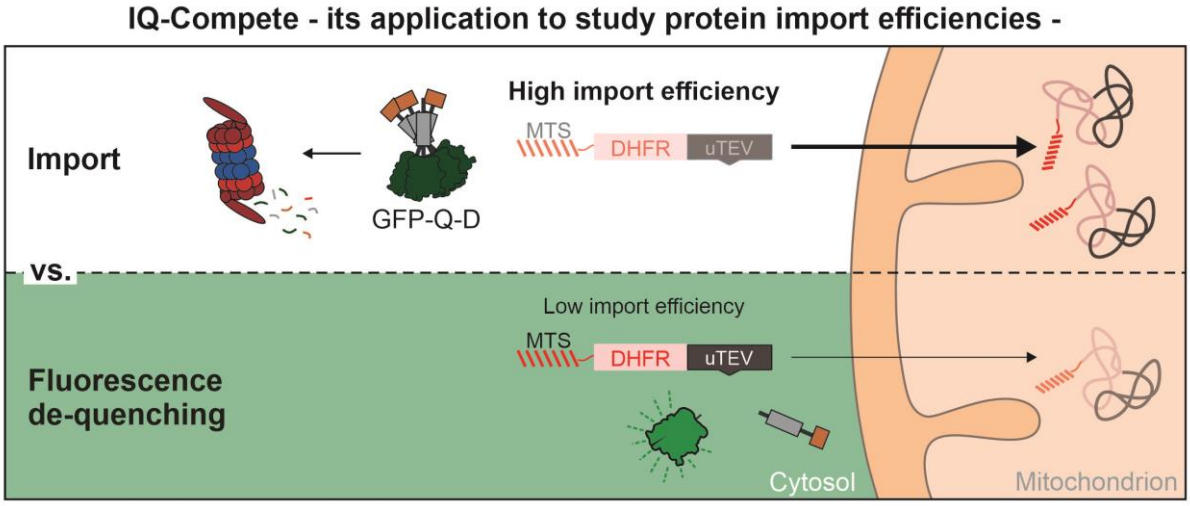

Figure 12: Schematic illustration of the application of the IQ-Compete assay for monitoring import efficiency *in vivo*. The uTEV protease was fused C-terminally to the tested presequences and DHFR. If presequences facilitate import with high efficiency, the protease is imported rapidly. Therefore, the GFP-Q-D reporter remains uncleaved and is degraded by the proteasome (upper panel). If presequences with low import efficiency are fused to the protease, this results in increased levels of the uTEV protease in the cytosol. Hence, uTEV cleaves the GFP-Q-D reporter, which results in fluorescence de-quenching and therefore in fluorescence (lower panel). The GFP-Q-D construct shown in this figure was drawn by Annika Egeler. Q = quencher, D = degron

In our experiments, a cytosolic protease without an MTS was used as a control to achieve maximal cleavage of the reporter and thus serving as benchmark for the maximal fluorescence intensity. Cells only expressing the GFP-Q-D reporter but no uTEV protease were used as a control to determine the minimal (background) fluorescence intensity of the cells. At first, we analyzed the levels of the cleaved GFP-Q-D reporter in our control cells and in cells expressing

the MTS-DHFR-uTEV constructs via Western blot. For this, cells expressing the indicated constructs were grown in glucose medium before harvesting them. The reporter was well detectable in cells expressing the cytosolic uTEV without an MTS, and absent in the control cells not expressing the protease (Figure 13B). Depending on the presequence fused to the protease, we detected strong to moderate levels of the GFP construct for Cor1, Atp5, Atp35 and Cox4, suggesting that these presequences were not efficient. However, very low or no GFP signals were observed for the "strong" presequences Oxa1, Su9 and Mdl2, indicating that these presequences facilitate efficient and rapid protein import of the protease *in vivo*.

These first findings were further supported by our results we obtained by fluorescence microscopy and flow cytometry. For both, cells were grown in glucose medium prior to the analysis. In accordance with the GFP signals detected via Western blot, the microscopy pictures showed strong to no GFP fluorescence for the cells expressing the different MTS-protease fusion proteins (Figure S4). Strong and no fluorescence was detected for the control cells expressing a cytosolic uTEV without an MTS or no uTEV, respectively. Next, we analyzed the fluorescence intensities in a quantitative way by using flow cytometry. We observed a presequence-dependent shift of the fluorescence intensity peaks, ranging from "strong fluorescence", like the cytosolic uTEV control, to "no/weak fluorescence", similar to the control cells lacking a uTEV (Figure 13C, D). The results revealed rather narrow peaks and very small standard deviations, indicating very low cell-to-cell heterogeneity due to the genomic integration of the constructs.

Next, I compared the results of the *in vitro* and the *in vivo* experiments to ensure consistency across my findings. For this, I correlated the mean values obtained with the *in vitro* imports shown in Figure 10B and the mean values obtained with IQ-Compete shown in Figure 13D. The analysis demonstrated strong correlation of the two assays. In both methods, Oxa1, Mdl2 and Su9 showed the highest import efficiencies among the tested presequences (Figure 13E). In contrast, Cox4, Atp25 and Atp5 exhibited lower import efficiencies, and Cor1 was not able to import the precursors at all.

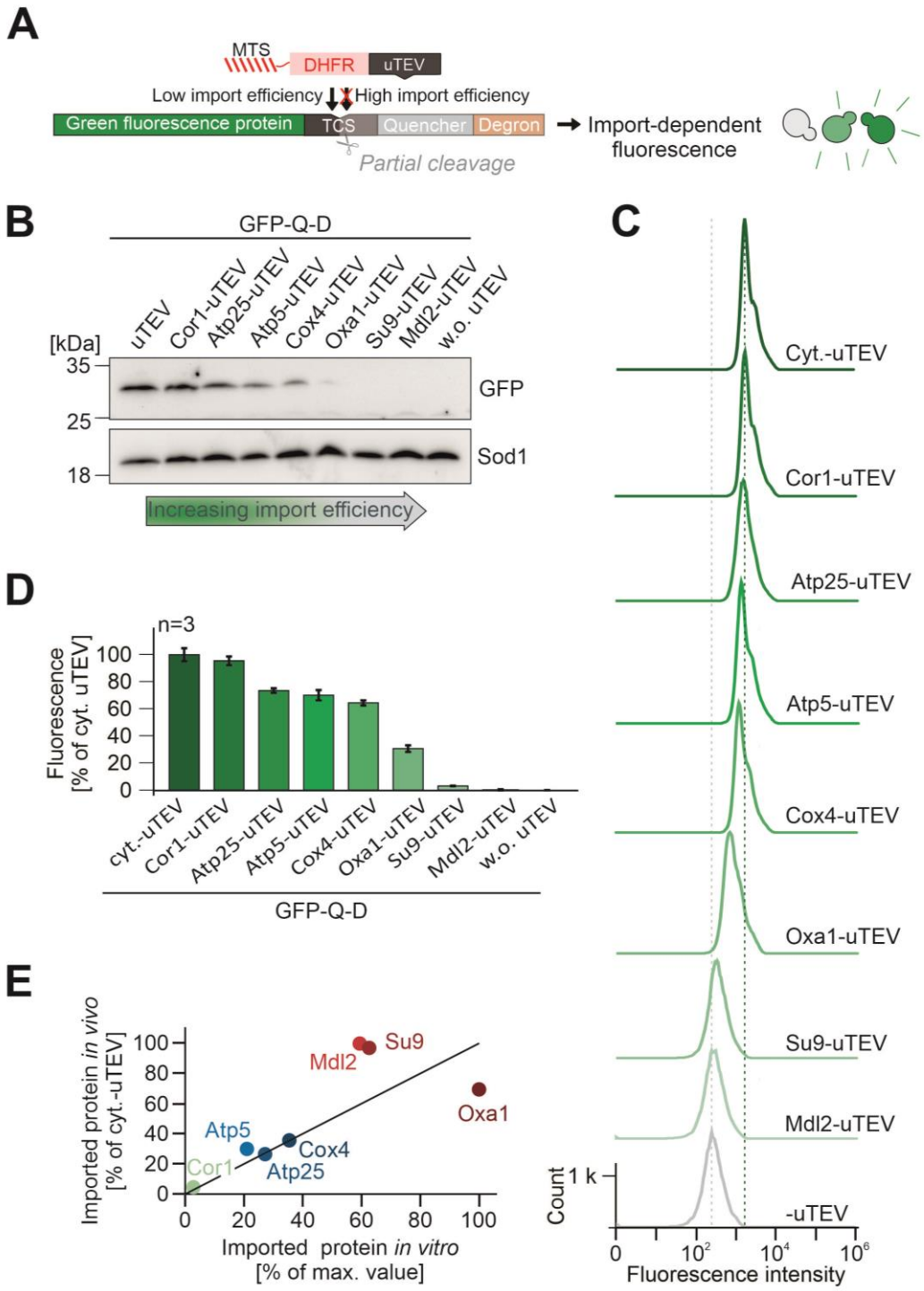

Figure 13: Presequences determine the import efficiency of precursor proteins in living cells. (A) Schematic illustration of the fusion proteins used in IQ-Compete to monitor import efficiency *in vivo*. A presequence with DHFR was fused to a uTEV protease to monitor the import efficiency of the presequence. The protease cleaves import-dependent in a linker region of the GFP-Q-D reporter in the cytosol. **(B)** WT cells expressing the indicated uTEV constructs and the GFP-Q-D reporter were grown in glucose medium to mid-log phase. Cells were harvested, lysed and then analyzed via Western blot. The GFP antibody detects the cleaved fragment of the GFP-Q-D reporter. **(C)** Fluorescence intensities of WT cells expressing the GFP-Q-D reporter and the indicated uTEV constructs in glucose medium were measured using flow cytometry. The dashed grey line marks the minimal fluorescence intensity of cells not expressing a uTEV protease. The dashed green line indicates maximal fluorescence intensity referring to cells expressing a cytosolic uTEV protease. **(D)** Quantification of the fluorescence intensities measured in C. The mean values and standard deviations of three biological replicates (n=3) are shown. **(E)** Correlation of the import efficiencies determined *in vitro* (Figure 10B, 15 min time point) and *in vivo* (Figure 13D). Adopted from [111].

Altogether, the results of the IQ-compete assay confirmed the previous findings I obtained using *in vitro* import experiments: Presequences determine the import efficiency of precursor proteins. Interestingly, these findings are also relevant for living cells.

In the next chapter, I will focus on the hypothesis that differences upstream of the translocation process are the reason for the observed differences in the import efficiencies. To do so, I tested if there is a particular factor in the cytosol, which influences the import behavior in reticulocyte lysate as well as in living cells.

3.3. The "strong" Oxa1 presequence recruits the cytosolic TPR protein TOMM34

For further analysis of the "strong" and "weak" presequences I decided to select one representative presequence from each group for detailed investigation. For the "strong" presequences I chose the MTS of Oxa1 and as a "weak" presequence that of Atp5 was chosen. To analyze if a cytosolic factor is responsible for the strong import efficiency of the MTS of Oxa1, I performed *in vitro* imports into mitochondria isolated from WT cells grown in galactose medium. This time, I compared the import of native proteins, synthesized in reticulocyte lysate as described before, with the import of denatured proteins. For denaturation, I precipitated the radiolabeled Atp5- and Oxa1-DHFR proteins with ammonium sulfate and denatured the proteins subsequently using 8 M urea. Atp5-DHFR was imported with higher efficiency after urea-induced denaturation (Figure 14A, B). This is consistent with previous findings reporting about accelerated import of precursors with "short" presequences after urea-stimulated denaturation [120]. In contrast, urea-denaturation of Oxa1-DHFR led to reduced import of the protein. Assuming that denaturation of both test proteins causes unfolding of the DHFR domain, thereby generally improving protein import, this result suggests that a cytosolic factor acting upstream of protein unfolding on the mitochondrial surface, is crucial for the high import efficiency of the Oxa1 presequence.

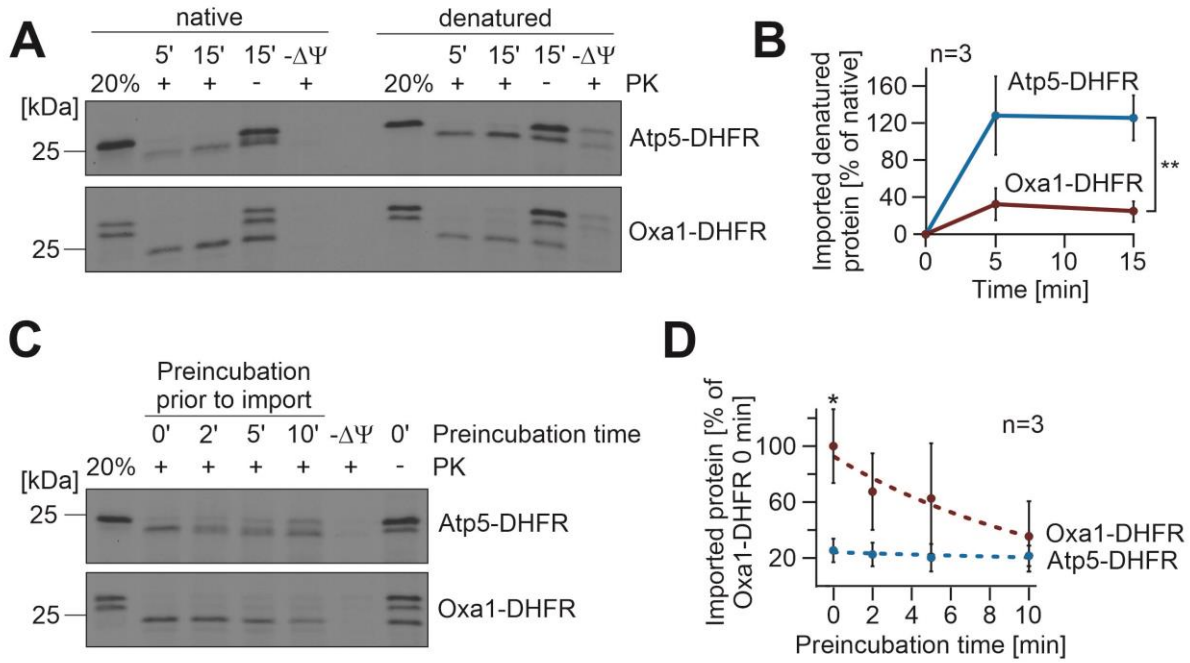

Figure 14: A cytosolic factor increases the import efficiency of the Oxa1 presequence. (A) The radiolabeled proteins indicated were imported either in their native state or as a denatured species. For denaturation, the proteins were precipitated using ammonium sulfate and subsequently dissolved in 8 M urea, 100 mM DTT, and 20 mM Tris pH 7.4 and incubated for 5 min at 25°C. The proteins were imported for 5 and 15 min into mitochondria isolated from WT cells grown in galactose medium before PK was added. **(B)** Quantification of the +PK samples relative to the -PK samples shown in A. The mean values and standard deviations of three biological replicates (n=3) are displayed. Statistical differences were calculated with a student's t-test. Statistical significance was assigned as follows: p-value < 0.01= **. **(C)** The radiolabeled precursors indicated were diluted 100-fold into import buffer containing ATP and NADH. After incubating for the times displayed, import reactions were started by addition of isolated WT mitochondria. After 15 min, imports were stopped, and PK was added. **(D)** Quantification of the +PK samples relative to the non-preincubated Oxa1-DHFR sample shown in C. The mean values and standard deviations of three biological replicates (n=3) are shown. Statistical differences were calculated with a student's t-test. Statistical significance was assigned as follows: p-value < 0.1 = *. Modified from [111].

In the *in vitro* import experiments, the radiolabeled precursors were diluted 100-fold exactly at the time point when the import process is initiated. Consequently, the cytosolic factors of the reticulocyte lysate are around until the import reaction starts. Based on this fact and my previous findings, I next tested whether preincubation of the radiolabeled proteins in import buffer (lacking mitochondria and cytosolic factors) affects their import efficiency. For this, I added isolated WT mitochondria either directly to the precursors or after 2, 5 and 10 minutes of preincubation in import buffer. This buffer contained ATP and NADH to energize the mitochondria but lacked any cytosolic factors. Imports were performed for 15 minutes, and samples were treated with or without PK. Whereas preincubation did not affect the import efficiency of Atp5-DHFR, the efficiency of Oxa1-DHFR was strongly reduced with prolonged incubation (Figure 14C, D). This suggests, that the presequence of Oxa1 transiently interacts with a cytosolic factor, which is released upon prolonged incubation in the buffer prior to the start of the import reaction.

Especially for proteins which are imported in a Tom70-dependent manner it is known that cytosolic proteins like chaperones and co-chaperones participate in their targeting and import [8,121,122]. For this reason, I wondered, whether the double deletion of the receptor Tom70 and its homolog Tom71 impacts the import of my two test precursor proteins. To address this, I isolated mitochondria from Δ*tom70*Δ*tom71* cells which were grown in galactose medium and analyzed the import of radiolabeled precursors into the mutant relative to WT mitochondria. Imports were performed for 15 minutes, and samples were treated with or without PK. The import of Atp5-DHFR was not altered upon loss of Tom70 and Tom71 (Figure 15A, B). In contrast, deletion of the two TOM receptors resulted in a considerable reduction of the import efficiency of Oxa1-DHFR.

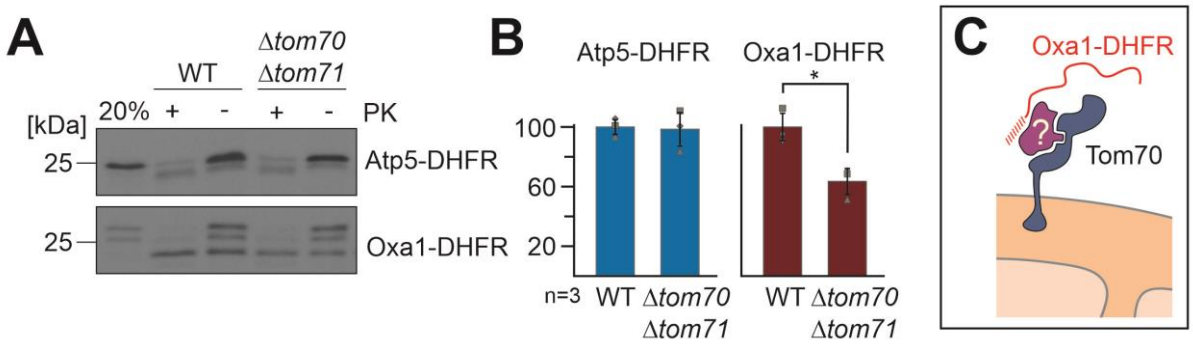

Figure 15: The Oxa1 presequence uses Tom70 for highly efficient protein import. (A) The radiolabeled proteins indicated were imported into mitochondria isolated from WT and Δ*tom70*Δ*tom71* cells grwon in galactose medium. After 15 min, the import reactions were stopped and PK was added. **(B)** Quantification of the +PK samples shown in A relative to the -PK samples. The mean values and standard deviations of three biological replicates (n=3) are shown. Statistical differences were calculated with a student's t-test. Statistical significance was assigned as follows: p-value < 0.1 = *. **(C)** Schematic illustration of a putative cytosolic factor that binds to the Oxa1 presequence and thus promotes Tom70-dependent import. Modified from [111].

Taken together, these results suggest that the "strong" presequence of Oxa1 transiently binds a cytosolic factor that, at least partially, promotes highly efficient protein import in a Tom70-dependent manner (Figure 15C).

Based on this hypothesis, I next identified proteins present in the reticulocyte lysate which are bound to the test presequences. To do so, I performed immunoprecipitation experiments and analyzed interaction partners using mass spectrometry (Figure 16A). I synthesized the test proteins ATP5-DHFR, Oxa1-DHFR, Su9-DHFR and DHFR without an MTS in reticulocyte lysate without radiolabeling. For pulldown of these proteins, I coupled DHFR-specific antibodies to Protein A beads and removed all unbound proteins through a washing step. I then added the prepared reticulocyte lysates to the antibody-bound beads. After incubation and subsequent washing, I eluted the proteins together with the interacting proteins and prepared

the samples for the analysis via mass spectrometry. The mass spectrometric measurement was performed by Markus Räschle and the statistical analysis was done by Annika Nutz.

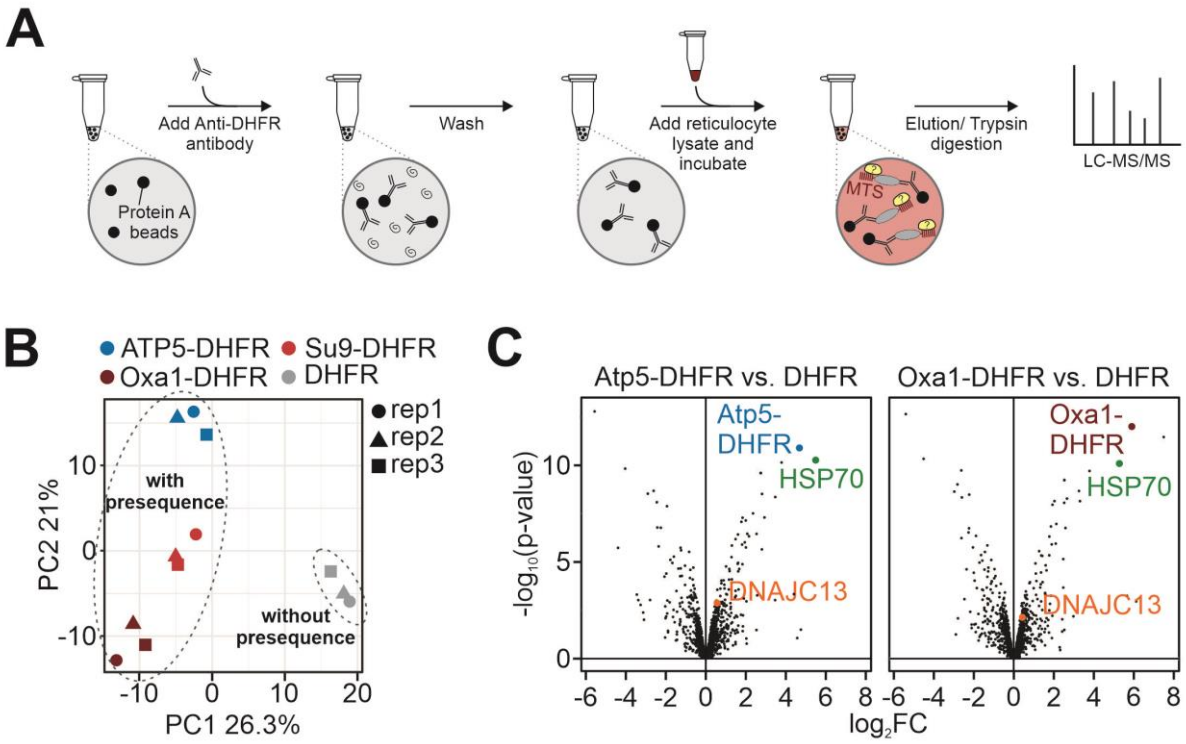

Figure 16: Presequences bind the chaperone Hsp70 in reticulocyte lysate. (A) Schematic illustration of the immunoprecipitation proteomics workflow. Atp5-DHFR, Oxa1-DHFR, Su9-DHFR, and DHFR without an MTS were synthesized in rabbit reticulocyte lysate without radiolabeling. DHFR-specific antibodies were coupled to Protein A beads and all non-bound proteins were removed by washing. The reticulocyte lysates were added to the antibody-bound beads and after incubation and subsequent washing, the samples were analyzed via mass spectrometry. **(B)** Principal component analysis of all samples after normalization. rep = replicate **(C)** Volcano plots showing the interactome comparisons of the indicated samples. HSP70 labels the data point for the rabbit heat shock cognate 71 kDa protein. B and C are modified from [111].

Principal component analysis revealed that the interactome of all presequence-containing samples remarkably differed from the DHFR control (Figure 16B). Moreover, direct comparisons of the Atp5-, Oxa1-, and Su9-DHFR interactomes with the DHFR control showed the Hsp70 protein 8 (homologous to the human HSP A8 protein) being strongly enriched in the presequence-containing samples (Figure 16C, Figure S5). This indicates, that the cytosolic Hsp70 serves as a general presequence-binding factor in reticulocyte lysate. In addition, DNAJC13, a J-domain protein, was also detected in all presequence-containing samples, albeit at lower levels.

Next, we analyzed which cytosolic factors of the reticulocyte lysate specifically interact with the “strong” presequence of Oxa1 but show no interaction with the “weak” presequence of Atp5. The corresponding comparison of the interactomes identified the protein TOMM34 as a possible candidate (Figure 17A). Interestingly, TOMM34 is a co-chaperone of the Hsp70/Hsp90 system that was found in previous studies to localize to the surface of mitochondria in human

cells and to promote protein import into mitochondria [68]. As shown in Figure 17B, TOMM34 contains six highly conserved tetratricopeptide repeats (TPR). This pattern is a common feature among co-chaperones which enables binding to chaperones of the Hsp70 and Hsp90 superfamilies [8,59,123].

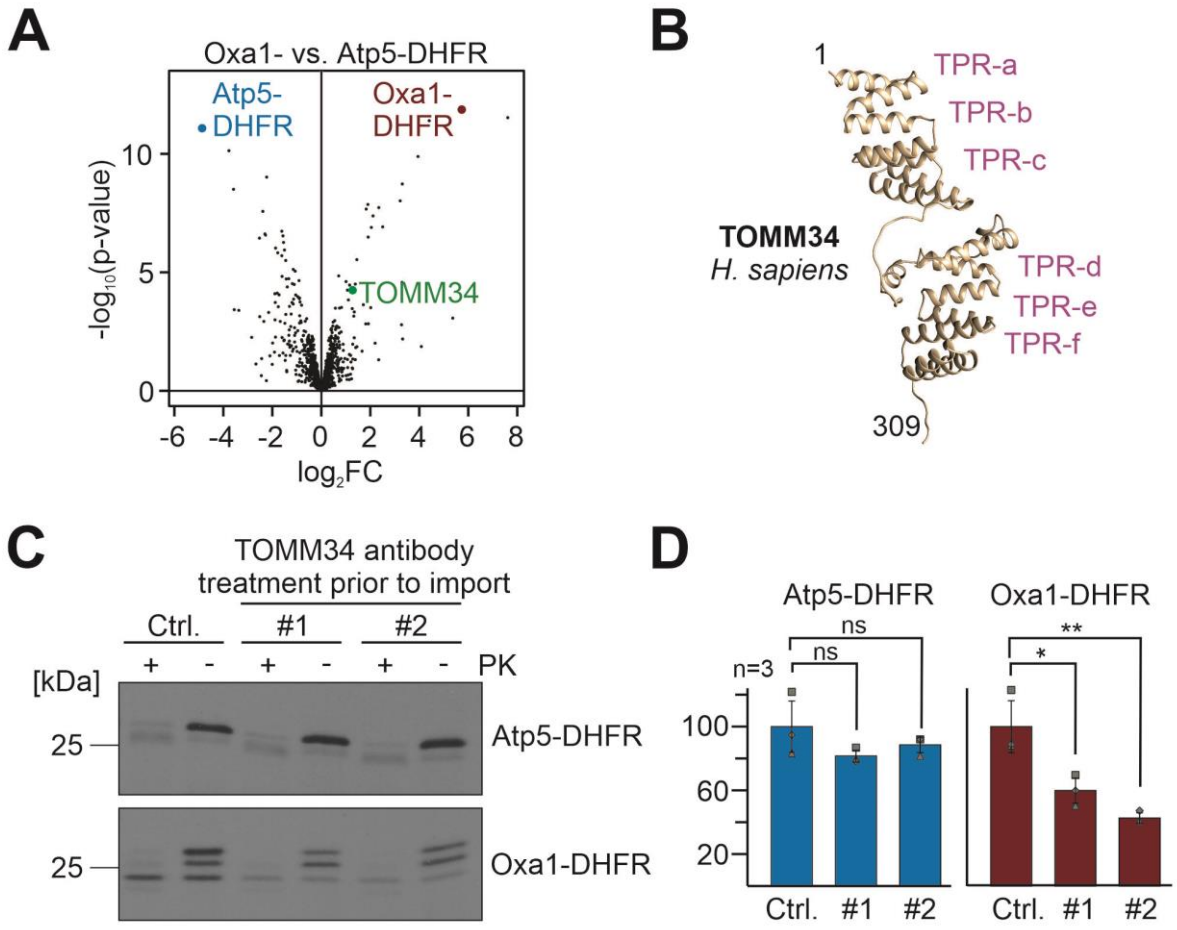

Figure 17: The presequence of Oxa1 recruits the TPR protein TOMM34 for efficient protein import. (A) Volcano plot showing the interactome comparison of the indicated samples from the immunoprecipitation proteomics analysis. **(B)** The alphafold structure of the human TOMM34 (accession number: Q15785) was modeled and visualized with UCSF Chimera [124]. Positions of the six TPR hairpins are indicated. **(C)** The radiolabeled proteins indicated were incubated with two different TOMM34-specific antibodies (#1 and #2), or with an Sod1-specific antibody as a control (Ctrl.) for 15 min at 25°C. Afterwards, the precursors were used for *in vitro* imports into mitochondria isolated from WT cells grown in galactose medium. Imports were stopped after 15 min and PK was added. **(D)** Quantification of the +PK samples shown in C relative to the -PK samples. The mean values and standard deviations of three biological replicates (n=3) are shown. Statistical differences were calculated with a student's t-test. Statistical significance was assigned as follows: p-value < 0.1 = *; < 0.01 = ** (ns = not significant). Modified from [111].

In the following step, I tested whether TOMM34 is in fact relevant for the high import efficiency of the Oxa1 presequence in *in vitro* imports. For this, I repeated *in vitro* import experiments into WT mitochondria isolated from cells grown in galactose medium. However, this time I added TOMM34-specific antibodies to the radiolabeled Atp5-DHFR and Oxa1-DHFR precursors for 15 minutes prior to the import reaction. The antibodies compete with the precursor proteins for

TOMM34 binding, making TOMM34 less accessible to the precursors. As a control, I added Sod1-specific antibodies. Imports were performed for 15 minutes, and samples were treated with or without PK. The import efficiency of Atp5-DHFR remained unchanged upon TOMM34 antibody pretreatment compared to the control (Figure 17C, D). However, the import of Oxa1-DHFR was strongly reduced when TOMM34 antibodies were added.

TOMM34 is a conserved protein in mammals but it is not found in fungi. However, its amino acid sequence resembles that of Cns1 (Figure S6), a co-chaperone of Hsp70 and Hsp90 in yeast. Like TOMM34, Cns1 also contains a TPR domain for chaperone binding [125,126].

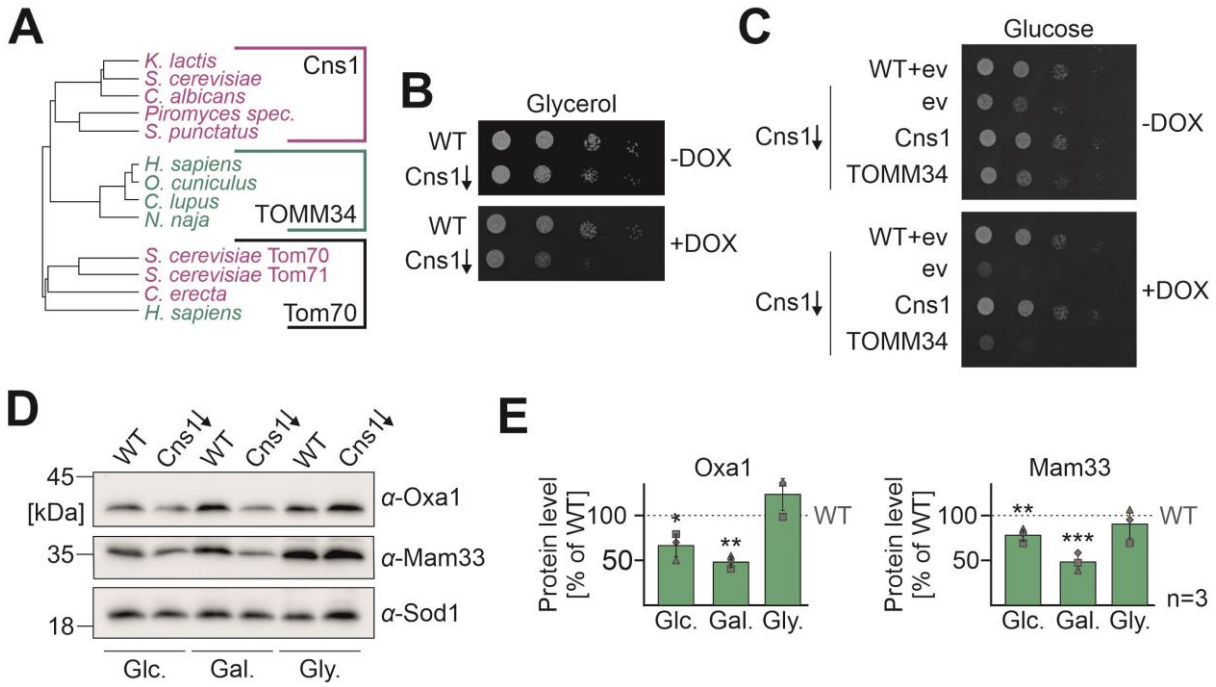

Figure 18: Oxa1 and Mam33 protein levels are reduced in cells depleted for the TPR protein Cns1. (A) Phylogenetic tree showing the relationship of Cns1, TOMM34 and Tom70 sequences. The sequences were aligned and trees were calculated with the MUSCLE Multiple Sequence Alignment tool [127] using the following sequences: Cns1 (*Kluyveromyces lactis* Q6CVR7; *S. cerevisiae* Cns1; *Candida albicans* A0A8H6BZ74; *Spizellomyces punctatus* A0A0L0HPW1), TOMM34 (*Homo sapiens* Q15785; *Oryctolagus cuniculus* G1SIU6; Canis lupus A0A8I3NTN0; Naja naja A0A8C6X204), Tom70 (*S. cerevisiae* Tom70/Tom71, *Coemansia erecta* A0A9W7XVH4; *H. sapiens* O94826). Species names of animals and fungi are shown in green or red, respectively. **(B)** The indicated strains were grown in galactose medium, and a ten-fold dilution series was dropped on plates containing glycerol as a carbon source. Plates were either prepared with or without 10 µg/ml doxycycline (DOX). **(C)** The indicated strains were grown in galactose medium first without and then for 24 h with the presence of 10 µg/ml DOX. A ten-fold dilution series was dropped on plates containing glucose as a carbon source. Plates were either prepared with or without 10 µg/ml DOX. **(D)** Cells of the designated strains were grown in glucose (Glc.), galactose (Gal.) or glycerol (Gly.) medium. All cultures were treated with 10 µg/ml DOX for 30 h to induce Cns1 depletion. Cells were harvested, lysed and analyzed via Western blot. **(E)** Quantification of the indicated protein levels shown in D relative to the WT. Shown are mean values and standard deviations of three biological replicates (n=3). Statistical differences were calculated with a student's t-test. Statistical significance was assigned as follows: p-value <0.1 = *; < 0.01 = **; < 0.001 = ***. Modified from [111].

The phylogenetic tree based on sequence alignments shown in Figure 18A supports a common evolutionary origin of TOMM34 in animals, Cns1 in fungi and Tom70 in both species. Just like TOMM34 and Cns1, Tom70 also harbors TPR domains for the binding of Hsp70 and Hsp90

chaperones [128]. Therefore, I tested whether Cns1, like TOMM34, is involved in mitochondrial biogenesis. For this, I used a Cns1 depletion strain, as Cns1 is an essential protein. In this strain, Cns1 expression is repressed when doxycycline (DOX) is added to the medium [125]. To first test the growth behavior of the Cns1 mutant strain, I performed a drop dilution assay and compared the growth of cells with depleted Cns1 levels with cells containing normal protein levels of Cns1. Depletion of Cns1 resulted in reduced growth on respiratory medium compared to the WT (Figure 18B). To check, if expression of TOMM34 restores this growth phenotype, I expressed either yeast Cns1 or human TOMM34 constitutively in the Cns1 depletion strain. DOX was added to the cultures for 24 hours prior to the experiment. Expression of an empty vector (ev) served as a control. Growth was analyzed by a drop dilution assay using glucose plates prepared with and without DOX. Whereas Cns1 expression restored the growth defect of the Cns1 depletion strain to WT growth rates, expression of TOMM34 did not suppress the growth phenotype. My results indicate that TOMM34 cannot take over the functions of Cns1, or at least it is not able to restore normal cell growth. Lastly, I analyzed the protein levels of the two mitochondrial proteins Oxa1 and Mam33 in the Cns1 depletion strain. For this, I cultivated WT and Cns1 mutant cells in galactose, glucose and glycerol medium and added DOX to all cultures for 30 h to deplete Cns1. I harvested the cells and analyzed them via Western blot. Interestingly, Oxa1 and Mam33 protein levels were strongly reduced in the Cns1 depletion strain compared to the WT in glucose and galactose medium (Figure 18D, E). However, in glycerol medium the protein levels were not altered. This suggests that under respiratory conditions, when mitochondrial protein import is highly required, cells can compensate the depletion of Cns1. Nevertheless, this result provides initial indications of Cns1 being involved in mitochondrial biogenesis. Whether Cns1 is indeed the functionally equivalent of the mammalian TOMM34 remains elusive so far.

At this stage, it became clear that the N-terminal presequences of precursor proteins and presumably cytosolic co-chaperones greatly impact the import efficiency into mitochondria. The involvement and rather complex interplay of numerous import components in the actual import process suggests that in addition from specific co-chaperones also other factors play a substantial role in modulating protein import. The most obvious aspects might include the proper functionality of the cytosolic targeting, degradation and import machineries. Based on a genetic screen in yeast, recent studies successively identified factors that are crucial for proper import of precursor proteins due to their involvement in any of these processes [86,129,130]. However, this is just the beginning of unraveling all the different factors involved in maintaining effective protein targeting to and import into mitochondria.

3.4. Ubc8-deficiency leads to the accumulation of precursor proteins in the cytosol

The just mentioned genetic screen was conducted by *Hansen et al.* with the aim to identify novel factors which are critical for efficient biogenesis of precursor proteins [86]. The goal of Hansen and co-cworkers was the identification of yeast mutants which fail to import a mitochondrial reporter protein which therefore accumulates in the cytosol (Figure 19A)

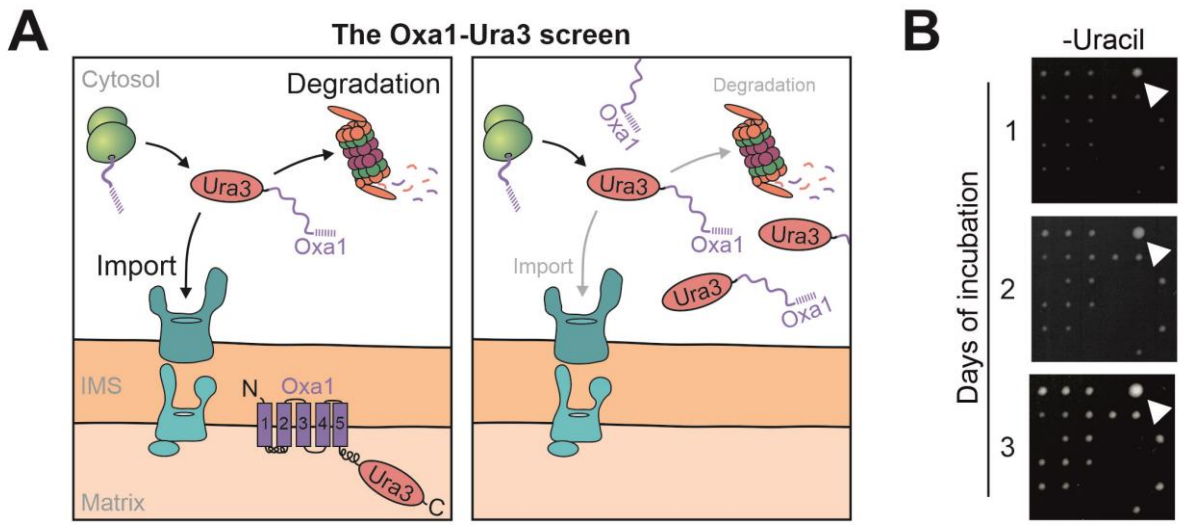

Figure 19: The Oxa1-Ura3 screen revealed a cytosolic accumulation of the Oxa1-Ura3 reporter in Ubc8 deletion cells. (A) Schematic illustration of the Oxa1-Ura3 screen in yeast. Cells with efficient biogenesis of the Oxa1-Ura3 reporter construct are uracil-deficient. The cytosolic accumulation of the reporter causes uracil independence. **(B)** Yeast deletion and DamP mutants expressing the Oxa1-Ura3 reporter were screened for uracil-independent growth. Here, parts of an uracil-free plate are shown after incubation for 1, 2 and 3 days, respectively. The colony of the Ubc8 deletion strain is marked by arrows. See Figure S7A for the entire plate. The result was obtained by Dr. Katja Hansen.

In the screen, Ura3, a protein functioning in uracil biosynthesis, was fused C-terminally to the mitochondrial IM protein Oxa1. This reporter construct was genomically expressed in a yeast deletion and a decreased abundance by mRNA perturbation (DAmP) library to screen for mutants that show impaired biogenesis of this reporter. Efficient protein targeting, import or degradation of the reporter results in the depletion of the precursor from the cytosol and therefore in uracil-deficiency of these cells (Figure 19A, left panel). In contrast, impairment in any of these steps causes the accumulation of the reporter in the cytosol and therefore allows growth on uracil-free medium (Figure 19A, right panel). Besides others, *Hansen et al.* observed the deletion strain Δ*ubc8* being able to grow on medium without uracil, indicating increased precursor levels in the cytosol (Figure 19B, Figure S7A). Ubc8 is a cytosolic ubiquitin conjugase that is mainly known to be involved in the glucose-induced degradation of enzymes [103,107,131]. However, a connection of Ubc8 to mitochondrial protein import was unknown.

The reason why this specific component of the UPS is crucial for maintaining efficient protein import will be investigated in more detail in this study.

To verify the initial finding of the screen, I replicated the experiment for Δ*ubc8* using a plasmid-based version of the reporter construct. I performed growth curves in either uracil-rich or uracil-free medium to compare the growth of WT and Δ*ubc8* cells. The cells either expressed the Oxa1-Ura3 reporter or a version, which lacks the N-terminal presequence of Oxa1 (ΔN-Oxa1-Ura3). This truncated version is not imported and therefore served as a control for maximal growth on uracil-free medium. Cells transformed with an ev served as a negative control. As expected, the growth of all strains was similar in uracil-rich medium (Figure 20A, left panel). WT and Δ*ubc8* cells carrying an ev were not able to grow in uracil-free medium, which was expected since these cells lack the Ura3 protein. The expression of the truncated version of the reporter did not affect the growth behavior of Δ*ubc8* compared to the WT in this medium. In contrast, Δ*ubc8* expressing the full length Oxa1-Ura3 reporter exhibited an increased growth rate compared to the WT (Figure 20A, right panel), supporting the previous findings of the genetic screen. It seems like the loss of Ubc8 results in an accumulation of the Oxa1-Ura3 reporter in the cytosol.

To check if the deletion of Ubc8 also affects the cytosolic level of other precursor proteins, I expressed the well-studied model protein b2Δ-DHFR in WT and Δ*ubc8* cells and analyzed its stability via Western Blot. b2Δ-DHFR is a fusion protein consisting of the presequence of the *S. cerevisiae* cytochrome b2 (amino acids 1-167), that lacks its TMD, and DHFR. The protein was controlled by a galactose-inducible *GAL1* promotor, which allowed inducible protein synthesis. First, protein synthesis was induced by addition of galactose. By switching to galactose-free medium protein synthesis was stopped and samples were taken in consecutive time intervals. For both, WT and Δ*ubc8*, the precursor levels declined over time (Figure 20B, C). However, I observed that the decline in Δ*ubc8* was significantly slower compared to that in the WT cells. To transfer these findings to real, non-artificial precursor proteins, I analyzed the precursor level of the two mitochondrial proteins Mdj1 and Rip1 via Western Blot. For better detection of precursors, I treated the cells with carbonyl cyanide m-chlorophenylhydrazone (CCCP) for different time periods. CCCP depletes the membrane potential and thereby impairs protein import into the matrix of mitochondria. In this experiment, Δ*ubx2* served as a positive control since it has previously been shown that upon CCCP treatment the precursors of Rip1 and Mdj1 accumulate in this strain [93]. Like Δ*ubx2*, Δ*ubc8* also exhibited increased precursor levels for both Rip1 and Mdj1 (Figure 20D). However, it has to be mentioned that the precursors

levels, compared to the amount of the mature forms of the proteins, was rather low. To further analyze the CCCP sensitivity of the yeast cells, halo assays were performed. For this, WT and Δ*ubc8* cells were pre-cultured in galactose medium. Cells were harvested and spread on galactose-containing plates. A filter disk containing CCCP was placed to the center of the plate and after incubation at 30°C the areas with inhibited cell growth were measured. Filter disks with Dimethyl sulfoxide (DMSO) served as a control. I observed that Δ*ubc8* cells were hypersensitive to CCCP relative to the WT (Figure S7B). As a next step, I tested if the cytosolic accumulation of precursors induces the Rpn4-mediated stress response. To do so, I expressed a yellow fluorescent protein (YFP) being controlled by a proteasome-associate control element (PACE) in WT and Δ*ubc8* cells. It was previously shown that the accumulation of precursors in the cytosol can trigger a stress response mediated by binding of the transcription factor Rpn4 to PACE elements, which control the expression of specific genes [85]. However, I did not observe any changes in the YFP intensity for Δ*ubc8* compared to the WT (Figure 20E), showing that this stress response is not induced in the mutant cells. In conjunction with the previous detection of relatively low precursor levels in the Western blot, this result hints towards a rather mild precursor accumulation in Δ*ubc8* cells.

In conclusion, my results suggest a direct or indirect role of Ubc8 in mitochondrial precursor depletion from the cytosol. In the following step, I analyzed the mitochondria-related effects of an Ubc8 deletion more comprehensively using mass spectrometry.

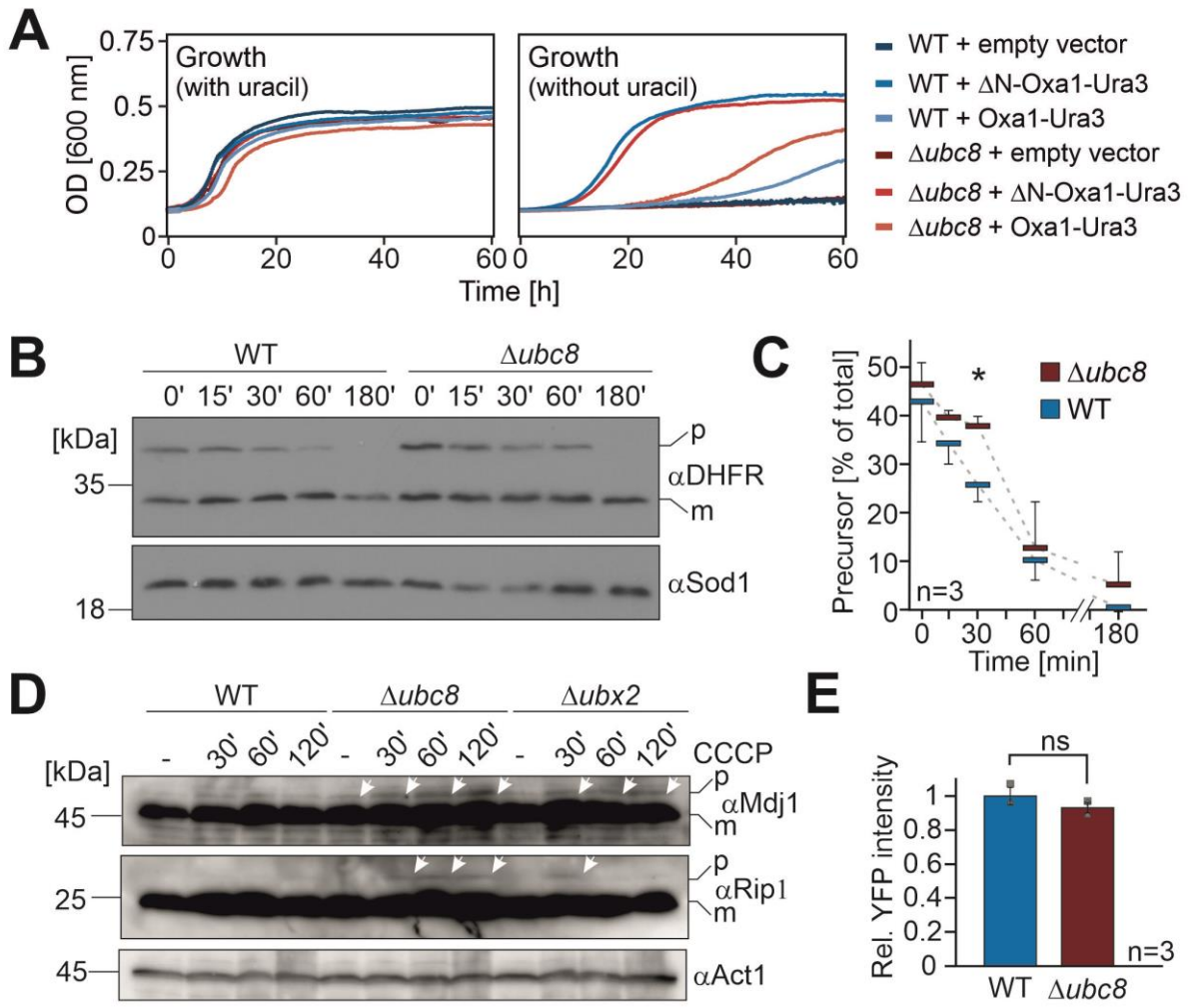

Figure 20: Precursor proteins accumulate in the cytosol of Δ*ubc8* cells. (A) Wild-type (WT) and Δ*ubc8* cells expressing a plasmid-based version of the Oxa1-Ura3 reporter, a truncated version lacking the presequence of Oxa1 (ΔN-Oxa1-Ura3) or an empty vector as control were grown in medium either with or without uracil. OD_{600} was continuously measured for 60 hours. The mean values of three technical replicates are shown. **(B)** WT and Δ*ubc8* cells carrying a galactose-inducible b_2Δ-DHFR expression plasmid were first grown in galactose medium to induce expression of b2Δ-DHFR and then shifted to galactose-free medium to stop its synthesis. Cells were harvested after the times indicated, lysed and analyzed via Western Blot. The precursor (p) and mature (m) forms of b2Δ-DHFR are indicated. **(C)** Quantification of the amount of b2Δ-DHFR precursor shown in B. The mean values and standard deviations of three biological replicates (n=3) are displayed. Statistical differences were calculated with a student's t-test and significance was assigned as follows: p-value < 0.1 = *. **(D)** Cells of the designated strains were grown in galactose medium and treated with 40 µM CCCP for the times indicated. Cells were harvested, lysed and analyzed via Western blot. Precursor (p) and mature (m) forms of Mdj1 and Rip1 are marked. **(E)** The Rpn4-mediated stress response was analyzed in the indicated strains using a plasmid that allows stress-induced expression of YFP that is under control of a PACE element **[85]**. The mean values of three biological replicates (n=3) are shown. Significance testing was performed using a student's t-test (ns = not significant). Modified from [112].

3.5. Ubc8 is involved in the catabolite degradation and maintains mitochondrial protein levels

Since Ubc8 is known to be involved in the glucose-induced degradation of enzymes, I analyzed the proteomes of WT and Δ*ubc8* from cultures either continuously grown in lactate medium or from cultures which were subjected to a switch from lactate to lactate + glucose medium. This

medium shift leads to glucose-induced protein degradation. To be able to distinguish between "old" proteins being synthesized prior to the medium switch and newly synthesized proteins, being expressed after the medium shift, I used a switch of media in a dynamic stable isotope labeling by amino acids in cell culture (SILAC) approach (Figure 21A). For this, I cultivated the cells in lactate medium containing "light" amino acids ([$^{14}N_2$, $^{12}C_6$]-lysine and [$^{14}N_4$, $^{12}C_6$]-arginine). I harvested these cells and prepared them for mass spectrometric analysis. The mass spectrometric measurement and the statistical analysis was performed by Markus Räschle. Comparison of the proteomes of lactate grown WT and Δ*ubc8* cells allows to investigate the extent to which the deletion of Ubc8 affects the proteome under physiological, respiratory conditions (we named this "Ubc8 effect"). The rest of the cultures were shifted to "heavy" medium ([$^{15}N_2$, $^{13}C_6$]-lysine and [$^{15}N_4$, $^{13}C_6$]-arginine) containing either lactate or lactate + 2% glucose. The cells were harvested after one doubling time and prepared for mass spectrometry. The comparison of the proteomes of the same strain before and after the glucose shift allows the investigation of the glucose-induced proteome changes, which we called "catabolite effect". Principal component analysis revealed that, firstly, the deletion of Ubc8 already caused major changes in the proteome of respiring cells compared to the WT ("Ubc8 effect") (Figure 21B). Secondly, the shift to glucose-containing medium caused drastic changes in the proteomes of both strains ("catabolite effect"). However, these changes are similar in WT and Δ*ubc8* cells. The analysis of the glucose-induced proteome changes in WT and Δ*ubc8* showed that the abundance of the four well-studied gluconeogenic enzymes Fbp1, Mdh2, Icl1 and Pck1 are strongly reduced in WT but remain unchanged in Δ*ubc8* (Figure 21C). This indicates that Ubc8 is a major player in the glucose-induced degradation of these proteins, which is consistent with previous findings [103,107]. Furthermore, we discovered a striking effect on mitochondrial protein levels in the Ubc8 deletion strain compared to the WT. Although the WT also showed reduced abundance of many mitochondrial proteins, this effect was even more pronounced in Δ*ubc8*.

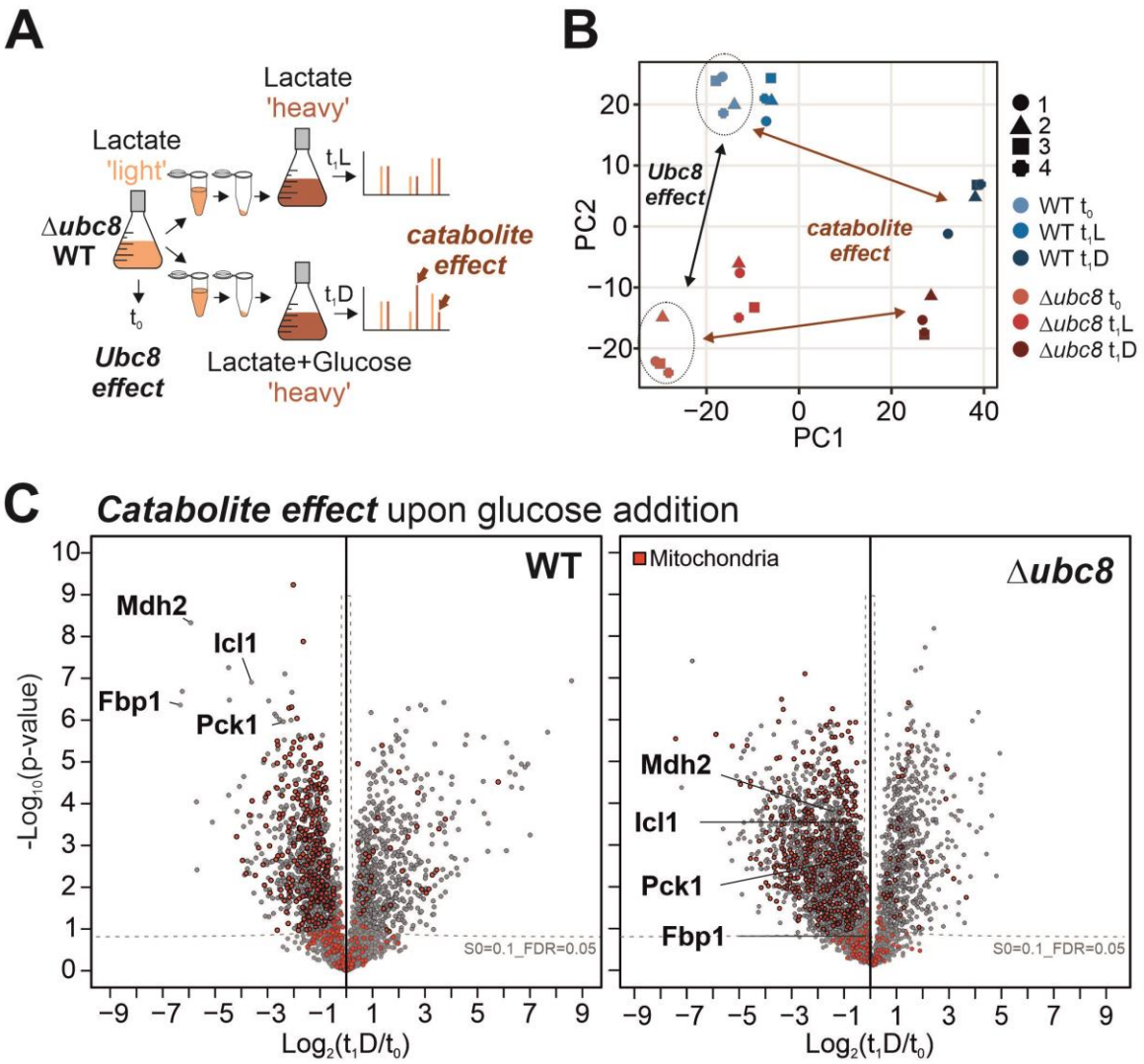

Figure 21: Mitochondrial protein levels are reduced in Δ*ubc8*. (A) Scheme of the SILAC-based proteomics workflow. Indicated strains were either continuously grown in "light" lactate medium or shifted to "heavy" lactate or "heavy" glucose medium for one doubling time. Cells were harvested and analyzed by mass spectrometry. **(B)** Principal component analysis of all samples after normalization. **(C)** Volcano plots showing the proteome comparisons of WT (left panel) and Δ*ubc8* cells (right panel) after switching from lactate to glucose medium. Data points of the gluconeogenic enzymes, that get degraded in an Ubc8-dependent manner, are labeled. Mitochondrial proteins are highlighted in red [2]. Modified from [112].

This reduction on mitochondrial protein level became even clearer after hierarchical clustering of the proteomics data (Figure 22A). In this clustering, all measured proteins were sorted into five groups (group 1,2, 3, 4a and 4b) based on their abundance in the different media in WT and Δ*ubc8*, respectively. In addition to proteins which were reduced or increased in the mutant strain (group 1 and 3, respectively), we also identified a cluster containing proteins with generally elevated protein abundances in glucose medium (group 2). Furthermore, we found one cluster enclosing all glucose-repressed proteins, meaning that they were less abundant after the metabolic shift (group 4). About half of these proteins showed higher abundances in Δ*ubc8* (group 4a), whereas the remaining ones were less abundant in the mutant strain (group 4b). As expected, the gluconeogenic enzymes clustered in group 4a, meaning they are more abundant

in Δ*ubc8* since they do not get degraded. Interestingly, group 4b was characterized by an enrichment of mitochondrial proteins of the IM, the OM, the matrix and the IMS, and in addition also of peroxisomal proteins (Figure 22B). This indicates that especially mitochondrial proteins are negatively affected by the loss of Ubc8.

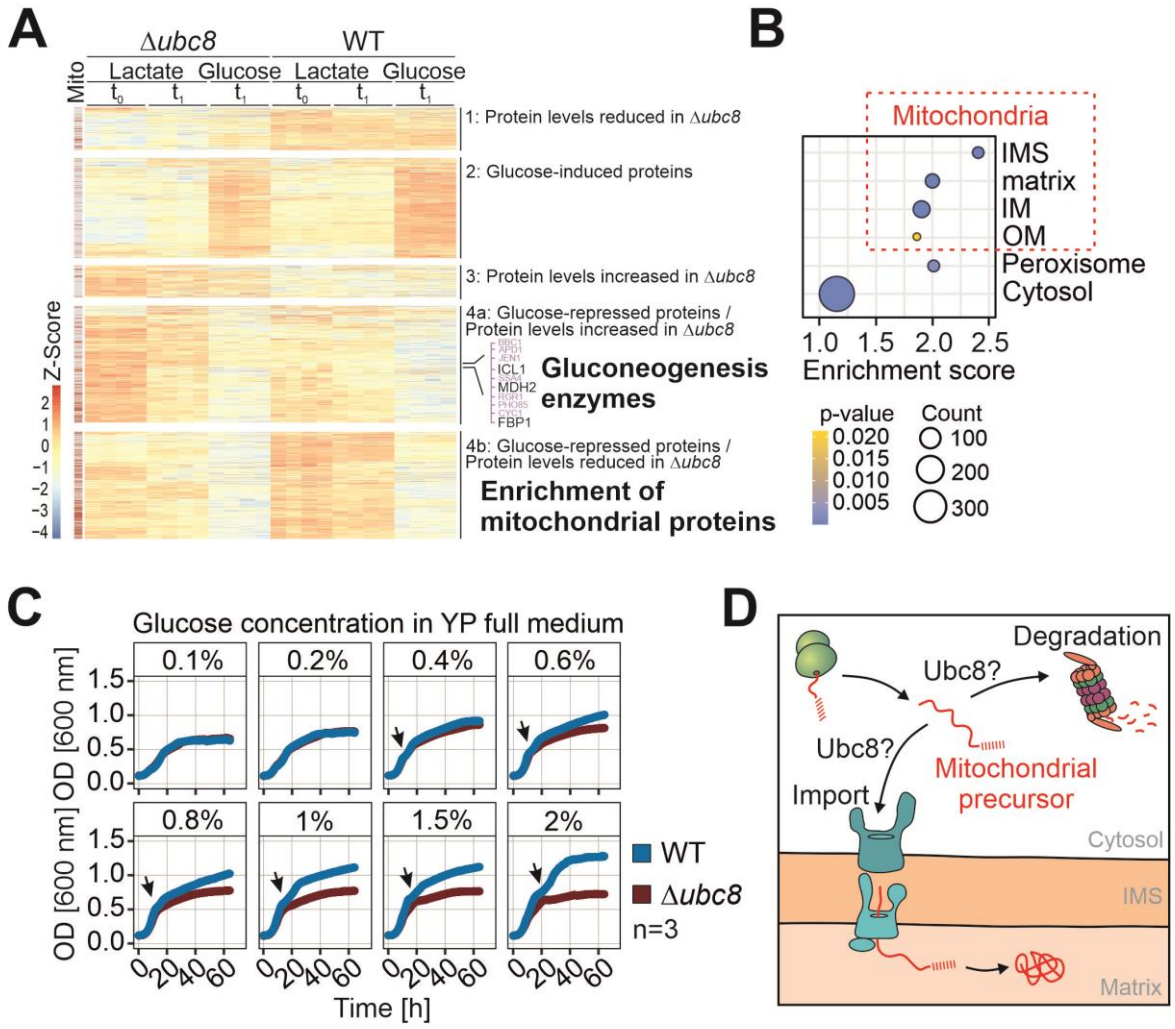

Figure 22: Ubc8 is important for the metabolic remodeling of yeast cells. (A) Hierarchical clustering of the data gained in the SILAC-based proteomics experiment. Five distinct groups were identified based on the protein abundance in the indicated media and strains. Mitochondrial proteins are highlighted in red on the left. **(B)** Enrichment scores for proteins of group 4b. **(C)** Respective strains were pre-cultured in glycerol medium. Subsequent growth in glycerol medium containing the indicated glucose concentrations was analyzed by measuring the OD_{600} over time. The mean values of three technical replicates are shown. The diauxic shift is marked by arrows. **(D)** Schematic illustration of Ubc8 playing a role in mitochondrial precursor biogenesis. Modified from [112].

In conjunction with these findings, I wondered if Δ*ubc8* cells show any limitations in mitochondrial fitness. To test this, I cultivated WT and Δ*ubc8* cells in glycerol medium (respiratory conditions) and analyzed their growth behavior after dilution of the cells in glycerol medium with varying glucose concentrations (0.1 to 2%) (Figure 22C). When grown in these media, cells initially use fermentation for energy production and then switch back to respiration

once the glucose is depleted. This switch is called “diauxic shift” and is characterized by a temporary slowdown of growth during the metabolic remodeling. Interestingly, I observed that cells lacking Ubc8 exhibited reduced growth once they reached the diauxic shift compared to the WT (Figure 22C). This suggests problems in the metabolic remodeling of the cells, possibly related to the upregulation of mitochondria, a crucial process during the transition from fermentation to respiration.

In total, these findings indicate that Ubc8 plays an important role in the biogenesis or stability of many mitochondrial proteins. In the same context, Ubc8 seems to be relevant for the rapid adaptation when cells are shifted from fermentative to respiratory growth conditions. In addition, the initial findings of the Oxa1-Ura3 screen [86] were further substantiated by my results. Next, I elucidated which step of precursor biogenesis, either targeting, import or degradation, is impaired upon deletion of Ubc8 (Figure 22D).

3.6. Ubc8 is crucial for efficient TOM complex assembly

Since the well-established *in vitro* import assay represents a straightforward method to analyze import defects, I decided to first check whether the deletion of Ubc8 affects protein import into mitochondria using this method. In my experiments, I used isolated mitochondria from WT and Δ*ubc8* cells which were grown in galactose medium. I incubated them with radiolabeled Oxa1 and Pet9 precursors for 2 and 5 minutes before adding PK. Oxa1 is an inner membrane protein using the TOM-TIM23 import route whereas Pet9 is a carrier being imported via the TOM-TIM22 pathway. Surprisingly, the import efficiencies of both, Oxa1 and Pet9, were strongly reduced in Δ*ubc8* mitochondria compared to the WT (Figure 23). This implies that the previously observed precursor accumulation in the cytosol results from import deficits into mitochondria that are caused by the loss of Ubc8. Since Oxa1 and Pet9 both use the TOM complex during their import process, this leads to the suggestion that either the biogenesis or the stability of this complex is affected.

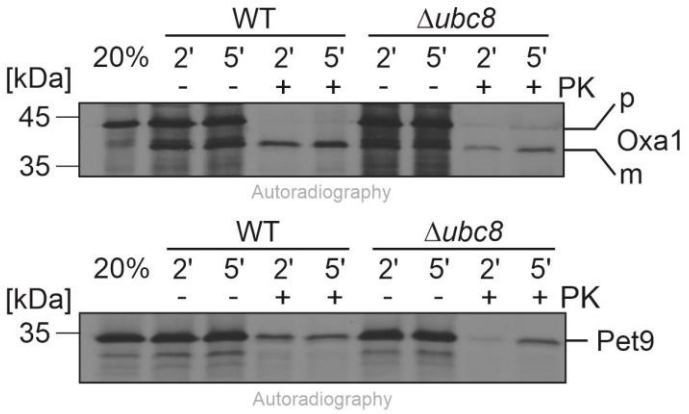

Figure 23: Protein import into isolated mitochondria is less efficient in Δ*ubc8*. Radiolabeled Oxa1 and Pet9 were incubated with mitochondria isolated from the indicated strains grown in galactose medium at 30°C. After 2 and 5 minutes, the import reactions were stopped, and the samples were treated with or without Proteinase K (PK). Proteins were analyzed via Autoradiography. Precursor (p) and mature (m) forms of Oxa1 are indicated. B is adopted from [112].

To further investigate the cause of the import defect, I analyzed the level of the components of the import machinery in whole cells by label-free mass spectrometry. To this end, I cultivated WT and Δ*ubc8* cells either solely in glycerol medium or shifted them to glucose medium for 4 hours. Samples were taken and analyzed by mass spectrometry. The mass spectrometric measurement was performed by Markus Räschle. Focusing on the components of the import machinery, the TOM receptor Tom22 was the protein whose abundance was mostly reduced in Δ*ubc8* compared to the WT, at least in the glucose shifted cells (Figure 24A). Also, in the continuously grown cells, Tom22 showed reduced protein levels in the mutant strain, however less pronounced (Figure S8). To confirm this finding, I prepared whole cell lysates of WT and Δ*ubc8* cells, that were shifted from glycerol to glucose medium for 4 hours and compared the Tom22 protein levels via Western blot. This way, I was able to confirm the decreased abundance of Tom22 in the deletion strain (Figure 24B, C). In collaboration with Fabian den Brave and Thomas Becker (University of Bonn), we next analyzed the Tom22 protein levels in isolated mitochondria. The corresponding data shown in Figure 24D and E were obtained by the collaboration partners from Bonn. They grew WT and Δ*ubc8* cells in glycerol medium, added glucose for 4 hours, isolated mitochondria and subsequently analyzed protein levels via Western blot. The results showed that in isolated mitochondria the protein levels Tom22 were also strongly reduced in the Ubc8 deletion strain (Figure 24D). In contrast, the levels of the pore-forming TOM component Tom40, as well as another TOM receptor Tom70, were unaffected. This result implies that the overall reduction of Tom22 is caused by diminished Tom22 levels in mitochondria.

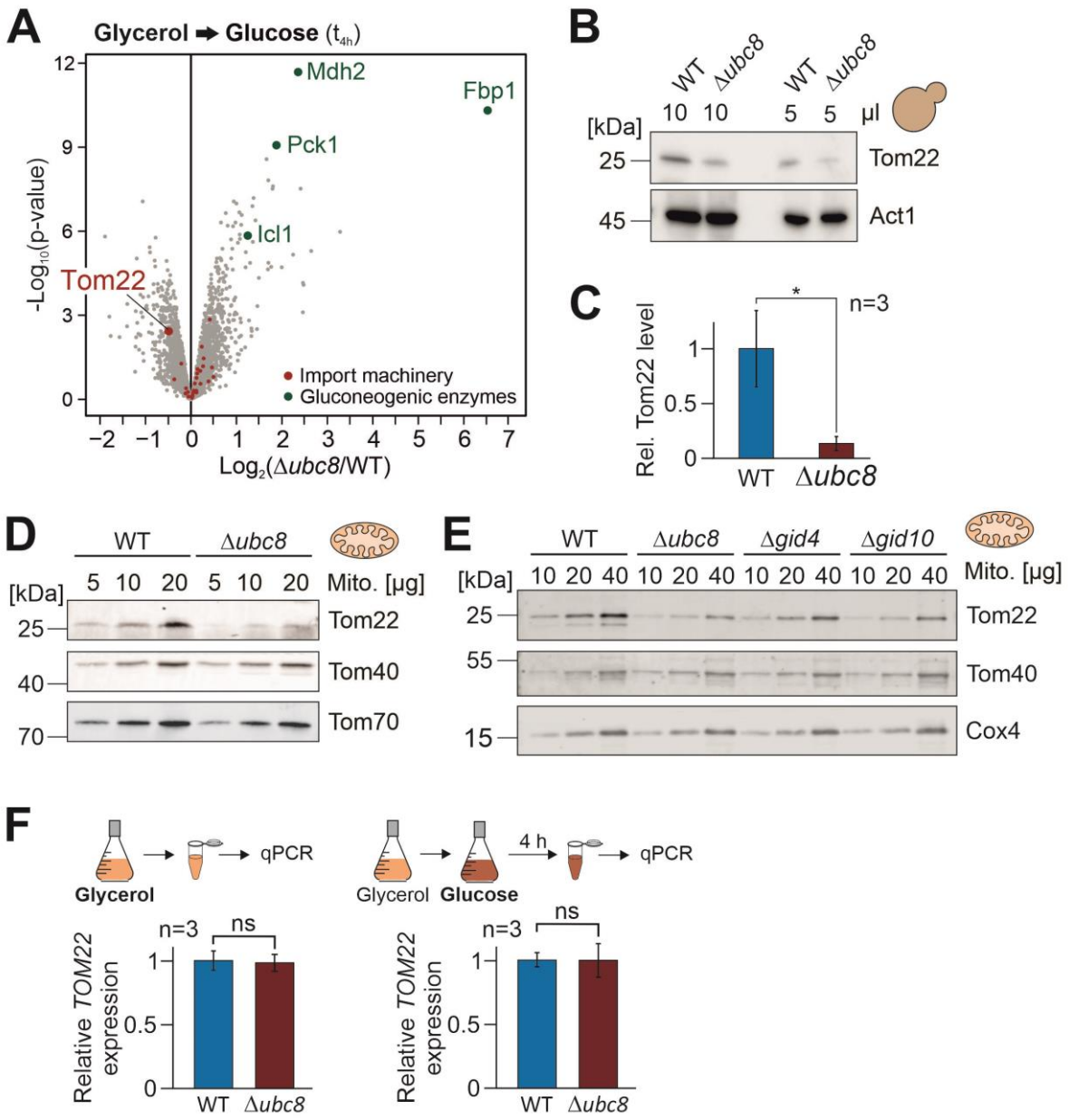

Figure 24: Deletion of Ubc8 or other components of the GID-complex results in reduced Tom22 protein levels. (A) Volcano plot showing the proteome comparison of Δ*ubc8* and WT cells. Cells were grown in glycerol medium and shifted to glucose medium for 4 h. Data points of gluconeogenic enzymes are labeled in green and components of the import machinery are highlighted in red. **(B)** Cells of the designated strains were grown in glycerol medium and shifted to glucose medium for 4 h. Cells were harvested, lysed and analyzed via Western blot. **(C)** Quantification of the Tom22 protein levels shown in B. The mean values and standard deviations of three biological replicates (n=3) are displayed. Statistical differences were calculated with a student's t-test and significance was assigned as follows: p-value < 0.1 = *. **(D, E)** Cells of the designated strains were grown in glycerol medium and shifted to glucose medium for 4 hours. Mitochondria were isolated and analyzed via Western blot. Experiments were performed by Fabian den Brave and Thomas Becker (University of Bonn). **(F)** Tom22 mRNA levels were analyzed by qRT-PCR. Indicated strains were either solely grown in glycerol medium (left panel) or shifted to glucose medium for 4 hours (right panel). The mean values and standard deviations of three biological replicates (n=3) are displayed. Statistical differences were calculated with a student's t-test (ns = not significant). Modified from [112].

It is known that during the glucose-induced degradation of enzymes Ubc8 works in conjunction with the GID-complex as a E3 ligase [104]. The two subunits Gid4 and Gid10 both serve as substrate binding proteins of the GID-complex [106,107]. We wondered if impairment of the

GID-complex also leads to reduced Tom22 levels in mitochondria. To answer this question, we included Δ*gid4* and Δ*gid10* into our analysis. Together with the WT and Δ*ubc8*, we analyzed the Tom22 protein levels in isolated mitochondria from these strains. Similar to the observed decline of Tom22 in Δ*ubc8*, we also found diminished Tom22 levels in Δ*gid4* and Δ*gid10* mitochondria (Figure 24E). The protein levels of Tom40, as well as the cytosolic control Cox4, remained unchanged in all mutant strains.

To exclude that the reduced Tom22 protein levels are caused by transcriptional changes, I compared the mRNA levels of Tom22 in WT and Δ*ubc8* cells using qRT-PCR. For this, either cells of continuously grown glycerol cultures or cells of cultures shifted to glucose medium for 4 hours were analyzed. Under both growth conditions, Tom22 mRNA levels were not altered upon deletion of Ubc8 (Figure 12F).

In summary, with these findings we were able to provide first explanations as to why the import efficiency in Δ*ubc8* cells is reduced. Although Ubc8 does not influence the expression ofTom22, it has a direct or indirect effect on the Tom22 protein levels in mitochondria.

Since Tom22 is a major component of the TOM complex, we tested if the reduced Tom22 levels affect the abundance or stability of the TOM complex. We also analyzed which step of Tom22 biogenesis is impaired in Δ*ubc8* cells. The data shown in Figure 25A-D were obtained by Fabian den Brave and Thomas Becker (University of Bonn).

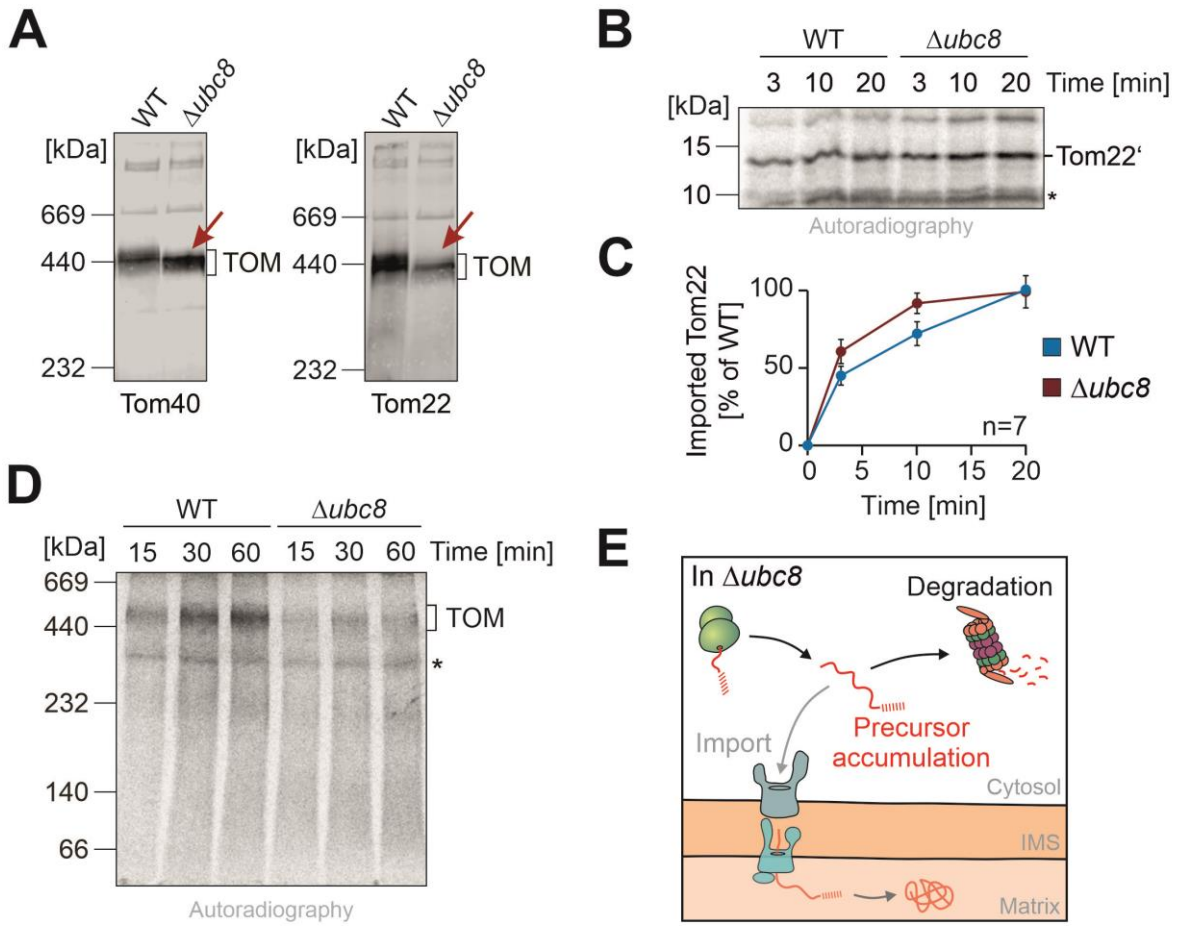

Figure 25: Ubc8 is required for complete TOM complex assembly. (A) Cells of the designated strains were grown in glycerol medium, and glucose was added for 4 hours. Mitochondria were isolated and analyzed via BN-PAGE. The trimeric TOM complex is marked with arrows **(B)** Radiolabeled Tom22 was incubated with mitochondria isolated from the indicated strains grown as described for A. After 3, 10 and 20 minutes, the import reactions were stopped, and all samples were treated with PK. Proteins were analyzed via Autoradiography. The protease-protected fragment of Tom22, that is inserted into the membrane (Tom22'), is indicated. Unspecific bands are marked with an asterisk (*). **(C)** Quantification of the Tom22' levels shown in B. The mean values and standard deviations of seven biological replicates (n=7) are shown. The signal for the WT strain after 20 min of import was set to 100%. **(D)** Radiolabeled Tom22 was incubated with mitochondria isolated from the indicated strains grown as described for A. After 15, 30 and 60 min the import reactions were stopped, and the samples were subjected to BN-PAGE and analyzed via Autoradiography. Size of the TOM complex is indicated as well as unspecific bands (*). **(E)** Schematic illustration showing that the deletion of Ubc8 impairs the import of precursor proteins. All the results shown in this figure were obtained by Fabian den Brave and Thomas Becker (University of Bonn). Modified from [112].

To answer the question regarding the effect on the TOM complex, we analyzed the size and abundance of the TOM complex via blue native polyacrylamide gel electrophoresis (BN-PAGE). BN-PAGE is a well-established method to study protein complexes and was performed as described by *Priesnitz et al.* [132]. For this, we isolated mitochondria from WT and Δ*ubc8* cells grown in glycerol medium with glucose addition for 4 hours and subjected them to BN-PAGE. When using a Tom40-specific antibody for detection, the abundance of the TOM complex was not changed in Δ*ubc8* compared to the WT (Figure 25A). However, we found that the TOM complex was slightly smaller when Ubc8 is deleted. This was also observed when a

Tom22-specific antibody was used for detection. This hints towards an incomplete assembly of the TOM complex. Consistent with our previous results, our data again revealed reduced Tom22 levels in the TOM complex of Δ*ubc8* cells. To test, if deletion of Ubc8 impairs the import of Tom22 itself, and thereby causes the reduced protein levels, we performed an adapted *in vitro* import assay. For this, we used a radiolabeled Tom22 variant containing three additional methionine residues to improve detection of a characteristic PK-resistant and membrane-inserted Tom22 fragment (Tom22') [133]. A detailed description about the Tom22 import assay can be found in my publication [112]. Mitochondria were isolated from WT and Δ*ubc8* cells which were grown in glycerol medium and shifted to glucose medium for 4 hours. Radiolabeled Tom22 was imported for up to 20 minutes and all samples were treated with PK. We found Tom22 to be imported with the same efficiency into Δ*ubc8* as into WT mitochondria (Figure 25B, C). To assess the amount of Tom22 being assembled into the TOM complex after import, we performed an *in vitro* import assay using the same Tom22 variant as described before, but in addition monitored its assembly into the TOM complex via BN-PAGE. This experiment revealed that the amount of newly imported Tom22 being incorporated into the TOM complex is strongly diminished in the Ubc8 deletion strain (Figure 25D).

In summary, I demonstrated in this study that TOMM34, a cytosolic co-chaperone, and Ubc8, a specific component of the UPS both play crucial roles in modulating protein import into mitochondria. On the one hand TOMM34 binds to selected presequences and thereby determines the preferred import pathway. On the other hand, Ubc8 is involved in enabling efficient assembly of the receptor Tom22 into a fully functional TOM complex.

4. DISCUSSION AND FUTURE PERSPECTIVES

The previous chapters have highlighted the rather complex journey of mitochondrial precursor proteins. This journey comprises many intermediate steps, including the interaction with cytosolic binding partners for proper targeting to the mitochondrial surface and the interaction with the import receptors allowing translocation across the mitochondrial membranes. To enable a smooth and efficient sequence of all steps, mitochondria closely collaborate with the cytosolic chaperone network and the UPS. This thesis aimed to elucidate different ways to modulate protein import into mitochondria. In this regard, I identified two mechanisms how cells modulate import efficiencies. First, the co-chaperone TOMM34 seems to selectively promote highly efficient import of some matrix-destined proteins by determining the preferred import route. Second, the UPS component Ubc8 enables efficient assembly of the main entry gate into mitochondria, the TOM complex. In the following, the relevance of these two surveilling mechanisms will be discussed. On the one hand, I will point out the reason why TOMM34 represents a suitable candidate to modulate mitochondrial import. On the other hand, I will demonstrate mechanisms of how Ubc8 might interfere with the assembly of the TOM complex. In addition, I will present perspectives for future research.

4.1. Presequences are not all the same

The common task of presequences comprises the targeting of precursor proteins from the cytosol to mitochondria. N-terminal targeting sequences directing precursor proteins to mitochondria were discovered already in the 1980s [18,110]. Investigations using artificially constructed presequences revealed that even very simple presequences only consisting of arginine, serine and leucine residues are sufficient for Cox4 import [134]. This suggests that targeting by presequences is most likely not only dependent on complicated amino acid sequences. However, secondary structures like amphipathic α-helices tend to be more critical for the recognition by the import receptors. Until today, hundreds of N-terminal targeting sequences have been identified in various organisms, including human [135], mouse [11] and yeast [10]. The published lists of presequences demonstrate the enormous versatility of N-terminal targeting sequences. Considering the fact of rather simple presequences being sufficient for import, the relevance of the huge diversity of presequences remains elusive. To address this aspect, I generated a test set of nine precursor proteins, all containing an N-terminal presequence of yeast, fused to DHFR (Figure 9). The selected presequences differed in their respective lengths ranging from 17 to 80 amino acid residues. Interestingly, the presequences

facilitated import of DHFR with strongly varying efficiencies *in vitro* and in *vivo* (Figure 10A, B, Figure 13C, D). This is consistent with recent findings reporting high variations in the protein import kinetics of numerous precursor proteins [136–138].

We initially assumed "stronger" presequences, as opposed to "weaker" ones, being able to maintain efficient import under competitive import conditions. This hypothesis about a "prioritized import" regarding a greater competitiveness of some proteins would have provided an explanation for the great versatility of presequences. However, adding increasing amounts of purified Su9-DHFR as a competitor to the *in vitro* import reactions of the test set precursors did not result in a clear reduction of the import efficiencies of only specific precursors. Instead, it affected all tested precursors to similar degrees (data not shown). Therefore, the initial hypothesis could not be confirmed, at least not for this competitor. Likewise, the efficiencies of all presequences were affected to a similar degree by depletion of either the membrane potential or ATP levels in Δ*cox18* or Δ*atp6* mitochondria (Figure 10E, F, Figure S2). This indicates that "stronger" presequences are not advantageous even under conditions of impaired energization of the import process. This is consistent with the findings of a previous *in vivo* study reporting about CCCP treatment causing an overall effect on mitochondrial protein import rather than affecting a specific subset of proteins [136].

Hitherto, only very few systematic analyses on targeting sequences were conducted. Due to the great diversity of presequences we wondered whether they share similarities in their amino acid sequences and can therefore be classified into distinct subgroups. In collaboration with Felix Jung and Timo Mühlhaus (Computational Systems Biology, University of Kaiserslautern), we used an unbiased machine learning approach for a solely sequence-based analysis of previously identified presequences of yeast (for details see [111]). The analysis of only the presequences that were included in this study's test set but also that of all yeast presequences identified by *Vögtle et al*. [10], revealed the formation of distinct groups (Figure 26A, B). Interestingly, the analysis of the test set presequences demonstrated that the "strong" and "weak" presequences, as defined previously by the *in vitro* and *in vivo* experiments, clustered accordingly. This suggests that the amino acid sequences of presequences contain information determining the import efficiency of the precursors. The identification of seven separate groups among all yeast presequences in addition substantiates the hypothesis that "presequences are not all the same". Correlating these groups with different properties revealed a group-specific length distribution of the presequences (data not shown, see [111]). In how far the presequence length and the

possible information about the import efficiency might be connected will be discussed in the section 4.2.

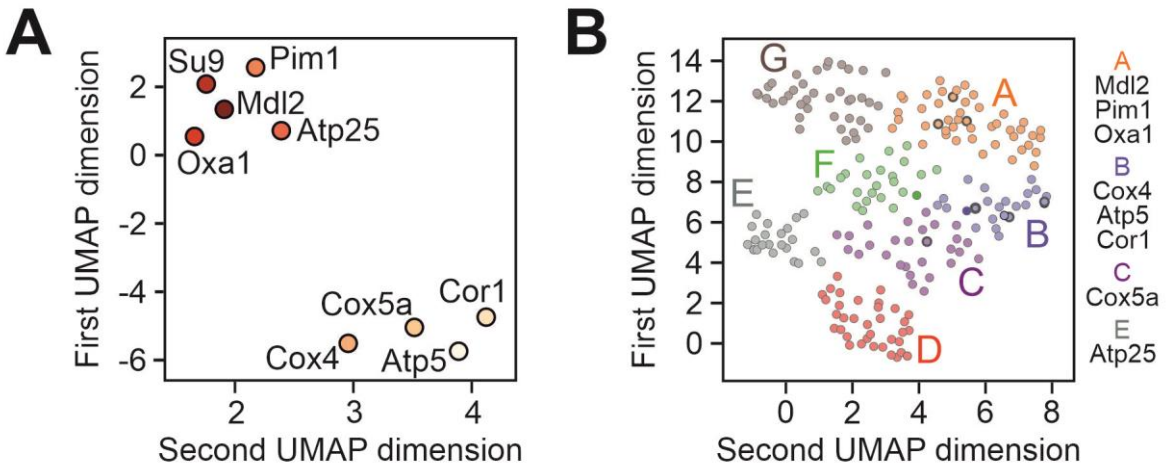

Figure 26: Presequences can be classified based on their amino acid sequences. (A) Physiochemical embedding of the presequences included in this study's test set for the import experiments. The embedding is solely based on the sequence information transformed by language model features representing physiochemical properties, **(B)** Spectral clustering of the physiochemical embedding of all presequences from the *S. cerevisiae* dataset obtained from [10] and extended by Oxa1. This figure and the legend are adopted from my publication [111]. A detailed description about the methodological procedure can be found in the Materials and Methods section of my unpublished manuscript [111] in the paragraph entitled "Bioinformatic analysis of mitochondrial presequences". This analysis was performed by Felix Jung and Timo Mühlhaus (Computational Systems Biology, RPTU Kaiserslautern-Landau).

The identification of sequence-based specificities among presequences appears to be relevant for all eukaryotes, as the inclusion of sequences from animals, plants and other fungi has demonstrated the preservation of the identified groups (data not shown, see [111]). However, a previous comparative study of mouse, human and yeast presequences claimed poor conservation of mouse presequences on the level of amino acid sequences [11]. This suggests that the features responsible for the clustering have been more conserved during evolution than the overall sequences of presequences, at least for mice. Although, it should be mentioned that the clustering of the presequences depends on the settings selected during the analysis, it became clear that in eukaryotes the amino acid sequence of presequences exhibits specific properties which allows presequences to differ from each other. Furthermore, it seems as if these features are relevant to determine the import behavior of the proteins.

Several outcomes have already been reported for precursors containing presequences with different properties. For example, the presequence length impacts the speed of the precursor unfolding on the mitochondrial surface and therefore modulates also the speed of the import process. It seems as if precursors with short presequences rely on spontaneous unfolding whereas long presequences improve import by interacting with the mitochondrial Hsp70 [120]. Furthermore, a sequence analysis revealed that some presequences possess hydrophobic amino

acids at position 2 which enables acetylation of these precursors by a specific acetyltransferase [139]. It is postulated that in conjunction with specific arrangements of downstream arginine residues this promotes protein import via binding to Tom20 and the OM. However, 30-40% of presequences from *S. cerevisiae* lack the hydrophobic residue at position 2. This further demonstrates that specific differences in the amino acid sequence of presequences can modulate the import process. Furthermore, Tom70-dependent import has been reported for some presequence-containing proteins, whereas most of them are imported via Tom20. This indicates that presequences are able to modulate protein import by determining the import route [137].

In summary, it became clear that the presequences are not all the same in terms of the characteristics of their amino acid sequence. A sequence-based analysis revealed groups of presequences that share similar features which seem to influence the import efficiency. However, the group-specific features in the amino acid sequences still need to be determined in the future. In line with the question of why presequences are not identical, the next section discusses a newly identified mechanism that makes it possible to modulate import efficiency at the presequence level.

4.2. Cytosolic co-chaperones might be relevant for the efficient import of some but not all presequence-containing proteins

Many precursor proteins contain hydrophobic stretches within their sequence which increase the potential of premature folding or the formation of cytosolic aggregates. Therefore, cells face the vital challenge of keeping all precursor proteins in a soluble and import-competent state to ensure proper import. In this regard, several cytosolic proteins which sustain cytosolic proteostasis also play crucial roles in the surveillance of precursor proteins. Chaperones of the Hsp70 and Hsp90 superfamilies and other factors, including the nascent-polypeptide-associated complex (NAC), the ribosome-associated complex (RAC) and the mitochondrial import stimulation factor (MSF), assist the cytosolic precursors and promote their targeting and import [8,140–142]. The importance of chaperones for protein import has been discovered long time ago [8,49,50]. Hsp70s and Hsp90s support the precursors throughout their whole journey in the cytosol. They bind to the nascent chain as soon as it emerges from the ribosomal exit tunnel [143], provide guidance through the cytosol and promote binding to the mitochondrial import receptors [121]. A previous study reports about the chaperones being part of a multi-chaperone complex which interacts with precursor proteins in mammalian cells [68]. Immunoprecipitation experiments revealed that this multi-chaperone complex comprises Hsp70, Hsp90 and the co-

chaperones TOMM34, HOP (Hsp70-Hsp90 organizing protein)/p60 and CDC37/p50. TOMM34 and HOP contain TPR domains which are employed by numerous proteins to interact with Hsp70s and Hsp90s ([144,145]). Initially, TOMM34 was discovered as a component of the mitochondrial import machinery in mammals [146]. TOMM34 has been shown to be distributed between the cytosol and the mitochondrial OM. However, in contrast to initial assumptions, fractionation experiments revealed that TOMM34 is more abundant in the cytosol than at the OM [147,148]. This suggests that TOMM34 plays a more important role during the early steps of precursor biogenesis. Interestingly, I observed a selective interaction of TOMM34 with the "strong" presequence of Oxa1, but not with the "weak" presequence of Atp5 in immunoprecipitation experiments using reticulocyte lysate of rabbits (Figure 17A). In contrast, HSP70 was binding to all tested presequences (Figure 16C, Figure S5). Besides HSP70 and TOMM34, none of the other components of the multi-chaperone complex mentioned above were identified in this experiment. This hints towards a rather transient or weak interaction between the chaperones and co-chaperones or towards TOMM34 being able to function in a CDC37- and HOP-independent manner. The binding of TOMM34 to precursors and its role in protein import was reported before, however the substrate spectrum was not identified with certainty. A study by Faou and co-workers suggests that TOMM34 is important for the import of matrix proteins and that its function may not be restricted to the Tom70-mediated import of IM proteins [68]. In contrast, another study claims that TOMM34 does not bind to presequences at all, but it exclusively binds to the mature part of some precursor proteins [149]. The discrepancies in the current literature might be explained by my finding on the binding of TOMM34 to only a subset of presequence-containing proteins.

Although, this raises the question of how this selective interaction is mediated. One possible answer might be the presence of specific motifs in the appropriate presequences, which enable selective recruitment of TOMM34. Since TOMM34 contains specialized TPR domains to recognize the short EEVD motifs of Hsp70/90 proteins [144], it is likely that the co-chaperone is also able to recognize further motifs of other protein families. In this regard, an unbiased motif search via machine learning could be useful to identify novel motifs in presequences which enable co-chaperone binding. As discussed in the previous section, machine learning was already used classify presequences based on their amino acid sequence. The data revealed that the long and "strong" presequences of my test set clustered in one group (Figure 26A). Combining this observation with the idea of TOMM34 recognizing specific motifs leads to the hypothesis that long presequences, in addition to their targeting information, might contain another segment comprising the appropriate binding motif for specific co-chaperone binding.

In case such a motif will be determined in the future, *in vitro* import experiments and IQ-Compete could be performed to test the efficiency of the Oxa1 presequence, that either contains a mutated version of this motif or lacks this motif completely. If the identified motif proves to be crucial for the enhanced import efficiency of the Oxa1 presequence due to TOMM34 binding, lower import efficiencies of the modified presequences would be expected, analogous to my observations upon precursor denaturation or preincubation (Figure 14A-D). Notably, the predicted TargetP 1.0 scores of most of the test set presequences were similar to each other (Figure 9). This indicates that the predicted scores are unlikely to provide information on improved TOMM34-mediated import efficiency. Nevertheless, it should be mentioned that the TargetP score of Oxa1 (0.966) was higher than that of Atp5 (0.826). It is therefore not certain that TargetP completely excludes possible motives from its calculations.

As mentioned before, the recruitment of TOMM34 to the presequence of Oxa1 massively enhances its import efficiency. Although the mechanistic details remain elusive, there are several possibilities regarding the extent to which TOMM34 might promote protein import. The corresponding binding partner of TOMM34 on the mitochondrial surface has not been identified with certainty. However, I observed that the import efficiency of the Oxa1 presequence was reduced when imported into mitochondria isolated from Δ*tom70*Δ*tom71* cells (Figure 15A, B). This indicates that TOMM34 might directly interact with the receptors Tom70/71 and therefore improves targeting of the bound precursor to the TOM complex. Alternatively, TOMM34 could exhibit regulatory functions by modulating the chaperone activities of the Hsp70 and Hsp90 proteins being bound to a precursor protein. As a result, TOMM34 might be beneficial for protein import by improving precursor unfolding or by increasing the ability of chaperones to maintain the precursors in an import-competent state. Whether TOMM34 therefore preferentially or exclusively binds to presequences of hydrophobic proteins, is not clear so far. Lastly, it might be possible that TOMM34 enhances protein import of Oxa1-DHFR by enabling Tom70-dependent import in addition to TOMM34-independent import via Tom20. In this regard, a recent study claims that substrates of Tom20 and Tom70 can be imported simultaneously through the different Tom40 pores of one TOM complex [150]. Therefore, Oxa1-DHFR might be imported at the same time via two different import pathways. In contrast, Atp5-DHFR, which does not interact with TOMM34, might only be imported in a Tom20-mediated fashion, and therefore import might be less efficient. Interestingly, TOMM34 is a mammalian protein which is not found in fungi. Nonetheless, the results obtained by the newly established IQ-Compete assay reliably showed that the import efficiencies of the tested presequences also varied considerably in living yeast cells (Figure

13B-D). Comparison of the gained *in vitro* and *in vivo* results demonstrated a good correlation between the findings (Figure 13E), indicating that the different "strengths" of presequences are also relevant for living cells. This leads to the assumption that a similar mechanism, possibly including the participation of a TOMM34-related protein, surveils the import of matrix-destined proteins *in vivo*. Fungi contain several co-chaperones with similar structural and functional properties to TOMM34. For example, Sti1, the homolog of the mammalian co-chaperone HOP, is a TPR domain-containing co-chaperone of Ssa1 (Hsp70) and Hsp82 (Hsp90) in yeast [151]. A role of Sti1 in mitochondrial protein import has been demonstrated for proteins located in different mitochondrial subcompartments [69]. In addition to Sti1, yeast cells express the TPR-domain-containing co-chaperone Cns1. In contrast to *STI1*, *CNS1* is not induced upon heat stress [152,153]. However, Cns1 is involved in several cellular processes including translation elongation [125]. Although Cns1 is not known to be involved in mitochondrial protein import so far, the sequence alignment of human TOMM34 and yeast Cns1 showed numerous conserved amino acid residues throughout their sequences (Figure S6). Interestingly, I observed diminished Oxa1 protein levels in cells depleted for Cns1 when grown in glucose or even more pronounced in galactose medium (Figure 18D, E). Surprisingly, the Oxa1 protein levels were not altered in these cells when they were grown in glycerol medium. The same was observed for the mitochondrial protein Mam33. Notably, Mam33 represents a protein whose presequence was classified into the same group as the one of Oxa1 in the bioinformatic analysis (Figure 26). The unaffected protein levels in glycerol medium indicate that in Cns1-depleted cells, compensatory mechanisms enable proper mitochondrial biogenesis when cells strongly depend on mitochondrial functionality. One possibility would be that under these conditions Sti1 or another co-chaperone substitutes Cns1, at least in terms of mitochondrial protein import. For β-barrel proteins, a compensatory mechanism of Sti1 and further co-chaperones of the Hsp40 protein family has been demonstrated, supporting this hypothesis [154]. Nevertheless, my results suggest that Cns1 might represent a novel co-chaperone being important for mitochondrial biogenesis in yeast. However, expression of TOMM34 in a Cns1 depletion strain did not rescue the growth defect of these cells (Figure 18C). This indicates that TOMM34 is note able to restore all the functions of Cns1, at least not to the extent required for normal cell growth. Notably, these are only the first experiments performed to investigate a possible role of Cns1 in mitochondrial import until now. Further investigation is required to demonstrate a crucial role of Cns1 in presequence binding and promoting protein import and to investigate whether Cns1 might be the yeast homolog of TOMM34.

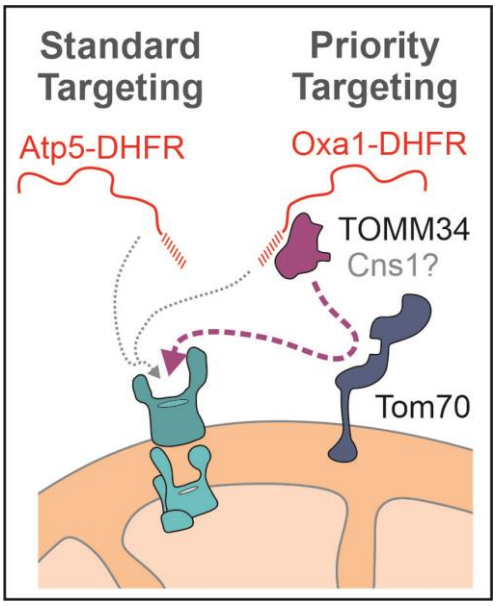

Figure 27: Some presequences recruit cytosolic co-chaperones for highly efficient import via Tom70. Schematic illustration of my findings on TOMM34 being recruited by the Oxa1 presequence and promoting highly efficient protein import via Tom70 ("priority targeting"). "Standard targeting" comprises TOMM34-independent import in a Tom20-dependent manner. Adopted from [111].

Summarizing my findings, the co-chaperones TOMM34 and possibly Cns1 might enable highly efficient import of some presequence-containing proteins in a Tom70-dependent manner, a process we termed "priority targeting" (Figure 27). In contrast, the "standard targeting" comprises TOMM34-independent import via Tom20, which seems to be less efficient compared to "priority targeting" route.

In accordance with my observation of TOMM34 binding to the presequence of Oxa1 but not to the one of Atp5, it might be interesting to analyze whether Cns1 exhibits a similar binding behavior. To address this aspect, proximity labeling experiments based on the specific and efficient BirA-dependent biotinylation of the AviTag could be performed [155]. In case Cns1 interacts with the Oxa1 presequence, the biotin ligase BirA fused to Cns1 would selectively biotinylate the AviTag attached to the either only the presequence of Oxa1 or to Oxa1-DHFR. In contrast, no biotinylation should be observed for the presequence of Atp5 or Atp5-DHFR if Cns1 indeed does not interact with this precursor. Furthermore, split-GFP represents another commonly used method to investigate protein-protein interactions. Fusion of the GFP β-sheets 1-10 to Cns1 and attachment of the 11th β-sheet to Oxa1-DHFR, Atp5-DHFR or DHFR as a control would enable to measure and compare the fluorescence intensities upon GFP reassembly [156]. In case of Cns1 interacting with the presequence-containing protein, GFP signals should be detectable. However, the reassembly of the two GFP fragments is irreversible which, on the one hand, might interfere with the import process of the precursor proteins and, on the other hand, might lead to an overestimation of the protein interactions. Nonetheless, this

method might prove to be a valid tool for the qualitative analysis of the rather transient or weak interactions between co-chaperones and precursors. For a more comprehensive investigation, one could analyze the whole cell proteomes of WT and Cns1 depletion cells via mass spectrometry and compare the mitochondrial protein levels in these strains. If Cns1 is involved in mitochondrial biogenesis, one would expect that the abundance of many related mitochondrial proteins would be decreased in the mutant strain. In this regard, it might be exciting to perform Gene Ontology enrichment analyses to analyze whether specific groups of mitochondrial proteins particularly depend on Cns1. In addition, by identifying the proteins showing an increased abundance in the mutant strain, the mass spectrometry data might reveal factors which compensate for the Cns1 depletion. To investigate the interaction of Cns1 with mitochondrial precursor proteins in a global way, proximity labeling experiments using TurboID could be conducted [157]. In this case, the biotin ligase TurboID would be fused to Cns1 and all proteins in proximity to Cns1 would be biotinylated and subsequently be identified via mass spectrometry. The potential of this method to study the interaction of mitochondrial proteins with cytosolic co-chaperones was recently shown by Annika Nutz, a colleague of our lab. Interestingly, in her study she observed Sgt1, another TPR domain-containing co-chaperone in yeast [158], being biotinylated by TurboID fused to a protein of the IM (data not shown). Her observation further substantiates the idea that several co-chaperones play critical roles in mitochondrial protein import. In addition, it might be interesting to investigate whether the depletion of Cns1 leads to the disruption of the mitochondrial morphology or if it causes a diminished volume of the mitochondrial network. In this context, morphological changes have been reported for a Sti1 deletion mutant and a diminished mitochondrial network volume was observed upon impairment of Tom70-dependent import [69,159]. Both aspects can be examined by fluorescence microscopy analyses. A very common way to visualize the mitochondrial network is to express GFP fused to the presequence of Su9. However, this might not be a suitable method in this case since it is unclear if the depletion of Cns1 affects the import efficiency of Su9. Instead, GFP could be fused to the TMD of Tom70 to stain the mitochondrial OM. Other useful alternatives might be the application of fluorescent antibodies recognizing OM proteins or the usage of MitoTracker, a fluorescent dye staining mitochondria [160]. For these experiments, as well as for the mass spectrometric identification of altered mitochondrial protein levels, it would be worthwhile to also include Cns1 depleted cells expressing TOMM34. Although TOMM34 did not rescue cell growth in my study (Figure 18C), these experiments would provide more precise insights into TOMM34 being able to rescue mitochondria-specific phenotypes caused by a Cns1 depletion. Moreover, a synthetic growth defect has been

previously observed for the double deletion Δ*sti1*Δ*tom20* [69]. Drop dilution assays and growth curves could be performed to investigate possible negative genetic interactions between Cns1 and Tom20 or Tom70, respectively. To do so, Cns1 depleted cells with either additionally deleted Tom20 or Tom70 can be used. In case of a negative genetic interaction with the import receptors, a role of Cns1 in mitochondrial protein import would be further substantiated. Lastly, it would be very interesting to investigate whether Cns1 and Sti1 or also Sgt1 can rescue the mitochondrial phenotypes of the other proteins. It would be particularly exciting to elucidate if Sti1 or Sgt1 are responsible for maintaining normal Oxa1 and Mam33 protein levels in Cns1 depleted cells grown in glycerol but not when grown in galactose or glucose medium (see Figure 18D, E).

Altogether, the recruitment of different co-chaperones by certain precursor proteins represents a very exciting research field that will certainly be investigated further in the future. I am sure that more details about the well-orchestrated interplay between different co-chaperone involved in protein import under different growth and stress conditions will be revealed over time.

4.3. Ubc8 enables efficient protein import by promoting complete TOM assembly

In addition to chaperones, the UPS is also crucially involved in preserving proper mitochondrial biogenesis (see 1.3.2). Numerous cytosolic UPS components facilitate the degradation of mature mitochondrial proteins and balance the individual cytosolic precursor levels. Furthermore, they enable smooth import by clearing the TOM complex from stalled precursor proteins. This is essential for the unrestricted functionality of cells since impaired mitochondrial protein import causes precursor accumulation in the cytosol, which in turn represents a proteotoxic challenge for the cell and induces stress responses [85]. Interestingly, a previous study suggests the ubiquitin conjugase Ubc8 as another, so far unrelated, UPS protein to be involved in the depletion of precursor proteins from the cytosol [86]. So far, Ubc8 is known to be crucially involved in the glucose-induced shutdown of gluconeogenesis by selective degradation of the specific gluconeogenic enzymes [103,104]. In agreement with this, I observed Fbp1, Mdh2, Icl1 and Pck1 to be strongly reduced in WT but not altered in Ubc8 deletion cells upon glucose addition (Figure 21C), confirming the role of Ubc8 in catabolite protein degradation. The GID complex acts as the related E3 protein with its subunits Gid4 and Gid10 being responsible for substrate binding [105,106]. Based on the finding of the genetic screen, I aimed to elucidate the previously unknown role of Ubc8 in mitochondrial biogenesis.

In accordance with the results obtained by Hansen and co-workers [86], I detected elevated precursor levels in Δ*ubc8* cells (Figure 20B-D). However, my results clearly demonstrated that the deletion of Ubc8 only causes a mild accumulation of the precursors and therefore no stress response was triggered in these cells (Figure 20E). Nevertheless, mass spectrometry revealed reduced abundances of many mitochondrial proteins in the Δ*ubc8* strain, hinting towards disturbed mitochondrial biogenesis (Figure 21C). In line with this, Δ*ubc8* exhibited impaired growth after the diauxic shift, suggesting impaired upregulation of mitochondria, an essential process taking place during the metabolic remodeling (Figure 22C). *In vitro* import experiments revealed that the previous findings are caused by diminished import efficiencies into mitochondria isolated from Δ*ubc8* cells. Thus, in this case, the UPS is not involved in the direct degradation of cytosolic precursors, but rather enables efficient protein import. Additionally, I discovered Ubc8 to be crucial for the full assembly of the TOM complex. The TOM complex represents the main entry gate into mitochondria. Most proteins, apart from some minor exceptions, use the TOM machinery as a common entrance into the organelle (Figure 2). Components of this complex comprise the pore-forming subunit Tom40, small Tom proteins that take over regulatory functions and act as scaffolding proteins, and the receptors Tom20 and Tom70 which recognize precursors for import [34,161–164]. The third receptor, Tom22, is also involved in precursor binding and, remarkably, serves as a crucial modulator of the higher-order organization of the TOM complex [165]. Thus, Tom22 determines the number of Tom40 channels assembling either in dimeric (100K) or trimeric (400K) TOM complexes [166]. Thereby, the trimeric complex represents the major variant facilitating protein import [34,167]. Whereas the trimeric TOM complex contains three Tom22 subunits, the dimer entirely lacks Tom22. The conversion of these complex variants is a dynamic process. The deletion of Tom22 causes a dissociation of the trimeric complex, resulting in the dimer variant. Due to its multitude of functions, Tom22 is also known as a "multifunctional organizer" [165]. Surprisingly, this study revealed reduced Tom22 protein levels in cells lacking Ubc8 (Figure 24A-D). Though, qRT-PCR analyses and *in vitro* import experiments showed neither a reduction in the expression of Tom22 (Figure 24F), nor an alteration in its import efficiency (Figure 25B, C).

This negative effect on Tom22 was observed upon switching cells from glycerol to glucose medium, but also when cells were continuously grown in glycerol medium (Figure 24A, Figure S8). However, in the continuously grown cultures, the effect was less pronounced. Beyond that, Tom22 protein levels were diminished upon glucose addition in both, Gid4 and Gid10 deletion cells (Figure 24E). These results indicate that the effect of Ubc8 and the GID complex on the biogenesis of Tom22 is not restricted to specific growth conditions and not to a single substrate-

specifying factor. It is furthermore possible that a so far unidentified Gid protein is also responsible for the substrate recognition. BN-PAGE analyses revealed considerably diminished levels of Tom22 being assembled into the trimeric TOM complex in Δ*ubc8* (Figure 25D), explaining the previously observed reduction of Tom22 protein levels. Size analyses of the TOM complex in Δ*ubc8* cells demonstrated that firstly, although Tom22 protein levels are strongly reduced, Tom22 is still part of the trimeric complex (Figure 25A, right panel). Secondly, the lower Tom22 levels, caused by the deletion of Ubc8, did not result in a dissociation of the trimeric TOM complex. However, I observed that the size of the TOM trimer shifted towards a slightly smaller size (Figure 25A, left panel). Lastly, the overall amount of the trimeric complex was not altered in the Δ*ubc8* strain (Figure 25A, left panel). Altogether, these findings demonstrate, that Ubc8 is crucial for the efficient assembly of newly imported Tom22 into the TOM complex. However, cells can maintain the overall number of trimeric TOM complexes. This indicates that the overall stability of the trimeric TOM complex does not necessarily rely on the presence of three Tom22 subunits and the complex might sustain its structure via additional mechanisms. Nevertheless, the altered trimeric TOM complex in Δ*ubc8* cells exhibits compromised functionality since precursors tend to accumulate in the cytosol and mitochondrial biogenesis is impaired (Figure 28).

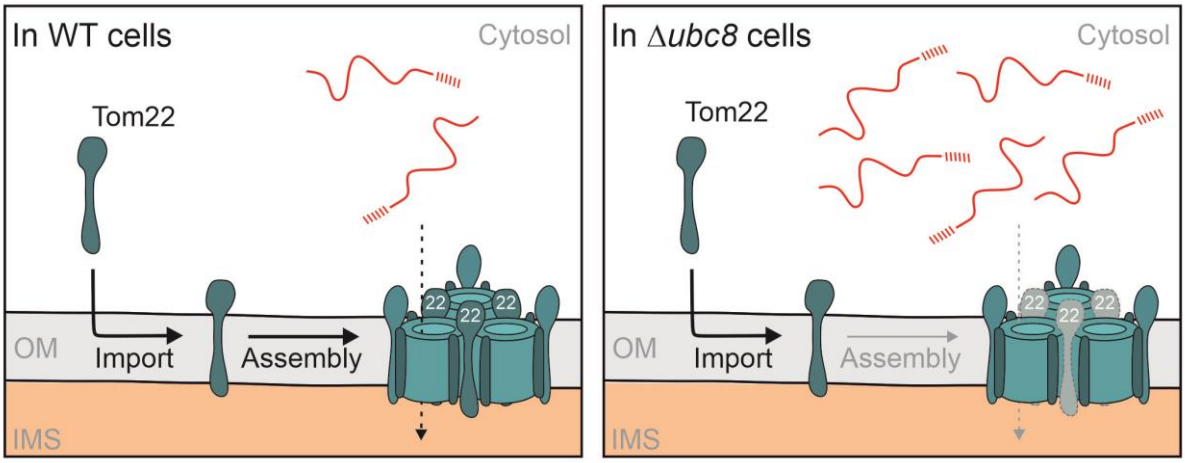

Figure 28: Ubc8 enables efficient assembly of Tom22 into a fully functional TOM complex. In WT cells, Tom22 is efficiently imported and assembled into the trimeric TOM complex which is fully functional and imports precursors without any restrictions (left panel). Deletion of Ubc8 impairs assembly of Tom22 resulting in an altered trimeric TOM complex with impaired functionality. Consequently, precursors tend to accumulate in the cytosol (right panel).

How the deletion of Ubc8 interferes with the assembly of Tom22 remains elusive. Ubc8 directly degrading Tom22 seems unlikely, since in this case the protein levels of Tom22 are expected to increase upon the deletion of Ubc8. Instead, I have observed the opposite effect. Nevertheless, other explanations are conceivable. On the one hand, several TOM components are known to

be tightly regulated by a complex interplay of cytosolic kinases. Especially Tom22 is phosphorylated site-specific by three kinases, namely protein kinase A (PKA), casein kinase 1 and 2 (CK1, CK2) [168,169]. Interestingly, PKA and CK1 are both induced under fermentative growth conditions [170]. However, PKA phosphorylates the precursor of Tom22 in the cytosol and therefore acts upstream of CK1. CK1, in contrast, mainly localizes to the OM in fermentative medium and phosphorylates membrane-bound Tom22. To increase the complexity even more, phosphorylation by PKA inhibits the import of Tom22, whereas phosphorylation by CK1 stimulates the assembly of Tom22 into the TOM complex [168,169,171]. It might be possible that PKA itself is degraded in an Ubc8- and GID-complex-dependent manner and that therefore the loss of any of these components causes increased levels of PKA. Since the PKA-mediated phosphorylation of Tom22 negatively impacts the levels of Tom22 in mitochondria, this could explain the reduced Tom22 levels I observed in Δ*ubc8* cells. However, mass spectrometric analyses do not provide indications for Ubc8 affecting the abundances of Tpk1 and Bcy1, two subunits of PKA, neither when cells were continuously grown in glucose (data not shown, see [112] for details) nor after shifting cells from glycerol to glucose medium (Figure 24A).

On the other hand, the highly abundant OM protein porin (Por1) has been reported to bind and sequesters newly imported Tom22 and thereby modulates assembly of Tom22 into the TOM complex [172]. Consequently, assembly of Tom22 is enhanced in cells depleted for Por1. Combining this knowledge with my observations leads to the assumption that Ubc8 and the GID complex mediate the degradation of Por1. Consequently, in a Ubc8 or Gid deletion strain, porin might be more abundant. In turn, increased amounts of newly imported or dissociated Tom22 would be sequestrated and therefore less Tom22 might be available for assembly into the TOM complex. However, the mass spectrometric analyses mentioned before also do not hint towards an increased abundance of Por1 in Δ*ubc8* cells (see [112] for details). A recent study reported about porin to be degraded by Ubc8 and thus about Ubc8 accelerating the assembly of the TOM complex [173]. However, the details remain elusive to date.

Beyond that, Ubc8 could also alter the SAM-Mdm10-dependent biogenesis of Tom22. The SAM complex and Mdm10 both are involved in the assembly of the TOM complex and direct SAM-Mdm10 interactions are crucial for the proper biogenesis of Tom22 [133,174,175]. BN-PAGE experiments revealed slightly diminished levels of the SAM-Mdm10 complex in cells lacking Ubc8 (data not shown, see [112]). Whether this observation might explain the inefficient assembly of Tom22 in Δ*ubc8* cells is unclear.

The last paragraphs highlighted the extremely complex process of Tom22 biogenesis. Numerous cytosolic and mitochondrial factors are involved, collaborate and fine-tune each step. Although the details of how Ubc8 modulates the assembly of Tom22 were not uncovered, this study revealed Ubc8 and the GID complex as components of the UPS which modulate the assembly of the mitochondrial import pore and therefore modulate protein import. As future perspectives, it might be interesting to identify the substrate(s) being degraded via Ubc8 and the GID complex thereby causing less efficient Tom22 assembly. For this, proteins that are in close proximity to Ubc8 and the GID-complex could be identified via proximity labeling experiments. By this, it might be possible to identify one or more of the previously discussed proteins. Additionally, it would be exciting to further investigate the Ubc8-dependent alteration of the TOM complex which causes the size shift in the BN gel (Figure 25A). The minor difference in size indicates no major alterations. Possible explanations include the partial absence of small Tom proteins, loss of single Tom22 proteins or missing posttranslational modifications of the TOM complex. For a detailed investigation, the band representing the trimeric TOM complex could be extracted from the BN gel and the components could subsequently be determined via mass spectrometry.

In summary, specific components of the UPS, namely Ubc8 and the GID complex, were identified to modulate the assembly of the mitochondrial import machinery. They were proven to be crucial for efficient protein import and therefore for preventing the accumulation of precursors in the cytosol. Although new insights were gained in this study, further research is required to better understand the involvement of the UPS in the assembly of Tom22 into the TOM complex.

4.4. Precursor proteins and the import machinery function as hubs to regulate mitochondrial protein import

Changes on the metabolic state of cells, cellular stress and pathophysiological conditions urge for the possibility to regulate mitochondrial protein import. Furthermore, different organisms and cell types require distinct regulatory mechanisms even under physiological, non-stressed conditions. Lately, a great diversity of mechanisms was described which regulate mitochondrial protein import at distinct steps of the process [176]. The cytosolic expression of most mitochondrial proteins enables cells to regulate import at two hubs. Firstly, regulatory processes can act directly on the precursor proteins by modulating the targeting and binding of the

precursor proteins to the mitochondrial surface. Secondly, the import machinery can be used as an additional target for regulation processes.

Numerous mechanisms are known which regulate mitochondrial precursor proteins. These regulatory processes include the binding of cofactors or cytosolic binding partners to the precursor proteins and cleavage of precursors by cytosolic proteases [177–179]. In addition, phosphorylation and spontaneous protein folding also modulate the import behavior of precursors [171,180,181]. However, most of these regulatory mechanisms are highly specific for individual proteins or restricted to small, related protein groups. Interestingly, this study identified a new mechanism for the modulation of protein import at the level of precursors. According to our model, some presequences specifically recruit a cytosolic co-chaperone which, in addition to Tom20-dependent import, mediate highly efficient import via Tom70, a process we termed “priority targeting” (Figure 27). In contrast, presequence-containing precursors that do not recruit this co-chaperone are imported less efficiently in a solely Tom20-dependent manner, which was termed “standard targeting”. Unlike the previously known regulatory mechanisms, the process of co-chaperone recruitment might not be restricted to single proteins. However, since the details about the co-chaperone recruitment still need to be elucidated, the scope of this regulatory mechanism remains unclear. It seems likely, that the newly identified mechanism allows to simultaneously modulate the import behavior of a broader spectrum of precursors.

The mitochondrial import machinery, as the second hub for regulation, is modulated by a complex network of cytosolic kinases. Importantly, this regulation is not restricted to physiological conditions, but also comprises adaptations to changes in the rate of cell growth and metabolic changes. Regulated mitochondrial protein import thus enables an appropriate adaptation of the mitochondrial proteome. Three kinases are known to regulate the TOM complex by phosphorylating different import components, including Tom40, Tom70 and Tom22 [168,169,171]. Interestingly, on the one hand, phosphorylation of import components by CK2 stimulates their import into mitochondria and thus increasing mitochondrial biogenesis. In rapidly growing cells the activity of CK2 is increased to improve import and therefore boosting the mitochondrial activity required in this growth phase [182]. On the other hand, the kinase PKA is activated when cells are shifted to fermentative growth conditions [170]. PKA phosphorylates several components of the import machinery and thereby inhibits their import into mitochondria. PKA therefore counteracts CK2 activity, as the speed of cell growth increases massively after cells are shifted to fermentative medium. This study demonstrates that

import regulation at the level of the import machinery is not restricted to the activity of kinases, but that it also includes the activity of specific UPS components. Under physiological conditions, and especially under glucose-induced growth conditions, Ubc8 and the GID complex regulate the amount of Tom22 being incorporated into the TOM complex (Figure 28). Since these UPS components promote the proper biogenesis of Tom22 and thereby ensure efficient import, one can assume that the activity of CK2 is supported by the UPS. The results of this study suggest that the UPS enables efficient protein import under physiological conditions to a certain extent and is particularly important for modulating the import machinery during metabolic changes. As the mechanistic details of how Ubc8 affects Tom22 assembly remain elusive, it is not clear whether the UPS and the kinases act in conjunction or in separate regulatory processes. However, this study indicates that several regulatory pathways converge at the TOM complex, as the main entry gate into mitochondria.

In summary, several cytosolic mechanisms are involved in the regulation of mitochondrial protein import. They act either on precursor proteins or on the import machinery and thereby modulate the import efficiency into mitochondria. This study reveals novel insights into previously unknown regulatory mechanisms of mitochondrial biogenesis.

4.5. How meaningful is the well-established method of *in vitro* imports?

In this study the remarkable potential of proteomic analyses became apparent. However, the multitudinous use of the well- and long-established *in vitro* import experiments validates the persistent relevance and importance of this method. But are *in vitro* imports still the way to go? Using *in vitro* import experiments was indispensable during the last 30 to 40 years to uncover numerous details of the mitochondrial protein import process. Over time, additional methods including the *in vitro* import into semi-intact cells [183], a split NanoLuc luciferase-based *in vitro* import [184] and the *in vivo* analysis of mitochondrially targeted fluorescent proteins [185] were established as additional methods to study protein import. Still, all these methods are largely limited to the investigation of a single protein at a time. Because of this, it is almost impossible to draw conclusions about the entire mitochondrial proteome from these experiments. As pointed out previously, mitochondria function in a closely linked network encompassing a multitude of cytosolic factors and other organelles. *In vitro* experiments however do not reflect the physiological conditions of living cells, comprising the total loss of the cellular environment. Therefore, the involvement of numerous cellular processes in protein import are neglected in *in vitro* imports. Keeping these limitations in mind, the application of

in vivo and more comprehensive assays is crucial to investigate import efficiencies across the whole mitochondrial proteome in a cellular context. This becomes particularly essential when the role of cytosolic factors in protein import is analyzed, as was done in this thesis. A recent study demonstrated the potential of SILAC-based mass spectrometry for the global analysis of mitochondrial import rates in living cells [136]. Due to the incorporation of heavily labeled amino acids, SILAC is suitable to monitor time-dependent changes in protein levels and is therefore a very powerful method to study protein turnover rates. By including a fully SILAC-labeled mitochondrial booster channel, Schäfer and co-workers increase the sensitivity for heavily labeled proteins. Consequently, the import kinetics of more than 700 proteins were determinable in mammalian cells [136]. Thereby, the effects of depleting the membrane potential or inhibiting the MIA-pathway on the whole mitochondrial proteome were analyzed. They furthermore report a subset of mitochondrial proteins being affected in their translation rates upon CCCP treatment, further substantiating the importance of analyzing protein import in the entire cellular context. However, SILAC-based mass spectrometry depends on a high incorporation rate of the heavily labeled amino acids. Thus, time resolution is limited to the doubling time of the cells. Due to this reason, SILAC does not allow to monitor import kinetics in very short time scales of seconds or a few minutes.

In the present study, different approaches were applied for more systematic investigations of protein import. Instead of selecting only a single protein for the analysis, I initially generated a test set including several proteins and used this set for *in vitro* and *in vivo* experiments. Thus, I identified protein groups, which exhibit a similar import behavior. Although, I selected single representatives of these groups during this study, transferring the findings to the previously classified members of each group might be straightforward. Furthermore, Yasmin Hoffman and I established and applied the novel assay IQ-Compete, which enables the analysis of import efficiencies *in vivo*. Notably, the IQ-Compete assay is not suitable for the determination of import kinetics, but it enables reliable monitoring of the import efficiencies of precursor proteins under physiological conditions in a quantitative manner based on single cell analysis. Although only precursors of the test set were analyzed in this study, this method might prove to be a valid tool to assess the import efficiencies of all endogenous mitochondrial proteins by yeast genetics in the future. Using the recently published SWAp-Tag (SWAT) strategy [186], it should be possible to fuse the uTEV protease as a tag to all yeast proteins of the SWAT library. Transformation of these cells with the GFP-Q-D construct may enable to investigate all individual import efficiencies in a high-throughput screen using either fluorescence-activated cell sorting (FACS) or fluorescence microscopy. In contrast to the present study, application of

the SWAT library would allow protein expression to be controlled by the endogenous promotors of the genes. Furthermore, since the uTEV protease would be directly fused to the endogenous proteins, the import efficiencies would not be altered by the folding ability of DHFR, like it may be the case in this study. Still, it is not clear to what extent the fused uTEV protease affects the import process. However, the SWAT-based strategy may allow the analysis of proteome-wide alterations in protein import upon any selected growth condition or drug treatment *in vivo*. Moreover, this method may not be restricted to solely analyzing mitochondrial proteins but might enable to additionally investigate import alterations of ER, peroxisomal or other proteins.

This section points out the necessity to investigate mitochondrial protein import not only by analyzing single proteins *in vitro*. The establishment of new methods to investigate import efficiencies *in vivo* and in large scale analyses is required to analyze mitochondrial import in a cellular context. Nevertheless, *in vitro* imports remain relevant, as it is an easy-to-apply method and offers several advantages, including the possibility to selectively inhibit the translation of single mitochondrially encoded genes [187]. Therefore, the *in vitro* imports remain a valid tool for specifically investigating import efficiencies and for gaining fundamental insights into the import behavior of precursors.

5. LIMITATIONS OF THE STUDY

While this study provides novel insights into different cellular mechanisms modulating mitochondrial biogenesis, it is important to consider its limitations which may bias the interpretation of the data. Awareness of these limitations ensures transparency and highlights possible avenues for follow-up research.

While interpreting the findings regarding the different import efficiencies of N-terminal presequences, some limitations should be considered. First, one needs to be aware that in this study a test set comprising nine presequences originating from yeast was used. In addition, only two presequences were selected as representatives of the test set for the detailed investigations. Since yeast contains hundreds of presequence-containing proteins, it is apparent that due to the small sample size, it is not certain whether the findings can be transferred to all yeast presequences. As mentioned in the discussion, numerous yeast presequences were considered in the bioinformatic analysis, increasing the informative value of the presequence analysis. However, further comprehensive analyses will be required in the future to define a set of presequences which recruit the cytosolic chaperones TOMM34 and Cns1, respectively.

Second, one needs to take into account that the presequences were fused to DHFR as a mature part of the precursor proteins. DHFR has previously been shown to be imported by Su9 and other presequences. However, DHFR is also known to fold in the cytosol, and when anchored to the IM, it even clogs the import pores. Therefore, the folding ability of DHFR might interfere with the import efficiencies of the tested precursors which in turn might influence the results obtained for the presequences tested. To circumvent this limitation, it would be worthwhile to repeat the analyses with either DHFRmut, which is a DHFR variant which does not fold, or another soluble protein as a mature part of the precursors. This applies not only to the *in vitro* analyses, but also to the *in vivo* analyses, which were performed with the newly established IQ-Compete assay. In this case, fusion proteins consisting of a presequence, DHFR and a uTEV protease were analyzed. It is unclear to what extent the attached protease alters the protein import efficiency in addition. Furthermore, the expression of the fusion proteins was controlled by the strong TEF promoter. The resulting high expression levels might also interfere with the import efficiencies and might not resemble the physiological conditions.

Third, in *in vitro* import experiments, precursor proteins are synthesized *in vitro* using rabbit reticulocyte lysate originating and imported into mitochondria isolated from yeast. Although many components of mammalian and yeast cells are conserved, differences are expected which

may influence the results obtained with this method. The findings about the variable presequence efficiencies in this study are largely based on results obtained by analyzing precursors which were synthesized in rabbit reticulocyte lysate, either by using import experiments or by additional methods. Due to this, it is essential to reproduce and verify the findings in living yeast cells using precursors that are also expressed in yeast. This aspect is especially important in this study, since the identified mammalian protein TOMM34 is absent in yeast cells. Therefore, it is crucial to verify the existence of a similar co-chaperone-mediated surveillance mechanism in yeast.

In the same context, one needs to consider that due to the fact that the precursor proteins were synthesized *in vitro*, post-translational modifications of the presequences and of the entire precursors were neglected. This may alter the import efficiency of the presequences and might not resemble the physiological condition in living cells. As mentioned before, *in vivo* analyses are therefore indispensable to confirm the results obtained *in vitro*.

While this study provides novel insights into the UPS promoting efficient assembly of the mitochondrial import machinery, it is important to also consider the limitations that may impact these findings. Primary limitations include the observation of inconsistent phenotypes caused by the deletion of Ubc8 in different yeast background strains. The differences in the genetic backgrounds of yeast strains make each strain advantageous for specific experimental means. In addition, Ubc8 is involved in the metabolic remodelling of cells which might be highly dependent on the different origins and genetic backgrounds of the strains. For this reason, the experiments were performed using a wide range of yeast backgrounds and no generalized statements could be made across all these strains.

In the end, this study did not identify a specific target protein that is ubiquitinated in a Ubc8-dependent manner and therefore interferes with the assembly of Tom22. For this reason, the involvement of Ubc8 in the assembly of the main entry gate into mitochondria could not be fully clarified and only speculations could be made. Therefore, future research is needed to uncover the remaining mechanistic details.

6. MATERIALS AND METHODS

Unless it is not mentioned otherwise, all reagents were obtained from Sigma, Roth, Diagonal, Thermo Scientific, or Sarstedt.

6.1. Genetic methods

6.1.1. *E. coli* strains

For plasmid purification and isolation, the *Escherichia coli* (*E. coli*) strains MH1 and DH5α were used [188,189]. The strains are described in Table 1.

Table 1: Bacterial strains used in this study. Listed are the used E. coli strains with genotype and their references.

Strain	Genotype	Reference
MH1	MC1061 derivative; araD139, lacX74, galU, galK, hsr, hsm+, strA	[189]
DH5α	K12 derivative; F- φ80dlacZΔM15, Δ(lacZYAargF)U169, deoR, recA1, endA1, hsdR17(rk- mk+), phoA, supE44, λ -, thi-1, gyrA96, relA1	[188]

6.1.2. Transformation of chemo-competent *E. coli* cells

50 µl chemically competent *E. coli* cells were transformed for the amplification of plasmid DNA. Therefore, the cells were thawed slowly on ice and 10 µl of a ligation or 2 µl plasmid DNA were added. The mixture was incubated on ice for 30 min, subjected to heat shock treatment at 42°C for 90 s, and afterwards cooled down on ice for 1 min. Next, 800 µl Lysogeny broth (LB) medium were added to the cells, followed by incubation for 45 min at 37°C and 600 rpm. Depending on the used resistance cassette, the transformed cells were plated onto LB agar plates containing either100 µg/ml ampicillin, 30 µg/ml kanamycin (KAN), or 25 µg/ml chloramphenicol (CAM) and were incubated overnight at 37°C.

Bacterial plasmids used for *in vitro* expression of proteins are listed in Table 2.

Table 2: Bacterial plasmids used in this study. Listed are all plasmids used for *in vitro* experiments. The selection marker for *E. coli* and the promotor are given.

Identifier	Plasmid	Description	Reference
HHB2046	pGEM4-Oxa1	pSP6, AmpR, Oxa1	Herrmann Lab
HHB1608	pGEM4-Pet9	pSP6, AmpR, Pet9	Herrmann Lab

HHB2352	pGEM4-DHFR	pSP6, AmpR, DHFR	This study
HHB2354	pGEM4-Atp5 MTS-DHFR	pSP6, AmpR, Atp5- DHFR	This study
HHB2355	pGEM4-Atp25 MTS-DHFR	pSP6, AmpR, Atp25- DHFR	This study
HHB2356	pGEM4-Cor1 MTS-DHFR	pSP6, AmpR, Cor1 - DHFR	This study
HHB2357	pGEM4-Cox4 MTS-DHFR	pSP6, AmpR, Cox4 - DHFR	This study
HHB2358	pGEM4-Cox5a MTS-DHFR	pSP6, AmpR, Cox5a - DHFR	This study
HHB2359	pGEM4-Mdl2 MTS-DHFR	pSP6, AmpR, Mdl2 - DHFR	This study
HHB2360	pGEM4-Oxa1 MTS-DHFR	pSP6, AmpR, Oxa1 - DHFR	This study
HHB2361	pGEM4-Pim1 MTS-DHFR	pSP6, AmpR, Pim1 - DHFR	This study
HHB2362	pGEM4-Su9 MTS-DHFR	pSP6, AmpR, Su9 (*n. c.*) - DHFR	This study

6.1.3. *S. cerevisiae* strains and plasmids

Saccharomyces cerevisiae (*S. cerevisiae*) strains were stored in glycerol stocks and plated onto agar plates. Cultures were inoculated from plates in liquid media and cultivated shaking at 30°C and 130 rpm. Yeast strains and plasmids used in this study are listed in Table 3, Table 4 and Table 5.

Table 3: Overview of the *S. cerevisiae* strains used in this study. Listed are the wild type background strains and strains generated via homologous recombination with their genotype and references.

Identifier	Strain	Genotype	Reference
HHY392	BY4742 (WT)	*MATα his3Δ1 leu2Δ0 lys2Δ0 ura3Δ0*	[190]
134 E 11	Δ*ubc8*	BY4742 *UBC8::kanMX4*	[191]
145 G 11	Δ*gid4*	BY4742 *GID4::kanMX4*	[191]
SR64	Δ*gid10*	BY4742 *GID10::natNT2*	This study
103 D 4	Δ*ubx2*	BY4742 *UBX2::natNT2*	[191]
HHY495	YPH499 (WT)	*Mata ura3-52 lys2-801 ade2-101 trp1-Δ63 his3-Δ200 leu2-Δ1*	[192]

HHY1129	Δ*arg4*	YPH499 *ARG4::kanMX4*	[193]
SR48	Δ*ubc8*	YPH499 *UBC8::kanMX4*	This study
SR46	Δ*arg4*Δ*ubc8*	YPH499 *ARG4::kanMX4 UBC8::HisMX6*	This study
HHY0084	W303 (WT)	MATα *leu2-3,112 trp1-1 can1-100 ura3-1 ade2-1 his3-11,15*	[194]
HHΨ0776	Δ*cox18*	W303 *COX18::HISMX3*	[115]
HHΨ0621	MP6	*D273-10B MATα ade2-1 his3-11,15 trp1-1 leu2-3,112 ura3-1 CAN1 arg8::HIS3 rho+*	[116]
HHΨ0622	MR10	MR6 *ATP6::ARG8m*	[116]
HHY304	BY4741	*MATa his3Δ1 leu2Δ0 met15Δ0 ura3Δ0*	[195]
HHY4317	*tet07-CNS1*	*tet07-CNS1 R1158; URA3::CMV-tTA; MATa; his3D1; leu2D0; met15D0; pCNS1::kanR-tet07-TATA*	Dharmacon Cat# TH3647[1)]
HHY4242	EGFP-Quencher-CL1	W303, cHHYTK364-EGFP-Quencher-CL1	Master's thesis Y. Hoffman
HHY4283	EGFP-Quencher-CL1, cyt-uTEV3	W303, cHHYTK364-EGFP-Quencher-CL1_cHHYTK367_DHFR-uTEV3	Master's thesis Y. Hoffman
HHY4276	EGFP-Quencher-CL1, ATP5-DHFR-uTEV3	W303, cHHYTK364-EGFP-Quencher-CL1_cHHYTK368_Atp5-DHFR-uTEV3	Master's thesis Y. Hoffman
HHY4277	EGFP-Quencher-CL1, ATP25-DHFR-uTEV3	W303, cHHYTK364-EGFP-Quencher-CL1_cHHYTK357_Atp25-DHFR-uTEV3	Master's thesis Y. Hoffman
HHY4278	EGFP-Quencher-CL1, Cor1-DHFR-uTEV3	W303, cHHYTK364-EGFP-Quencher-CL1_cHHYTK358_Cor1-DHFR-uTEV3	Master's thesis Y. Hoffman
HHY4279	EGFP-Quencher-CL1, Cox4-DHFR-uTEV3	W303, cHHYTK364-EGFP-Quencher-CL1_cHHYTK359_Cox4-DHFR-uTEV3	Master's thesis Y. Hoffman
HHY4280	EGFP-Quencher-CL1, Mdl2-DHFR-uTEV3	W303, cHHYTK364-EGFP-Quencher-CL1_cHHYTK361_Mdl2-DHFR-uTEV3	Master's thesis Y. Hoffman
HHY4281	EGFP-Quencher-CL1, Oxa1-DHFR-uTEV3	W303, cHHYTK364-EGFP-Quencher-CL1_cHHYTK369_Oxa1-DHFR-uTEV3	Master's thesis Y. Hoffman

HHY4282	EGFP-Quencher-CL1, Su9-DHFR-uTEV3	W303, cHHYTK364-EGFP-Quencher-CL1_cHHYTK363_Su9-DHFR-uTEV3	Master's thesis Y. Hoffman

[1)] kind gift of Buchner lab

Table 4: Overview of the *S. cerevisiae* strains obtained by transformation. Listed are the strains used in this study with their genotype and references.

Identifier	Strain	Plasmid	Reference
HHY1880	BY4742 + pRS313	pRS313	This study
HHY1879	BY4742 + Oxa1-Ura3	pRS313-Oxa1-Ura3	This study
HHY1878	BY4742 + ΔNOxa1-Ura3	pRS313-ΔNOxa1-Ura3	This study
HHY1877	BY4742 Δ*ubc8* + pRS313	pRS313	This study
HHY1876	BY4742 Δ*ubc8* + Oxa1-Ura3	pRS313-Oxa1-Ura3	This study
HHY1881	BY4742 Δ*ubc8* + ΔNOxa1-Ura3	pRS313-ΔNOxa1-Ura3	This study
SR20	YPH499 + b2Δ-DHFR	pYX223- b2Δ-DHFR	This study
SR24	YPH499 Δ*ubc8* + b2Δ-DHFR	pYX223- b2Δ-DHFR	This study
HHY2244	W303 + PACE-YFP	pNH605-PACE-YFP	This study
-	W303 Δ*ubc8* + PACE-YFP	pNH605-PACE-YFP	This study
HHY3600	W303 + GFP	pYX142-GFP, pYX113 ev	Herrmann lab
HHY4052	W303 + EGFP-Quencher	cHHYTK330-EGFP-Quencher	Master's thesis Y. Hoffman
HHY4191	W303 + EGFP-Quencher-CL1	cHHYTK350-EGFP-Quencher-CL1	Master's thesis Y. Hoffman
HHY4118	W303 EGFP-Quencher-CL1, cyt-uTEV3	cHHYTK351-EGFP-Quencher-CL1, DHFR-uTEV3	Master's thesis Y. Hoffman
HHY4372	W303 cyt-uTEV3	W303, cHHYTK347-DHFR-uTEV3	Master's thesis Y. Hoffman

HHY4373	W303 EGFP-Quencher + uTEV3	cHHYTK403-EGFP-Quencher_DHFR-uTEV3	Master's thesis Y. Hoffman
HHY4361	BY4741 + ev	pYX122 ev	This study
HHY4362	tet07-CNS1 + ev	pYX122 ev	This study
HHY4363	tet07-CNS1 + Cns1	pYX122 Cns1	This study
HHY4364	tet07-CNS1 + TOMM34	pYX122 TOMM34	This study

Table 5: Yeast plasmids used in this study. Listed below are the plasmids used for yeast transformation in this thesis. The selection marker for yeast as well as the yeast origin are given.

Identifier	Plasmid	Description	Reference
HHB384	pRS313	CEN/ARS, *HIS3*, AmpR	[192]
HHB1025	pRS313-Oxa1-Ura3	CEN/ARS, *HIS3*, AmpR, Oxa1-Ura3	[86]
HHB1026	pRS313-ΔNOxa1-Ura3	CEN/ARS, *HIS3*, AmpR, ΔNOxa1-Ura3	[86]
HHB1721	pYX223-b_2Δ-DHFR	2μ, *HIS3,* AmpR, *pGAL1*, b_2Δ - DHFR	[85]
HHB1940	pNH605-PACE-YFP	INT, *HIS3*, AmpR, *pCYC1*-4xPACE-YFP	[85]
HHB1563	pYM17	AmpR, *6xHA-NatMX* for genomic tagging	[196]
HHB1185	pFA6α-*NatNT2*	AmpR, *NatNT2* for genomic deletions	[196]
HHB2136	pYX142-GFP	CEN, *LEU2,* AmpR, TPI, GFP	Herrmann lab
HHB0038	pYX122 ev	CEN, *HIS3,* AmpR, TPI	[197]
HHB2366	pYX122 Cns1	CEN, *HIS3,* AmpR, TPI, Cns1	This study
HHB2367	pYX122 TOMM34	CEN, *HIS3,* AmpR, TPI, TOMM34	This study
cHHYTK347	DHFR-uTEV3 (level 1 plasmid)	CEN/ARS, *URA3*, AmpR, pTEF2-DHFR-tTDH1	Master's thesis Y. Hoffman

cHHYTK350	EGFP-Quencher-CL1 (level 1 plasmid)	CEN/ARS, *URA3*, AmpR, pTEF2-EGFP-Quencher-CL1-tTDH1	Master's thesis Y. Hoffman
cHHYTK351	EGFP-Quencher-CL1_DHFR-uTEV3 (level 2 plasmid)	CEN/ARS, *URA3*, KanR, pTEF1-EGFP-Quencher-CL1-tENO2_pTEF2-DHFR-uTEV3-tTDH1	Master's thesis Y. Hoffman
cHHYTK367	DHFR-uTEV3 (genomic integration)	KanR, pTEV2-DHFR-uTEV3-tTDH1	Master's thesis Y. Hoffman
cHHYTK364	EGFP-Quencher-CL1 (genomic integration)	HygroR, pTEF1-EGFP-Quencher-CL1-tENO2	Master's thesis Y. Hoffman
cHHYTK368	Atp5-DHFR-uTEV3 (genomic integration)	KanR, pTEF2-Atp5-DHFR-uTEV3-tTDH1	Master's thesis Y. Hoffman
cHHYTK357	Atp25-DHFR-uTEV3 (genomic integration)	KanR, pTEF2-Atp25-DHFR-uTEV3-tTDH1	Master's thesis Y. Hoffman
cHHYTK358	Cor1-DHFR-uTEV3 (genomic integration)	KanR, pTEF2-Cor1-DHFR-uTEV3-tTDH1	Master's thesis Y. Hoffman
cHHYTK359	Cox4-DHFR-uTEV3 (genomic integration)	KanR, pTEF2-Cox4-DHFR-uTEV3-tTDH1	Master's thesis Y. Hoffman
cHHYTK361	Mdl2-DHFR-uTEV3 (genomic integration)	KanR, pTEF2-Mdl2-DHFR-uTEV3-tTDH1	Master's thesis Y. Hoffman
cHHYTK369	Oxa1-DHFR-uTEV3 (genomic integration)	KanR, pTEF2-Oxa1-DHFR-uTEV3-tTDH1	Master's thesis Y. Hoffman
cHHYTK363	Su9-DHFR-uTEV3 (genomic integration)	KanR, pTEF2-Su9-DHFR-uTEV3-tTDH1	Master's thesis Y. Hoffman
cHHYTK403	EGFP-Quencher_DHFR-uTEV3	CEN/ARS, *HIS3*, KanR, pTEF1-EGFP-uTEV3-tENO2	Master's thesis Y. Hoffman

6.1.4. *S. cerevisiae* transformation

S. cerevisiae cells were grown to exponential phase and 1.5 ml of the culture was harvested by centrifugation for 1 min at 16,000 g at room temperature (RT). The cell pellet was washed with

1 ml ddH_2O. The cells were resuspended in 1 ml of 0.1 M lithium acetate and incubated for 10 min at 30°C and 650 rpm. After centrifugation (1 min at 16,000 g at RT), the cell pellet was resuspended in 74 µl ddH_2O, 5 µl salmon sperm DNA (ssDNA, denatured at 96°C for 10 min and cooled down on ice prior to usage), 5 µl 100 ng/µl plasmid DNA, 36 µl 1 M lithium acetate (final concentration 0.1 M) and 240 µl 50% (w/v) polyethylene glycol (PEG) 4000. The mixture was thoroughly mixed for 1 min and incubated for 30 min at 30°C, followed by a heat shock for 25 min at 42°C. Afterwards, the cells were pelleted and resuspended in 100 µl sterile ddH_2O. The suspension was plated on selective media and the plates were incubated for 2 days at 30°C.

Homologous recombination was applied to generate yeast deletion strains via genomic integration of DNA cassettes. For this, 1 µg of PCR-amplified DNA and 34 µl ddH_2O were used. The residual procedure was the same as described above. When antibiotic cassettes were used, the cells were first plated onto YPD and incubated overnight and the next day replica plated onto YPD containing the appropriate antibiotic.

For genomic integration of plasmids generated with modular cloning (plasmids for the IQ-Compete assay), the integrating plasmids were linearized prior to the transformation process. For this, reactions with a final volume of 50 µl were set up, containing 5 µl 10x rCutSmart buffer, 1 µl of the restriction enzyme NotI-HF and 1 µg plasmid DNA. After incubation for 30 min at 37°C, the digested DNA was cleaned up using 35 µl pre-heated water for elution. 10 µl of the elution was used for subsequent transformation.

6.2. Molecular Biology Methods

6.2.1. Isolation of plasmid DNA from *E. coli*

Plasmid DNA was isolated from *E. coli* cells either in small (Mini-prep) or large scale (Midi-prep). For small-scale isolation of plasmids, 5 ml of selective $LB_{Amp/\ Cam/\ Kan}$ medium were inoculated with a single bacterial colony and incubated overnight at 37°C. To isolate plasmid DNA, 1.5 ml of the culture were harvested, and the DNA was extracted using the NucleoSpin Plasmid-Kit (Macherey-Nagel) according to the manufacturer's instructions.

For large-scale isolation, 150 ml selective $LB_{Amp/\ Cam/\ Kan}$ were inoculated with bacteria. The cells were cultured overnight at 37°C before the plasmid DNA of the whole culture was isolated using the *PureYield*^{TM} Plasmid Midiprep System (Promega) as described by the manufacturer.

6.2.2. Determination of DNA concentration

For determination of the DNA concentration and purity, the Spectrophotometer/Fluorometer DS-11 FX+ (DeNovix) was used. After calibration with 1 µl of ddH_2O, 1 µl of DNA was used for the measurement.

6.2.3. Polymerase Chain Reaction

DNA amplification for either homologous recombination or plasmid construction was achieved by polymerase chain reaction (PCR). A PCR reaction set up with a final volume of 50 µl containing 100 ng template DNA, 0.5 µM of each primer (forward and reverse), 0.2 mM dNTPs (deoxynucleotide triphosphates), 1 U Q5® High-Fidelity (HF) polymerase and 1x Q5® reaction buffer. In Table 6 the PCR program for the amplification of DNA is displayed. The elongation time was determined according to the insert length and the polymerase used (Q5: 1 kbp/20-30 s). Annealing temperatures were set according to the calculations obtained with the NEB Tm calculator (https://tmcalculator.neb.com/).

Table 6: PCR Program. Protocol for DNA amplification via PCR.

Temperature	Time	Cycle Number	Description
98°C	30 s		Initial DNA denaturation and nuclease inactivation
98°C	10 s		1. DNA denaturation
50-72°C	20 s	35x	2. Primer annealing
72°C	20-30 s/kb		3. Elongation
72°C	2 min		Final elongation
4°C	∞		Cooling

Colony PCR was performed for the verification of successful homologous recombination in yeast. Single yeast colonies were picked and mixed with 30 µl 0.2% sodium dodecyl sulfate (SDS). The samples were boiled for 10 min at 96°C and cell debris and intact cells were pelleted by centrifugation (1 min, 16,000 g, RT). 1 µl of the supernatant was used as template DNA and PCR reactions were set up as described above. The PCR program is displayed in Table 6. In Table 7 all primers used for PCR reactions in this study are listed.

Table 7: Primers used in this study. Listed are the names, sequences as well as a short description of the primers used in this thesis. For/fwd, forward primer; rev, reverse primer

Primer	Sequence [5'-3']	Description
gid10-for	GTATTGTGTTATGAGACTTTTCATTTAA AATATACTGTAGGTATGCTACGCTGCAG GTCGAC	Deletion of *GID10*
gid10-rev	GACATGGTTGACGAGTAAACAAACATA CATTGGTAATTCTATAAGGTCTTTAATC GATGAATTCGAGCTCG	Deletion of *GID10*
His3-for	CTAGCGGATGACTCTTTTTTTTCTTAG CG	*HIS3* amplification for deletion of *UBC8* in YPH499 Δ*arg4*
His3-rev	CATACTGTTCGTATACATACTTACTGAC ATTCATAGG	*HIS3* amplification for deletion of *UBC8* in YPH499 Δ*arg4*
ubc8_His3_for	GTATTTCATAAGGAATATTGGAAGAAAG GAGCGTAATACGAAAGATGCGTACGCT GCAGGTCGAC	Deletion of *UBC8* in YPH499 D*arg4*
ubc8_His3_rev	TTATACATACATACATATATATATATATAT ATATATGTGTGTGCTCGATCGATGAATT CGAGCTCG	Deletion of *UBC8* in YPH499 Δ*arg4*
ubc8_for	CGTAATTATCAAGCGAGATAG	Deletion of *UBC8* in YPH499
ubc8_rev	CCTTGTAGTTGCTTGATAG	Deletion of *UBC8* in YPH499
Tom22-fwd	AGACGAACCACAATTTTCCAG	qPCR SYBR Green
Tom22_rev	CACACCGAGTAACAAAGCAG	qPCR SYBR Green
DHFR-fwd	AttcgagctcggtacccggggatccACCATGGTTCG ACCATTGAAC	*In vitro* synthesis of DHFR
DHFR-rev	ctcactatagggagaccggaagcttTTAGTCTTTCTT CTCGTAGAC	*In vitro* synthesis of DHFR
Atp5 MTS-DHFR-fwd	tgacactatagaatacacgg*aattcACC*ATGTTTAAT AGAGTCTTTACCAGGTCATTTGCATCAA GCTTAAG	*In vitro* synthesis of Atp5-DHFR
Atp5 MTS-DHFR-rev	tgcagttcaatggtcgaacg*gatcc*CACCGGTGGGG GAGCAG	*In vitro* synthesis of Atp5-DHFR
Atp25 MTS-DHFR-fwd	Tgacactatagaatacacgg*aattcACC*ATGAATAA ATTCTGTCTACTACC	*In vitro* synthesis of Atp25-DHFR
Atp25 MTS-DHFR-rev	tgcagttcaatggtcgaacggatccTTCATGACTGTC ATTTTTGC	*In vitro* synthesis of Atp25 -DHFR

Cor1 MTS-DHFR-fwd	TgacactatagaatacacggaattcACCATGCTAAGAACAGTAACTTCAAAGACTGTATCTAACC	*In vitro* synthesis of Cor1-DHFR
Cor1 MTS-DHFR-rev	tgcagttcaatggtcgaacg*gatcc*TTCGGCCTTGGGGGTTG	*In vitro* synthesis of Cor1-DHFR
Cox4 MTS-DHFR-fwd	TgacactatagaatacacggaattcACCATGCTTTCACTACGTCAATC	*In vitro* synthesis of Cox4-DHFR
Cox4 MTS-DHFR-rev	tgcagttcaatggtcgaacg*gatcc*TTGGGCAGTTTTCACCAC	*In vitro* synthesis of Cox4-DHFR
Cox5a MTS-DHFR-fwd	TgacactatagaatacacggaattcACCATGTTACGTAACACTTTTACTAGAGC	*In vitro* synthesis of Cox5a-DHFR
Cox5a MTS-DHFR-rev	tgcagttcaatggtcgaacggatccAGCAGCGTTGGAAAGAG	*In vitro* synthesis of Cox5a-DHFR
Mdl2 MTS-DHFR-fwd	TgacactatagaatacacggaattcACCATGTTGAATGGTCGTTTAC	*In vitro* synthesis of Mdl2-DHFR
Mdl2 MTS-DHFR-rev	tgcagttcaatggtcgaacggatccCCTTGCTGATCCTTTAGATATG	*In vitro* synthesis of Mdl2-DHFR
Oxa1 MTS-DHFR-fwd	TgacactatagaatacacggaattcACCATGTTCAAACTCACCTCTC	*In vitro* synthesis of Oxa1-DHFR
Oxa1 MTS-DHFR-rev	tgcagttcaatggtcgaacggatccGACATCGTTGGCATTTGG	*In vitro* synthesis of Oxa1-DHFR
Pim1 MTS-DHFR-fwd	TgacactatagaatacacggaattcACCATGCTAAGAACAAGAACCACAAAGAC	*In vitro* synthesis of Pim1-DHFR
Pim1 MTS-DHFR-rev	tgcagttcaatggtcgaacggatccCTCTACGTCACGCACGGTC	*In vitro* synthesis of Pim1-DHFR
Su9 MTS-DHFR-fwd	TgacactatagaatacacggaattcACCATGGCCTCCACTCGTGTC	*In vitro* synthesis of Su9-DHFR
Su9 MTS-DHFR-rev	tgcagttcaatggtcgaacggatccGGAAGAGTAGGCGCGCTTC	*In vitro* synthesis of Su9-DHFR
YMC_DHFR_fix_f	TCGTCTCAGATCTACCCTGGCCTCC	Mutation of Bsa1 restriction site in DHFR for modular cloning
YMC_DHFR_fix_r	TCGTCTCAGATCTCCGTTCTTGCCAATCC	Mutation of BsaI restriction site in DHFR for modular cloning
YMC_DHFR_3a_r	ATGCCGTCTCAGGTCTCAAGAACCGTCTTTCTTCTCGTA GACTTCAAAC	*In vivo* expression of DHFR
YMC_DHFR_3a_f	GCATCGTCTCATCGGTCTCATATGGTTCGACCATTGAACTGCATCG	*In vivo* expression of DHFR

YMC_Atp5 MTS-DHFR_3a_f	GCATCGTCTCATCGGTCTCATATGTTTA ATAGAGTCTTTACCAGGTCATTTGCA	*In vivo* expression of Atp5-DHFR
YMC_Atp25 MTS-DHFR_3a_f	GCATCGTCTCATCGGTCTCATATGAATA AATTCTGTCTACTACCTTTCCATGGC	*In vivo* expression of Atp25-DHFR
YMC_Cor1 MTS-DHFR_3a_f	GCATCGTCTCATCGGTCTCATATGCTAA GAACAGTAACTTCAAAGACTGTATCTA ACC	*In vivo* expression of Cor1-DHFR
YMC_Cox4 MTS-DHFR_3a_f	GCATCGTCTCATCGGTCTCATATGCTTT CACTACGTCAATCTATAAGATTTTCAA GC	*In vivo* expression of Cox4-DHFR
YMC_Mdl2 MTS-DHFR_3a_f	GCATCGTCTCATCGGTCTCATATGTTGA ATGGTCGTTTACCACTTTTGC	*In vivo* expression of Mdl2-DHFR
YMC_Oxa1 MTS-DHFR_3a_f	GCATCGTCTCATCGGTCTCATATGTTCA AACTCACCTCTCGACTCG	*In vivo* expression of Oxa1-DHFR
YMC_Su9 MTS-DHFR_3a_f	GCATCGTCTCATCGGTCTCATATGGCCT CCACTCGTGTCC	*In vivo* expression of Su9-DHFR
YMC_CL1_4a_f	GCATCGTCTCATCGGTCTCAATCCATGG CTTGTAAAAATTGGTTTTC	CL1 fusion to C-terminus of DHFR
YMC_CL1_4a_r	ATGCCGTCTCAGGTCTCAGCCACTCGA GTTACAAATGTATAACAAAATGAGACA AAGA	CL1 fusion to C-terminus of DHFR

6.2.4. Restriction digest of DNA

For plasmid verification or the preparation of insert DNA and vectors for subsequent ligation, restriction digest was performed. The 50 µl reaction mix contained 15 U of the specific restriction enzymes, 5 µl 10x rCutSmart buffer, and 2 µg of DNA. The reaction mixture was incubated for 15-60 min at 37°C, analyzed by agarose gel electrophoresis or directly purified using the Monarch® PCR & DNA Cleanup Kit (NEB) according to the manufacturer's instructions.

6.2.5. Ligation of DNA fragments and vectors via classical cloning

Inserts were ligated into vector plasmid DNA in a 20 µl reaction volume. For this, 100 ng of vector DNA, a 3-fold molar excess of insert DNA to vector (5-fold if the DNA insert was smaller than 200 bp), 2 µl T4 DNA ligase, and 2 µl 10x T4 ligase reaction buffer were mixed. To molar ratios were calculated with the online NEB web tool (https://nebiocalculator.neb.com/#!/ligation). The samples were incubated for 1 h at RT. 10 µl

of the ligation reaction were used to transform *E. coli* cells. Single colonies were selected, and isolated plasmids were analyzed via restriction digest.

6.2.6. Gibson Assembly

The gene of interest was amplified via PCR using primers generated with NEBuilder (https://nebuilder.neb.com/) and purified as described before. Vector DNA was linearized via restriction digest in 100 µl approaches including 10 µl 10x rCutSmart buffer, 2 µg plasmid DNA, and 2.5 µl of the respective restriction enzymes. Samples were incubated for 15-60 min at 37°C, loaded on an Agarose gel, and DNA was purified using the Monarch® PCR & DNA Cleanup Kit (NEB) according to the manufacturer's instructions. Ligations were set up in 20 µl reaction volumes. 100 ng vector DNA, a 3-fold molar excess of insert DNA to vector (5-fold if the DNA insert was smaller than 200 bp), 10 µl 2x HiFi DNA Assembly MasterMix were mixed, and samples were incubated for 15 min at 50°C. 2 µl of the ligation reaction was used to transform *E. coli* cells. Single colonies were selected, and isolated plasmids were analyzed via restriction digest.

6.2.7. Modular Cloning

Modular cloning was performed to generate the plasmids used in the IQ-Compete assay. First, the desired parts were created in a first step called domestication (level 0 assembly). For this, the gene of interest was amplified via PCR and after purification it was assembled into a level 0 plasmid. The Yeast Toolkit Primer Design Tool (Yeast Toolkit Primer Design Tool (shinyapps.io) was used to generate the primers used the for the PCR reactions. The BsaI restriction site in the sequence of DHFR was removed by inserting a silent mutation using appropriate primers (see Table 7).

Domestication reactions were set up with a final volume of 20 µl containing 75 ng of entry vector DNA (pYTK001), 75 ng of insert DNA, 2 µl 10x T4 ligase reaction buffer, and 1 µl NEB GG Mix BsmBI. In Table 8 the program for the domestication of parts is displayed. 5 µl of the level 0 plasmids was transformed into *E. coli* cells and single, white colonies were selected on LB plates containing 25 µg/ml chloramphenicol (CAM). Plasmid assembly was analyzed via test digestion and verified by sequencing.

Table 8: Program for the domestication of parts (Level 0).

Temperature	Time	Cycle Number
42°C	5 min	30x
16°C	5 min	
60°C	5 min	
4°C	∞	

For expression in yeast, single (level 1) or multiple (level 2) transcriptional unit plasmids were generated using the level 0 plasmids. Level 1 assembly reactions were set up with a final volume of 20 µl, containing 75 ng of each desired part, 2 µl 10x T4 ligase reaction buffer, and 1 µl NEB GG Mix BsaI. Level 2 assemblies contained 75 ng of the entry vector cHHYTK002 (*URA3*, CEN6/ARS4), 75 ng of each transcriptional unit (level 1), 2 µl 10x T4 ligase reaction buffer, and 1 µl NEB GG Mix BsmBI. In Table 9 and Table 10 the programs for level 1 and level 2 assemblies are displayed. 5 µl of the assembled plasmids were used for transformation into *E. coli* cells and single, white colonies were selected on LB plates containing 100 µg/ml ampicillin or 30 µg/ml kanamycin (KAN), respectively. Plasmid assembly was analyzed via test digestion.

Table 9: Program for a level 1 assembly.

Temperature	Time	Cycle Number
37°C	5 min	30x
16°C	5 min	
60°C	5 min	
4°C	∞	

Table 10: Program for a level 2 assembly.

Temperature	Time	Cycle Number
42°C	5 min	30x
16°C	5 min	
60°C	5 min	
4°C	∞	

6.2.8. Agarose gel electrophoresis

Agarose gel electrophoresis was used for analytic (test of successful ligation) and preparative purposes (isolation of DNA fragments). To cast the gel matrix, 1% agarose (w/v) was entirely dissolved in 1x TAE buffer (40 mM Tris, 1.14% acetic acid, 10 mM EDTA pH 8.0) by heating the solution in a microwave. After cooling down the agarose solution, 0.5 µg/ml ethidium bromide was added to visualize DNA using ultraviolet light. The samples were supplemented with 6x loading dye (final concentration: 1x) (60 mM Tris/HCl pH 7.5, 30 mM sodium acetate, 12 mM EDTA, 60% (v/v) glycerol, 0.36% (w/v) orange G) before loading. The electrophoresis was performed in 1x TAE buffer at 10 V/cm. Separation of the DNA fragments was analyzed using ultraviolet light. To isolate DNA fragments of interest (for preparative purposes), the respective DNA band was cut out using a scalpel and purified with Monarch® PCR & DNA Cleanup Kit (NEB) according to the manufacturer's instructions.

6.2.9. RNA isolation and real-time quantitative polymerase chain reaction (qRT-PCR)

For total RNA extraction, yeast strains were cultivated in synthetic or full media to exponential growth phase. 4 OD_{600} of cells were harvested and RNA was extracted using the RNeasy Mini Kit (Qiagen) in conjunction with the RNase-Free DNase Set (Qiagen) according to the manufacturer's instructions. Yield and purity of the obtained RNA were determined with a Spectrophotometer/Fluorometer DS-11 FX+ (DeNovix). 500 ng RNA were reverse transcribed into cDNA using the qScript cDNA Synthesis Kit (Quanta Biosciences). For relative mRNA level measurements, the iTaq Universal SYBR Green Supermix (BioRad) was used with 2 µl of a 1:10 dilution of the cDNA sample. Measurements were performed in technical triplicates with the CFX96 Touch Real-Time PCR Detection System (BioRad). Calculations of the relative mRNA expressions were conducted following the 2-ΔΔCt method [198]. Due to its stability, the housekeeping gene *ACT1* was used for normalization. See Table 7 for primer sequences.

6.3. Cell Biology Methods

6.3.1. Cultivation media for *E. coli* cells

E. coli cells were grown in LB-medium or on LB-plates. 1% bacto-tryptone, 0.5% yeast extract, and 1% sodium chloride were used for liquid cultures. The pH was adjusted to 7.5 using sodium hydroxide (NaOH) and 100 µg/ml ampicillin, 30 µg/ml chloramphenicol, or 25 µg/ml kanamycin was added for plasmid selection. For agar plates, LB medium was supplemented with 2% (w/v) bacto-agar and autoclaved.

6.3.2. Cultivation media for *S. cerevisiae*

Yeast cells were grown in non-selective YP-medium, containing 1% yeast extract and 2% peptone, or YEP-medium, containing 3% (w/v) yeast extract peptone (YEP) broth (Formedium LTD). The pH was adjusted to 5.5 using HCl and the media were supplemented with 2% of the respective carbon source (D, glucose; Gal, galactose, G, glycerol). For plates, YP or YEP medium was supplemented with 2% (w/v) agar, autoclaved and subsequently supplemented with 2% of the respective carbon source. For selection, 100 µg/ml G418 or cloNAT was added.

Cells harboring plasmids were cultured in selective media (S-medium) or selective lactic acid-based medium (SLac-medium). For this purpose, 1,7 g/l yeast nitrogen base, and 5 g/l ammonium sulfate were mixed with drop-out mix lacking auxotrophic markers and 2% of the respective carbon source (D, glucose; Gal, Galactose; G, glycerol). For SLac medium, 1,7 g/l yeast nitrogen base, 5 g/l ammonium sulfate, and 2.2% lactic acid (90% (v/v)) were mixed with drop-out mix lacking auxotrophic markers. In SLac-medium, 0.5% galactose could be added to induce protein expression from a *GAL*-promotor. In Table 11, the components of a 20x drop-out mix are listed. For plates containing selective media, half of the volume consisting of water supplemented with 2% (w/v) agar was autoclaved. The agar-solution was mixed with S-medium or SLac-medium, drop-out mix, and the respective carbon source and poured into petri dishes.

6.3.3. Dropout-mix

The dropout-mix contains all amino acids. For plasmid selection individual amino acids were not added. The composition of the dropout-mix is listed in Table 11.

Table 11: Composition of the 20x dropout-mix. Depending on the selection markers, appropriate amino acids were not added.

Amino acid/Nucleobase	Amount [mg/l]
L-adenine hemi sulfate salt	400
L-Arginine	400
L-Histidine HCl Monohydrate	400
L-Isoleucine	600
L-Leucine	2000
L-Lysin HCl	600
L-Methionine	400
L-Phenylalanine	1000
L-Threonine	400
L-Tryptophan	400
L-Tyrosine	400

L-Uracil	400
L-Valine	3000

6.3.4. Growth assays

For drop dilution analysis, the respective yeast strains were grown in liquid media. During the exponential growth phase, 1 OD_{600} of yeast cells was harvested. The cells were washed with sterile ddH_2O and a ten-fold dilution series (starting OD = 0.5) was prepared. 3 µl of these serial dilutions were spotted on plates containing the respective media. If specified, plates were supplemented with 10 µg/ml doxycycline (DOX, Doxycycline hyclate; Sigma, CAS Number: 24390-14-5). After incubation at 30°C for several days, pictures were taken.

Growth curves were performed in 96-well plates, using the ELx808™ Absorbance Microplate Reader (BioTek®) for automated measurements. Yeast cells were grown in liquid media until mid-log phase, 1 OD_{600} of yeast cells were harvested (16,000 g, 1 min, RT) and washed with sterile ddH_2O. The samples were set up in a final volume of 100 µl and with an initial OD_{600} of 0.1. The OD_{600} was measured every 10 min for 72 h at 30°C. The mean of technical triplicates was calculated and plotted in R.

6.3.5. Sensitivity assay/ Halo assay

To analyze the Carbonylcyanid-m-chlorphenylhydrazon (CCCP) sensitivity of yeast cells, halo assays were performed. For this, cells were precultured in YPG medium until mid-log phase. 1 OD_{600} were harvested (16,000 g, 1 min, RT) and washed with sterile ddH_2O. 100 µl of cells equal to OD_{600} 0.01 were plated out on YPG plates and a filter disk with 10 µl of 10 mM CCCP was placed to the center of the plate. Filter disks with 10 µl Dimethyl sulfoxide (DMSO) served as a control. After incubating the plates for 1 day at 30°C, halo areas were measured.

6.3.6. CCCP treatment assay

The protocol for the CCCP treatment assay was adapted from [93].Yeast cells were grown in YPGal at 19°C for 2 days and diluted continuously to ensure exponential cell growth. During the exponential growth phase, cells were treated with 40 µM CCCP and shifted to 30°C. After 30 min, 60 min, and 120 min cells equivalent to 4 OD_{600} were harvested (16,000 g, 1 min, RT), washed with sterile ddH_2O and cell lysates were prepared as described in 6.4.1. One sample was additionally taken before the addition of CCCP.

6.3.7. YFP reporter assay

The *PACE-YFP* reporter gene was integrated into the *LEU2* locus of the yeast genome. Cells were grown to mid-log phase, cells equivalent to 4 OD_{600} were harvested by centrifugation (12,000 g, 5 min, RT) and resuspended in 400 µl H_2O. 100 µl of the cell suspension were transferred to flat-bottomed black 96-well imaging plates (BD Falcon, Heidelberg, Germany) in technical triplicates. Cells were sedimented by gentle spinning (30 g, 5 min, RT) and fluorescence (excitation 497 nm, emission 540 nm) was measured using a ClarioStar Fluorescence plate reader (BMG-Labtech, Offenburg, Germany). The corresponding WT strain not expressing YFP was used for background subtraction of autofluorescence. Fluorescence intensities were normalized to the value obtained from the WT carrying an empty vector in each of the three independent biological replicates.

6.3.8. Isolation of mitochondria

For the isolation of mitochondria, cells were grown in SGal full or selective medium to mid-log phase. Cells were harvested (2,000 g, 5 min, RT) in exponential phase and after a washing step, cells were treated for 10 min with 2 ml per g wet weight MP1 buffer (10 mM Tris pH unadjusted, 100 mM DTT) at 30°C. After washing with 1.2 M sorbitol, cells were resuspended in 6.7 ml per g wet weight MP2 buffer (20 mM KPi buffer pH 7.4, 1.2 M sorbitol, 3 mg/g wet weight zymolyase 20T from Seikagaku Biobusiness) and incubated for 1 h at 30°C. Spheroplasts were collected via centrifugation at 4°C and resuspended in ice-cold homogenization buffer (13.4 ml/g wet weight) (10 mM Tris pH 7.4, 1 mM EDTA pH 8, 0.2% fatty acids free bovine serum albumin (BSA), 1 mM PMSF, 0.6 M sorbitol). Spheroplasts were disrupted by 10 strokes with a cooled glass potter. Cell debris was removed via centrifugation at 1,500 *g* for 5 min. To collect mitochondria, the supernatant was centrifuged at 12,000 *g* for 12 min. Mitochondria were resuspended in 1 ml of ice-cold SH buffer (0.6 M sorbitol, 20 mM Hepes pH 7.4). The Spectrophotometer/Fluorometer DS-11 FX+ (DeNovix) was used to determine the protein concentration and purity. Mitochondria were diluted to a protein concentration of 10 mg/ml.

6.3.9. Fluorescence microscopy

For fluorescence microscopy, cells were grown to mid-log phase in YEPD or SLac + 0.2% glucose medium and 1 OD was harvested via centrifugation. Cell pellets were resuspended in 30 µl PBS. 3 µl were pipetted onto a glass slide and covered with a cover slip. Manual microscopy was performed using a Leica Dmi8 Thunder Imager. Images were acquired using

an HC PL APO100x/1,44 Oil UV objective with Immersion Oil Type A 518 F. For the excitation of GFP, 475 nm was used. Image analysis was done with the LAS X software and further processing of images was performed in Fiji/ImageJ.

6.3.10. Flow cytometry

For fluorescence intensity measurements, yeast cells were either grown YEPD or SLac + 0.2% glucose medium to mid-log phase. 1 OD_{600} of cells was harvested and cell pellets were resuspended in 500 µl PBS. The fluorescence intensity of 100,000 cells per strain was measured using the Attune™ Flow Cytometer (Thermo Fisher). Each strain was measured in biological triplicates. Data analysis was performed using the FlowJo™ software, version 10. For quantification, the mean values of the fluorescence intensities measured for each strain were calculated.

6.4. Protein Biochemistry Methods

6.4.1. Whole cell lysates

For whole cell lysates, yeast strains were cultivated in liquid medium to mid-log phase. Cells equally to 4 OD_{600} were harvested by centrifugation (16,000 g, 1 min, RT), washed with sterile ddH_2O, and resuspended in 160 µl reducing loading buffer. Cells were transferred to screw-cap tubes containing 1 mm glass beads. Cell lysis was performed using a FastPrep-24 5G homogenizer (MP Biomedicals, Heidelberg, Germany) with 3 cycles of 30 s, speed 8.0 m/s, 120 s breaks, glass beads) at 4°C. Lysates were boiled at 96°C for 5 min and stored at -20°C until further use. Equal sample amounts were analyzed via SDS-PAGE.

6.4.2. SDS-Polyacrylamide gel electrophoresis

Sodiumdodecylsulfate polyacrylamide gel electrophoresis (SDS-PAGE) allows the separation of proteins by size. For the standard gel system, glass plates with a size of 160 x 180 mm and spacers with 1 mm thickness were sealed using a base gel, on top of which first the separation gel and then the stacking gel was placed. The composition of the gels is represented in Table 12. Before loading, samples were supplemented with reducing sample (Laemmli) buffer (50 mM Tris-HCl pH 6.8, 10% glycerin, 2% SDS, 0.01% bromophenol blue, 100 mM DTT). To determine protein sizes, the unstained marker from peQLab was used. The electrophoresis was conducted at 25 mA for 2.5 - 3 h in SDS running buffer (25 mM Tris-HCl pH 8.3, 190 mM glycine, 0.1% SDS).

Table 12: Gel composition for SDS-PAGE. Composition of the stacking, running and base gel.

Gel	Composition
Stacking gel	5% acrylamide 0.03% bisacrylamide 60 mM Tris-HCl at pH 6.8 0.1% SDS 0.05% ammonium persulfate 0.1% N,N,N',N'-Tetramethylethylenediamine
Running gel	16% acrylamide 0.11% bisacrylamide 375 mM Tris-HCl at pH 8.8 0.1% SDS 0.1% ammonium persulfate 0.03% N,N,N',N'-Tetramethylethylenediamine
Base gel	20% acrylamide 0.13% bisacrylamide 375 mM Tris-HCl at pH 8.8 0.1% SDS 0.05% ammonium persulfate 0.1% N,N,N',N'-Tetramethylethylenediamine

6.4.3. Transfer of proteins to nitrocellulose membranes (Western Blot)

The semi-dry blotting method was used to transfer proteins from SDS-gels to nitrocellulose membranes [199]. The gel was placed onto a nitrocellulose membrane. It was covered with two Whatman papers below and one Whatman paper on top of it. The stack was soaked in blotting buffer (20 mM Tris, 150 mM glycine, 0.08% SDS, 20% methanol), arranged in this order on the anode transfer module and covered with the cathode transfer module. The transfer of proteins from the gel onto the membrane was performed for 1.5 h at 1.3 mA/cm^2. To detect proteins on the nitrocellulose membrane, it was stained with Ponceau S solution (0.2% (w/v) Ponceau S, 3% (w/v) acetic acid) for 5 min.

6.4.4. Immune decoration of cellulose membranes

Proteins transferred onto a nitrocellulose membrane were visualized by immune decoration with specific antibodies. After staining the membrane with Ponceau S, it was incubated for 1 h at RT with 5% (w/v) nonfat dry milk in 1x TBS buffer (10 mM Tris/HCl at pH 7.5, 150 mM NaCl) to block non-specific protein binding sites. Then, the blocking solution was replaced by

a solution containing the specific primary antibody diluted in 5% milk in 1xTBS. The membrane was incubated in this solution overnight at 4°C, washed 3x 5 min with 1xTBS, followed by incubation with the secondary antibody (dilution of 1:10,000 in 5% milk in 1xTBS) for 1 h at RT. After washing 3x with 1x TBS, the membrane was coated with a 1:1 mix of ECL solutions (ECL 1: 100 mM Tris/HCl at pH 8.5, 0.044% (w/v) luminol, 0.0066% p-coumaric acid; ECL 2: 100 mM Tris/HCl at pH 8.5, 0.03% H_2O_2). Luminescence signals were detected using the ChemiDoc™ MP Imaging System (Bio-Rad). or Super RX Medical X-Ray Films (Fuji) using the Optimax Type TR-developer (MS Laborgeräte).

6.4.5. Antibodies used in this study

If not further specified, antibodies were raised in rabbits using recombinant purified proteins. The anti-rabbit secondary antibody was obtained from Bio-Rad (Goat Anti-Rabbit IgG (H+L)-HRP Conjugate #172-1019). The monoclonal anti-TOMM34 antibodies were raised in mice and were a gift from the Petr Müller lab (University of Brno, Czech Republic). Details about the antibodies used in this study are listed in Table 13.

Table 13: Antibodies used in this study. Listed are the antibody names, the used dilutions and their sources.

Name	Dilution	Source
Anti-Su9-DHFR	1:500	Herrmann lab
Anti-GFP	1:500	Herrmann lab
Anti-Oxa1	1:500	Herrmann lab
Anti-Mam33	1:500	Herrmann lab
Anti-Sod1	1:1,000	Herrmann lab
Anti-TOMM34 (2.1/#1), (3.1/#2)	undiluted	Kind gift from the Petr Müller lab

6.4.6. *In vitro* protein import into isolated mitochondria

For the synthesis of ^{35}S-methionine-labeled proteins in reticulocyte lysate, the TNT® Quick Coupled Transcription/Translation Kit from Promega was used. If not indicated otherwise, 50 µg of mitochondria were incubated in import buffer (500 mM sorbitol, 50 mM Hepes pH 7.4, 80 mM KCl, 10 mM and 2 mM KH_2PO_4), 2 mM ATP and 2 mM NADH for 10 min at 30°C and 650 rpm. As a negative control, 2% (v/v) VAO (55.6 µg/ml Valinomycin, 440 µg/ml Antimycin A, 850 µg/ml Oligomycin in ethanol (>99.8 %, p.a.)) was added to the import buffer instead of ATP and NADH. The import reaction was started by the addition of 1% (v/v)

reticulocyte lysate. Samples were taken after the indicated time points and the reaction was stopped by a 1:10 dilution in ice-cold SH buffer (0.6 M sorbitol, 20 mM HEPES/KOH at pH 7.4). For the removal of non-imported proteins, samples were supplemented with 100 µg/ml proteinase K (PK). After incubation for 30 min on ice, 2 mM phenylmethylsulfonyl fluoride (PMSF) was added to inhibit the protease. The samples were centrifuged for 15 min at 30,000 g and 4°C. The mitochondria were washed with 500 µl SH/KCl-buffer (0.6 M sorbitol, 20 mM HEPES/KOH at pH 7.4, 150 mM KCl) containing 2 mM PMSF. After centrifugation for 15 min at 30,000 g and 4°C, the mitochondria were resuspended in reducing sample buffer and analyzed via SDS-PAGE and autoradiography.

6.4.7. Ammonium sulfate precipitation and denaturation of proteins

A saturated ammonium sulfate (AS) solution was prepared by dissolving 400 mg AS in 500 µl H_2O. The solution was incubated for 30 min at 96°C and afterwards put on ice. After precipitation of excess AS, the supernatant was transferred into a fresh Eppendorf tube. For protein precipitation of ^{35}S-methionine-labeled proteins in reticulocyte, 8 µl of saturated AS solution were added to 10 µl of lysate and mixed thoroughly. Additional 8 µl of saturated AS solution were added in a second step and again mixed thoroughly. After incubating for 30 min on ice, the samples were centrifuged for 10 min at 16,000 g and 4°C. The supernatant was removed, and the precipitated proteins were resuspended in a denaturation buffer (8 M urea, 100 mM DTT, and 20 mM Tris pH 7.4) and incubated for 5 min at 25°C prior to the use in import experiments.

6.4.8. Autoradiography

Radioactive proteins can be detected by autoradiography. Therefore, the dried cellulose membrane was exposed to a radio-sensitive film (Fuji Medical X-Ray Film Super RX or Kodak BioMax MR Film). After the desired exposure time, the film was developed using the developing machine Optimax TR (MS Laborgeräte). For quantification, the membrane was exposed to an imaging plate (Fujifilm) for phospho-imaging with the Typhoon FLA 7000 (GE Healthcare). The films were scanned in a greyscale 8-bit format and quantification was performed using the ImageQuant software.

6.4.9. Sample preparation and mass spectrometric identification of proteins

6.4.9.1. Co-immunoprecipitation of proteins in reticulocyte lysate

Co-immunoprecipitation followed by mass spectrometry was used for the identification of interactors of *in vitro* synthesized precursor proteins. For protein synthesis in reticulocyte lysate the TNT® Quick Coupled Transcription/Translation System (Promega) was used and performed according to the manufacture's protocol employing 1 mM unlabeled methionine. Anti-Su9-DHFR antibody (Herrmann lab) was pre-coupled to activated Protein A beads (Amintra Protein A Resin #APA0100) in IP buffer (10 mM This/HCl at pH 7.5, 150 mM NaCl, 0.5 mM EDTA at pH 8.0, 1 mM PMSF) for 30 min at 4°C. Beads were washed once with IP buffer. Reticulocyte lysates were incubated with antibody-bound beads in IP buffer tumbling end-over-end for 15 min at 4°C. After discarding the supernatant, the beads were washed twice with wash buffer (50 mM Tris pH 7.5, 150 mM NaCl, 5% Glycerol). For on-bead digestion, elution buffer I (2 M Urea, 50 mM Tris pH 7.5, 1 mM DTT and 5 ng/µl Trypsin (Promega, #V5111)) was added and samples were incubated for 1 h at RT. The supernatant was transferred into a fresh Eppendorf tube. For a second elution step, elution buffer II (2 M urea, 50 mM Tris pH 7.5, 5 mM chloroacetaldehyde, 5 ng/µl trypsin) was added to the beads and the samples were incubated for 30 min at RT. The supernatant of the first and second elution steps were combined and incubated overnight in the dark at 37°C. Peptides were acidified to a pH<2 using Tris-fluoracetic acid and desalted on in-house-prepared StageTips containing Empore C_{18} disks [200]. StageTips were activated with 100 µl methanol and twice with 100 µl buffer A (0.1% formic acid). Acidified peptides were loaded onto the StageTips and washed with 100 µl buffer A. Peptides were eluted by addition of 40 µl buffer B (80% acetonitrile, 0.1% formic acid in MS grad water) and dried using a speed vac. Samples were resolubilized in 9 µl buffer A and 1 µl buffer A* (2% acetonitrile, 0.1% tri-flouracetic acid in MS grad water).

Half of the sample was separated with an EASY-nLC 1200 ultra-high-pressure liquid chromatography system connected in-line to a Q-Exactive HF Mass Spectrometer (Thermo Fisher Scientific). Chromatography columns (50 cm, 75 mm inner diameter) were packed in house with ReproSil-Pur C18-AQ 1.9 µm resin (Dr. Maisch GmbH). Peptides were loaded in buffer A (0.1% formic acid) and eluted with a non-linear gradient of 5–60% buffer B (0.1% formic acid, 80% acetonitrile) at a rate of 250 nl/min over 90 min. Column temperature was maintained at 60 °C. Data acquisition alternated between a full scan (60 K resolution, maximum injection time of 20 ms, AGC target of 3e6) and 15 data-dependent MS/MS scans (15 K

resolution, maximum injection time of 80 ms, AGC target of 1e5). The isolation window was 1.4 m/z, and normalized collision energy was 28. Dynamic exclusion was set to 20 s.

6.4.9.2. Dynamic SILAC experiment and whole cell measurements of Δubc8 cells

For dynamic SILAC mass spectrometry (MS), YPH499 *Δarg4* wild type and Δ*ubc8* cells were cultured in SLac medium containing light [$^{14}N_2$, $^{12}C_6$]-lysine and [$^{14}N_4$, $^{12}C_6$]-arginine isotopes. Cells were diluted continuously to keep them in the exponential growth phase while increasing the culture volume stepwise up to 300 ml. For timepoint t(0) 100 ml of each culture were harvested (5,000 *g*, 5 min, RT), washed with sterile water, and shock frozen with liquid nitrogen. Samples were stored at -80°C for further analysis. To analyze the metabolic shift (Fig.2, S2), 2x100 ml of every culture was harvested (5,000 *g*, 5 min, RT) and washed with 30 ml SLac medium without lysine and arginine (5,000 *g*, 5 min, RT). Cells were resuspended in 200 ml SLac+2% glucose or SLac as control. Both media only contained the heavy amino acid isotopes of lysine ($^{15}N_2$, $^{13}C_6$) and arginine ($^{15}N_4$, $^{13}C_6$). Cultures were incubated at 30°C and 130 rpm for one doubling time of the cells. Cell growth was continuously monitored by measuring OD_{600}. Samples (t(1) Gluc and t(1) Lac) were harvested and treated like described before for the samples t(0).

MS samples were prepared according to a published protocol with minor adaptations[201]. Cell lysates from 25 OD were prepared in 100 µl lysis buffer (6 M guanidinium chloride, 10 mM TCEP-HCl, 40 mM chloroacetamide, 100 mM Tris pH 8.5) using a FastPrep-24 5 G homogenizer (MP Biomedicals) with 3 cycles of 20 s, speed 8.0 m/s, 120 s breaks, glass beads (Ø 0.5 mm) at 4°C. Samples were heated for 10 min at 96°C and afterwards centrifuged twice for 5 min at 16,000 g. In between the supernatant was transferred to fresh Eppendorf tubes to remove all remaining glass beads. Protein concentrations were measured using the Pierce BCA Protein Assay (Thermo Scientific, #23225). For protein digestion, 36 µg of protein was diluted 1:10 with LT-digestion buffer (10% acetonitrile, 25 mM Tris at pH 8.8). Trypsin (Sigma-Aldrich #T6567) and Lys-C (Wako #125-05061) were added to the samples (1:50 w/w). Samples were incubated over night at 37°C and 700 rpm. After 16 h, fresh Trypsin (1:100 w/w) was added for 30 min (37°C, 700 rpm). pH of samples was adjusted to pH <2 with trifluoroacetic acid (10%) and samples were centrifuged for 3 min at 16,000 g and RT. Desalting/mixed-Phase cleanup with 3 layers SDB-RPS stage tips (cat 2241). Samples were dried down in speed-vac and resolubilized in 12 µl buffer A++ (buffer A (0.1% formic acid) and buffer A* (2% acetonitrile and 0.1% trifluoracetic acid) in a ratio of 9:1)).

To analyze the metabolic shift by label-free mass spectrometry (Figure 24A, Figure S8), the respective yeast strains were cultured either continuously in YPG or glucose (final concentration: 2%) was added to the cultures for 4 h. 10 OD_{600} of cells were harvested (5,000 *g*, 5 min, RT) and washed with sterile water. Pellets were snap frozen in liquid nitrogen and stored at -80°C for further analysis. Samples were prepared for mass spectrometry as described above with minor changes: Cell lysates of 10 OD were prepared in 200 µl lysis buffer and 25 µg of protein was used for trypsin and Lys-C digest.

For both MS experiments, digested peptides were separated on reversed-phase columns (50 cm, 75 µm inner diameter packed in-house with C18 resin ReproSilPur 120, 1.9 µm diameter (Dr. Maisch) using an Easy-nLC 1200 system (Thermo Scientific) directly coupled to a Q Exactive HF mass spectrometer (Thermo Scientific). A 3 h gradient from 5% - 95% Solvent B (Solvent A: aqueous 0.1% formic acid; Solvent B: 80 % acetonitrile, 0.1% formic acid) at a constant flow rate of 250 nl/min was used to elute bound peptides.

MS data were processed using the MaxQuant software (version 1.6.10.43) [202–204] and a *Saccharomyces cerevisiae* proteome database obtained from UniProt. The paragraph 6.4.9 was adopted from my publications [111,112].

6.4.10. Mass spectrometry data analysis

6.4.10.1. Data analysis of the co-immunoprecipitation experiment described in 6.4.9.1

Raw mass spectrometry data were processed using MaxQuant (2.0.1.0). Peak lists were searched against a Uniprot database (UP000001811_9986) and the sequences Atp5-, Oxa1-, and Su9 presequences fused to DHFR, alongside 262 common contaminants using the Andromeda search engine. A 1% false discovery rate was applied for both peptides (minimum length: 7 amino acids) and proteins. The "Match between runs" (MBR) function was activated, with a maximum matching time window of 0.7 min and an alignment time window of 20 min. Relative protein quantities were calculated using the MaxLFQ algorithm, requiring a minimum ratio count of two. The calculation of iBAQ intensities was enabled.

The protein groups identified in each mass spectrometry data set were processed and analyzed in parallel using the R programming language (R version 4.2.2; R Core Team (2022). R: A language and environment for statistical computing. R Foundation for Statistical Computing, Vienna, Austria. Available online at https://www.R-project.org/.). First, the MaxQuant output data was filtered to remove contaminants, reverse hits, proteins identified by site only as well

as proteins that were identified in less than three replicates (N = 3). This resulted in 1200 robustly identified protein groups whose label-free quantification (LFQ) intensities were log2-transformed, batchcleaned using limma [205] and further normalized using variance stable normalization [206]. Lastly, missing values were imputed by sampling N = 3 values from a normal distribution (seed = 90853375) and using them whenever there are no valid values in a triplicate of a condition. Different for each data set, the mean of this normal distribution corresponds to the 1% percentile of LFQ intensities. Its standard deviation is determined as the median of LFQ intensity sample standard deviations calculated within and then averaged over each triplicate. Proteins were tested for differential expression using the limma package for the indicated pairwise comparison of samples and a Benjamini-Hochberg procedure was used to account for multiple testing [207].

Principal component analysis was carried out for each data set using the package *pcaMethods* [208] on the processed and standardized LFQ intensities of those protein groups with an ANOVA F-statistic p-value < 0.05 between all replicate groups to filter for proteins with a discernable degree of variance between conditions.

6.4.10.2. Data analysis of the dynamic SILAC and whole cell measurements described in 6.4.9.2

MaxQuant output files were processed using Perseus and the R programming language. Each condition was measured in four replicates. For the lactate to glucose shift experiment (Figure 21), proteins were filtered to contain at least 3 valid values in at least one of compared conditions. Log2 protein intensities (combined intensity of the heavy and light channel) were mean centered. For the dynamic SILAC experiment, the same normalization factors were applied to the individual light and heavy channel. To compare conditions, a Student's t-Test was performed and p-values were adjusted for multiple testing [207]. Hierarchical clustering (Figure 22A) was carried out in Perseus. Mean centered log2 protein intensities were filtered using a multiple-sample ANOVA test (FDR > 0.01, S0=1) implemented in Perseus and Z-scored protein intensities were clustered according to Euclidean distance. The heatmap was visualized in R using the pheatmap package. Gene set enrichment analysis was performed using Fisher's exact test. *p*-values of gene set enrichments were adjusted for multiple hypothesis testing using the Benjamini-Hochberg procedure [207].

For the label-free experiment (Figure 24A, Figure S8) proteins were filtered as described above and label-free quantitation (LFQ) protein intensities were cleaned for batch effects using limma [205] and further normalized using variance stabilization normalization [206]. Proteins were

tested for differential expression using the limma package and *p*-values were adjusted for multiple hypothesis testing using the Benjamini-Hochberg procedure [207]. The paragraph 6.4.10 was adopted from my publications [111,112].

7. REFERENCES

1. Palade GE. An electron microscope study of the mitochondrial structure. *J Histochem Cytochem Off J Histochem Soc*. 1953;1(4):188-211. doi:10.1177/1.4.188

2. Morgenstern M, Stiller SB, Lübbert P, et al. Definition of a High-Confidence Mitochondrial Proteome at Quantitative Scale. *Cell Rep*. 2017;19(13):2836-2852. doi:10.1016/j.celrep.2017.06.014

3. Rath S, Sharma R, Gupta R, et al. MitoCarta3.0: an updated mitochondrial proteome now with sub-organelle localization and pathway annotations. *Nucleic Acids Res*. 2021;49(D1):D1541-D1547. doi:10.1093/nar/gkaa1011

4. Lesnik C, Cohen Y, Atir-Lande A, Schuldiner M, Arava Y. OM14 is a mitochondrial receptor for cytosolic ribosomes that supports co-translational import into mitochondria. *Nat Commun*. 2014;5(1):5711. doi:10.1038/ncomms6711

5. MUKHOPADHYAY A, NI L, WEINER H. A co-translational model to explain the in vivo import of proteins into HeLa cell mitochondria. *Biochem J*. 2004;382(1):385-392. doi:10.1042/BJ20040065

6. Williams CC, Jan CH, Weissman JS. Targeting and plasticity of mitochondrial proteins revealed by proximity-specific ribosome profiling. *Science*. 2014;346(6210):748-751. doi:10.1126/science.1257522

7. Busch JD, Fielden LF, Pfanner N, Wiedemann N. Mitochondrial protein transport: Versatility of translocases and mechanisms. *Mol Cell*. 2023;83(6):890-910. doi:10.1016/j.molcel.2023.02.020

8. Young JC, Hoogenraad NJ, Hartl FU. Molecular chaperones Hsp90 and Hsp70 deliver preproteins to the mitochondrial import receptor Tom70. *Cell*. 2003;112(1):41-50. doi:10.1016/s0092-8674(02)01250-3

9. Rödl S, Herrmann JM. The role of the proteasome in mitochondrial protein quality control. *IUBMB Life*. 2023;75(10):868-879. doi:10.1002/iub.2734

10. Vögtle FN, Wortelkamp S, Zahedi RP, et al. Global analysis of the mitochondrial N-proteome identifies a processing peptidase critical for protein stability. *Cell*. 2009;139(2):428-439. doi:10.1016/j.cell.2009.07.045

11. Calvo SE, Julien O, Clauser KR, et al. Comparative Analysis of Mitochondrial N-Termini from Mouse, Human, and Yeast. *Mol Cell Proteomics MCP*. 2017;16(4):512-523. doi:10.1074/mcp.M116.063818

12. von Heijne G. Mitochondrial targeting sequences may form amphiphilic helices. *EMBO J*. 1986;5(6):1335-1342. doi:10.1002/j.1460-2075.1986.tb04364.x

13. Hawlitschek G, Schneider H, Schmidt B, Tropschug M, Hartl FU, Neupert W. Mitochondrial protein import: identification of processing peptidase and of PEP, a processing enhancing protein. *Cell*. 1988;53(5):795-806. doi:10.1016/0092-8674(88)90096-7

14. Taskin AA, Kücükköse C, Burger N, Mossmann D, Meisinger C, Vögtle FN. The novel mitochondrial matrix protease Ste23 is required for efficient presequence degradation and processing. *Mol Biol Cell*. 2017;28(8):997-1002. doi:10.1091/mbc.E16-10-0732

15. Kambacheld M, Augustin S, Tatsuta T, Müller S, Langer T. Role of the novel metallopeptidase Mop112 and saccharolysin for the complete degradation of proteins residing in different subcompartments of mitochondria. *J Biol Chem*. 2005;280(20):20132-20139. doi:10.1074/jbc.M500398200

16. Rospert S, Junne T, Glick BS, Schatz G. Cloning and disruption of the gene encoding yeast mitochondrial chaperonin 10, the homolog of E. coli groES. *FEBS Lett*. 1993;335(3):358-360. doi:10.1016/0014-5793(93)80419-u

17. Boos F, Mühlhaus T, Herrmann JM. Detection of Internal Matrix Targeting Signal-like Sequences (iMTS-Ls) in Mitochondrial Precursor Proteins Using the TargetP Prediction Tool. *Bio-Protoc*. 2018;8(17):e2474. doi:10.21769/BioProtoc.2474

18. Hurt EC, Pesold-Hurt B, Schatz G. The cleavable prepiece of an imported mitochondrial protein is sufficient to direct cytosolic dihydrofolate reductase into the mitochondrial matrix. *FEBS Lett*. 1984;178(2):306-310. doi:10.1016/0014-5793(84)80622-5

19. Backes S, Hess S, Boos F, et al. Tom70 enhances mitochondrial preprotein import efficiency by binding to internal targeting sequences. *J Cell Biol*. 2018;217(4):1369-1382. doi:10.1083/jcb.201708044

20. Friedl J, Knopp MR, Groh C, et al. More than just a ticket canceller: the mitochondrial processing peptidase tailors complex precursor proteins at internal cleavage sites. *Mol Biol Cell*. 2020;31(24):2657-2668. doi:10.1091/mbc.E20-08-0524

21. Glick BS, Brandt A, Cunningham K, Müller S, Hallberg RL, Schatz G. Cytochromes c1 and b2 are sorted to the intermembrane space of yeast mitochondria by a stop-transfer mechanism. *Cell*. 1992;69(5):809-822. doi:10.1016/0092-8674(92)90292-k

22. Nunnari J, Fox TD, Walter P. A mitochondrial protease with two catalytic subunits of nonoverlapping specificities. *Science*. 1993;262(5142):1997-2004. doi:10.1126/science.8266095

23. Schneider A, Behrens M, Scherer P, Pratje E, Michaelis G, Schatz G. Inner membrane protease I, an enzyme mediating intramitochondrial protein sorting in yeast. *EMBO J*. 1991;10(2):247-254. doi:10.1002/j.1460-2075.1991.tb07944.x

24. Sideris DP, Petrakis N, Katrakili N, et al. A novel intermembrane space-targeting signal docks cysteines onto Mia40 during mitochondrial oxidative folding. *J Cell Biol*. 2009;187(7):1007-1022. doi:10.1083/jcb.200905134

25. Milenkovic D, Ramming T, Müller JM, et al. Identification of the signal directing Tim9 and Tim10 into the intermembrane space of mitochondria. *Mol Biol Cell*. 2009;20(10):2530-2539. doi:10.1091/mbc.e08-11-1108

26. Endres M, Neupert W, Brunner M. Transport of the ADP/ATP carrier of mitochondria from the TOM complex to the TIM22.54 complex. *EMBO J*. 1999;18(12):3214-3221. doi:10.1093/emboj/18.12.3214

27. Pfanner N, Hoeben P, Tropschug M, Neupert W. The carboxyl-terminal two-thirds of the ADP/ATP carrier polypeptide contains sufficient information to direct translocation into mitochondria. *J Biol Chem*. 1987;262(31):14851-14854.

28. Fölsch H, Guiard B, Neupert W, Stuart RA. Internal targeting signal of the BCS1 protein: a novel mechanism of import into mitochondria. *EMBO J*. 1996;15(3):479-487.

29. Meier S, Neupert W, Herrmann JM. Proline residues of transmembrane domains determine the sorting of inner membrane proteins in mitochondria. *J Cell Biol*. 2005;170(6):881-888. doi:10.1083/jcb.200505126

30. Kutik S, Stojanovski D, Becker L, et al. Dissecting Membrane Insertion of Mitochondrial β-Barrel Proteins. *Cell*. 2008;132(6):1011-1024. doi:10.1016/j.cell.2008.01.028

31. Jores T, Klinger A, Groß LE, et al. Characterization of the targeting signal in mitochondrial β-barrel proteins. *Nat Commun*. 2016;7:12036. doi:10.1038/ncomms12036

32. Brix J, Dietmeier K, Pfanner N. Differential Recognition of Preproteins by the Purified Cytosolic Domains of the Mitochondrial Import Receptors Tom20, Tom22, and Tom70*. *J Biol Chem*. 1997;272(33):20730-20735. doi:10.1074/jbc.272.33.20730

33. Zhou X, Yang Y, Wang G, et al. Molecular pathway of mitochondrial preprotein import through the TOM-TIM23 supercomplex. *Nat Struct Mol Biol*. 2023;30(12):1996-2008. doi:10.1038/s41594-023-01103-7

34. Araiso Y, Tsutsumi A, Qiu J, et al. Structure of the mitochondrial import gate reveals distinct preprotein paths. *Nature*. 2019;575(7782):395-401. doi:10.1038/s41586-019-1680-7

35. Fielden LF, Busch JD, Merkt SG, et al. Central role of Tim17 in mitochondrial presequence protein translocation. *Nature*. 2023;621(7979):627-634. doi:10.1038/s41586-023-06477-8

36. Sim SI, Chen Y, Lynch DL, Gumbart JC, Park E. Structural basis of mitochondrial protein import by the TIM23 complex. *Nature*. 2023;621(7979):620-626. doi:10.1038/s41586-023-06239-6

37. Ieva R, Schrempp SG, Opaliński L, et al. Mgr2 functions as lateral gatekeeper for preprotein sorting in the mitochondrial inner membrane. *Mol Cell*. 2014;56(5):641-652. doi:10.1016/j.molcel.2014.10.010

38. Mokranjac D. How to get to the other side of the mitochondrial inner membrane - the protein import motor. *Biol Chem*. 2020;401(6-7):723-736. doi:10.1515/hsz-2020-0106

39. Mesecke N, Terziyska N, Kozany C, et al. A disulfide relay system in the intermembrane space of mitochondria that mediates protein import. *Cell*. 2005;121(7):1059-1069. doi:10.1016/j.cell.2005.04.011

40. Sirrenberg C, Bauer MF, Guiard B, Neupert W, Brunner M. Import of carrier proteins into the mitochondrial inner membrane mediated by Tim22. *Nature*. 1996;384(6609):582-585. doi:10.1038/384582a0

41. Wiedemann N, Truscott KN, Pfannschmidt S, Guiard B, Meisinger C, Pfanner N. Biogenesis of the protein import channel Tom40 of the mitochondrial outer membrane: intermembrane space components are involved in an early stage of the assembly pathway. *J Biol Chem*. 2004;279(18):18188-18194. doi:10.1074/jbc.M400050200

42. Wiedemann N, Kozjak V, Chacinska A, et al. Machinery for protein sorting and assembly in the mitochondrial outer membrane. *Nature*. 2003;424(6948):565-571. doi:10.1038/nature01753

43. Takeda H, Tsutsumi A, Nishizawa T, et al. Mitochondrial sorting and assembly machinery operates by β-barrel switching. *Nature*. 2021;590(7844):163-169. doi:10.1038/s41586-020-03113-7

44. Takeda H, Busto JV, Lindau C, et al. A multipoint guidance mechanism for β-barrel folding on the SAM complex. *Nat Struct Mol Biol*. 2023;30(2):176-187. doi:10.1038/s41594-022-00897-2

45. Becker T, Wenz LS, Krüger V, et al. The mitochondrial import protein Mim1 promotes biogenesis of multispanning outer membrane proteins. *J Cell Biol*. 2011;194(3):387. doi:10.1083/jcb.201102044

46. Dimmer KS, Papić D, Schumann B, et al. A crucial role for Mim2 in the biogenesis of mitochondrial outer membrane proteins. *J Cell Sci*. 2012;125(14):3464-3473. doi:10.1242/jcs.103804

47. Papic D, Krumpe K, Dukanovic J, Dimmer KS, Rapaport D. Multispan mitochondrial outer membrane protein Ugo1 follows a unique Mim1-dependent import pathway. *J Cell Biol*. 2011;194(3):397-405. doi:10.1083/jcb.201102041

48. Doan KN, Grevel A, Mårtensson CU, et al. The Mitochondrial Import Complex MIM Functions as Main Translocase for α-Helical Outer Membrane Proteins. *Cell Rep*. 2020;31(4):107567. doi:10.1016/j.celrep.2020.107567

49. Murakami H, Pain D, Blobel G. 70-kD heat shock-related protein is one of at least two distinct cytosolic factors stimulating protein import into mitochondria. *J Cell Biol*. 1988;107(6 Pt 1):2051-2057. doi:10.1083/jcb.107.6.2051

50. Deshaies RJ, Koch BD, Werner-Washburne M, Craig EA, Schekman R. A subfamily of stress proteins facilitates translocation of secretory and mitochondrial precursor polypeptides. *Nature*. 1988;332(6167):800-805. doi:10.1038/332800a0

51. Zhu X, Zhao X, Burkholder WF, et al. Structural analysis of substrate binding by the molecular chaperone DnaK. *Science*. 1996;272(5268):1606-1614. doi:10.1126/science.272.5268.1606

52. Flaherty KM, DeLuca-Flaherty C, McKay DB. Three-dimensional structure of the ATPase fragment of a 70K heat-shock cognate protein. *Nature*. 1990;346(6285):623-628. doi:10.1038/346623a0

53. Blond-Elguindi S, Cwirla SE, Dower WJ, et al. Affinity panning of a library of peptides displayed on bacteriophages reveals the binding specificity of BiP. *Cell*. 1993;75(4):717-728. doi:10.1016/0092-8674(93)90492-9

54. Flynn GC, Pohl J, Flocco MT, Rothman JE. Peptide-binding specificity of the molecular chaperone BiP. *Nature*. 1991;353(6346):726-730. doi:10.1038/353726a0

55. Fourie AM, Sambrook JF, Gething MJ. Common and divergent peptide binding specificities of hsp70 molecular chaperones. *J Biol Chem*. 1994;269(48):30470-30478.

56. Gragerov A, Zeng L, Zhao X, Burkholder W, Gottesman ME. Specificity of DnaK-peptide binding. *J Mol Biol*. 1994;235(3):848-854. doi:10.1006/jmbi.1994.1043

57. Endo T, Mitsui S, Nakai M, Roise D. Binding of mitochondrial presequences to yeast cytosolic heat shock protein 70 depends on the amphiphilicity of the presequence. *J Biol Chem*. 1996;271(8):4161-4167. doi:10.1074/jbc.271.8.4161

58. Nemoto T, Ohara-Nemoto Y, Ota M, Takagi T, Yokoyama K. Mechanism of dimer formation of the 90-kDa heat-shock protein. *Eur J Biochem*. 1995;233(1):1-8. doi:10.1111/j.1432-1033.1995.001_1.x

59. Chen S, Smith DF. Hop as an Adaptor in the Heat Shock Protein 70 (Hsp70) and Hsp90 Chaperone Machinery*. *J Biol Chem*. 1998;273(52):35194-35200. doi:10.1074/jbc.273.52.35194

60. Schmid AB, Lagleder S, Gräwert MA, et al. The architecture of functional modules in the Hsp90 co-chaperone Sti1/Hop. *EMBO J*. 2012;31(6):1506-1517. doi:10.1038/emboj.2011.472

61. Hernández MP, Sullivan WP, Toft DO. The assembly and intermolecular properties of the hsp70-Hop-hsp90 molecular chaperone complex. *J Biol Chem*. 2002;277(41):38294-38304. doi:10.1074/jbc.M206566200

62. Lott A, Oroz J, Zweckstetter M. Molecular basis of the interaction of Hsp90 with its co-chaperone Hop. *Protein Sci Publ Protein Soc*. 2020;29(12):2422-2432. doi:10.1002/pro.3969

63. Das AK, Cohen PW, Barford D. The structure of the tetratricopeptide repeats of protein phosphatase 5: implications for TPR-mediated protein-protein interactions. *EMBO J*. 1998;17(5):1192-1199. doi:10.1093/emboj/17.5.1192

64. Sikorski RS, Boguski MS, Goebl M, Hieter P. A repeating amino acid motif in CDC23 defines a family of proteins and a new relationship among genes required for mitosis and RNA synthesis. *Cell*. 1990;60(2):307-317. doi:10.1016/0092-8674(90)90745-z

65. Perez-Riba A, Itzhaki LS. The tetratricopeptide-repeat motif is a versatile platform that enables diverse modes of molecular recognition. *Curr Opin Struct Biol*. 2019;54:43-49. doi:10.1016/j.sbi.2018.12.004

66. Chen S, Sullivan WP, Toft DO, Smith DF. Differential interactions of p23 and the TPR-containing proteins Hop, Cyp40, FKBP52 and FKBP51 with Hsp90 mutants. *Cell Stress Chaperones*. 1998;3(2):118-129. doi:10.1379/1466-1268(1998)003<0118:diopat>2.3.co;2

67. Scheufler C, Brinker A, Bourenkov G, et al. Structure of TPR domain-peptide complexes: critical elements in the assembly of the Hsp70-Hsp90 multichaperone machine. *Cell*. 2000;101(2):199-210. doi:10.1016/S0092-8674(00)80830-2

68. Faou P, Hoogenraad NJ. Tom34: A cytosolic cochaperone of the Hsp90/Hsp70 protein complex involved in mitochondrial protein import. *Biochim Biophys Acta BBA - Mol Cell Res*. 2012;1823(2):348-357. doi:10.1016/j.bbamcr.2011.12.001

69. Hoseini H, Pandey S, Jores T, et al. The cytosolic cochaperone Sti1 is relevant for mitochondrial biogenesis and morphology. *FEBS J*. 2016;283(18):3338-3352. doi:10.1111/febs.13813

70. Belle A, Tanay A, Bitincka L, Shamir R, O'Shea EK. Quantification of protein half-lives in the budding yeast proteome. *Proc Natl Acad Sci U S A*. 2006;103(35):13004-13009. doi:10.1073/pnas.0605420103

71. Finley D, Ulrich HD, Sommer T, Kaiser P. The ubiquitin-proteasome system of Saccharomyces cerevisiae. *Genetics*. 2012;192(2):319-360. doi:10.1534/genetics.112.140467

72. McGrath JP, Jentsch S, Varshavsky A. UBA 1: an essential yeast gene encoding ubiquitin-activating enzyme. *EMBO J*. 1991;10(1):227-236. doi:10.1002/j.1460-2075.1991.tb07940.x

73. Peng J, Schwartz D, Elias JE, et al. A proteomics approach to understanding protein ubiquitination. *Nat Biotechnol*. 2003;21(8):921-926. doi:10.1038/nbt849

74. Chau V, Tobias JW, Bachmair A, et al. A multiubiquitin chain is confined to specific lysine in a targeted short-lived protein. *Science*. 1989;243(4898):1576-1583. doi:10.1126/science.2538923

75. Finley D. Recognition and processing of ubiquitin-protein conjugates by the proteasome. *Annu Rev Biochem*. 2009;78:477-513. doi:10.1146/annurev.biochem.78.081507.101607

76. Welchman RL, Gordon C, Mayer RJ. Ubiquitin and ubiquitin-like proteins as multifunctional signals. *Nat Rev Mol Cell Biol*. 2005;6(8):599-609. doi:10.1038/nrm1700

77. Twomey EC, Ji Z, Wales TE, et al. Substrate processing by the Cdc48 ATPase complex is initiated by ubiquitin unfolding. *Science*. 2019;365(6452):eaax1033. doi:10.1126/science.aax1033

78. Rumpf S, Jentsch S. Functional division of substrate processing cofactors of the ubiquitin-selective Cdc48 chaperone. *Mol Cell*. 2006;21(2):261-269. doi:10.1016/j.molcel.2005.12.014

79. Wu X, Li L, Jiang H. Doa1 targets ubiquitinated substrates for mitochondria-associated degradation. *J Cell Biol*. 2016;213(1):49-63. doi:10.1083/jcb.201510098

80. Vitali DG, Drwesh L, Cichocki BA, Kolb A, Rapaport D. The Biogenesis of Mitochondrial Outer Membrane Proteins Show Variable Dependence on Import Factors. *iScience*. 2020;23(1):100779. doi:10.1016/j.isci.2019.100779

81. Anton F, Dittmar G, Langer T, Escobar-Henriques M. Two deubiquitylases act on mitofusin and regulate mitochondrial fusion along independent pathways. *Mol Cell*. 2013;49(3):487-498. doi:10.1016/j.molcel.2012.12.003

82. Bragoszewski P, Gornicka A, Sztolsztener ME, Chacinska A. The ubiquitin-proteasome system regulates mitochondrial intermembrane space proteins. *Mol Cell Biol*. 2013;33(11):2136-2148. doi:10.1128/MCB.01579-12

83. Kowalski L, Bragoszewski P, Khmelinskii A, Glow E, Knop M, Chacinska A. Determinants of the cytosolic turnover of mitochondrial intermembrane space proteins. *BMC Biol*. 2018;16(1):66. doi:10.1186/s12915-018-0536-1

84. Wrobel L, Topf U, Bragoszewski P, et al. Mistargeted mitochondrial proteins activate a proteostatic response in the cytosol. *Nature*. 2015;524(7566):485-488. doi:10.1038/nature14951

85. Boos F, Krämer L, Groh C, et al. Mitochondrial protein-induced stress triggers a global adaptive transcriptional programme. *Nat Cell Biol*. 2019;21(4):442-451. doi:10.1038/s41556-019-0294-5

86. Hansen KG, Aviram N, Laborenz J, et al. An ER surface retrieval pathway safeguards the import of mitochondrial membrane proteins in yeast. *Science*. 2018;361(6407):1118-1122. doi:10.1126/science.aar8174

87. Shakya VP, Barbeau WA, Xiao T, Knutson CS, Schuler MH, Hughes AL. A nuclear-based quality control pathway for non-imported mitochondrial proteins. *eLife*. 2021;10:e61230. doi:10.7554/eLife.61230

88. Fry MY, Saladi SM, Cunha A, Clemons WM. Sequence-based features that are determinant for tail-anchored membrane protein sorting in eukaryotes. *Traffic Cph Den*. 2021;22(9):306-318. doi:10.1111/tra.12809

89. Matsumoto S, Nakatsukasa K, Kakuta C, Tamura Y, Esaki M, Endo T. Msp1 Clears Mistargeted Proteins by Facilitating Their Transfer from Mitochondria to the ER. *Mol Cell*. 2019;76(1):191-205.e10. doi:10.1016/j.molcel.2019.07.006

90. Dederer V, Khmelinskii A, Huhn AG, Okreglak V, Knop M, Lemberg MK. Cooperation of mitochondrial and ER factors in quality control of tail-anchored proteins. *eLife*. 2019;8:e45506. doi:10.7554/eLife.45506

91. Qin Q, Zhao T, Zou W, Shen K, Wang X. An Endoplasmic Reticulum ATPase Safeguards Endoplasmic Reticulum Identity by Removing Ectopically Localized Mitochondrial Proteins. *Cell Rep*. 2020;33(6):108363. doi:10.1016/j.celrep.2020.108363

92. McKenna MJ, Sim SI, Ordureau A, et al. The endoplasmic reticulum P5A-ATPase is a transmembrane helix dislocase. *Science*. 2020;369(6511):eabc5809. doi:10.1126/science.abc5809

93. Mårtensson CU, Priesnitz C, Song J, et al. Mitochondrial protein translocation-associated degradation. *Nature*. 2019;569(7758):679-683. doi:10.1038/s41586-019-1227-y

94. Schulte U, den Brave F, Haupt A, et al. Mitochondrial complexome reveals quality-control pathways of protein import. *Nature*. 2023;614(7946):153-159. doi:10.1038/s41586-022-05641-w

95. Ishii T, Funakoshi M, Kobayashi H. Yeast Pth2 is a UBL domain-binding protein that participates in the ubiquitin-proteasome pathway. *EMBO J*. 2006;25(23):5492-5503. doi:10.1038/sj.emboj.7601418

96. Funakoshi M, Sasaki T, Nishimoto T, Kobayashi H. Budding yeast Dsk2p is a polyubiquitin-binding protein that can interact with the proteasome. *Proc Natl Acad Sci U S A*. 2002;99(2):745-750. doi:10.1073/pnas.012585199

97. Kinner A, Kölling R. The yeast deubiquitinating enzyme Ubp16 is anchored to the outer mitochondrial membrane. *FEBS Lett*. 2003;549(1-3):135-140. doi:10.1016/s0014-5793(03)00801-9

98. Weidberg H, Amon A. MitoCPR-A surveillance pathway that protects mitochondria in response to protein import stress. *Science*. 2018;360(6385):eaan4146. doi:10.1126/science.aan4146

99. Basch M, Wagner M, Rolland S, et al. Msp1 cooperates with the proteasome for extraction of arrested mitochondrial import intermediates. *Mol Biol Cell*. 2020;31(8):753-767. doi:10.1091/mbc.E19-06-0329

100. Kostova KK, Hickey KL, Osuna BA, et al. CAT-tailing as a fail-safe mechanism for efficient degradation of stalled nascent polypeptides. *Science*. 2017;357(6349):414-417. doi:10.1126/science.aam7787

101. Izawa T, Park SH, Zhao L, Hartl FU, Neupert W. Cytosolic Protein Vms1 Links Ribosome Quality Control to Mitochondrial and Cellular Homeostasis. *Cell*. 2017;171(4):890-903.e18. doi:10.1016/j.cell.2017.10.002

102. Verma R, Reichermeier KM, Burroughs AM, et al. Vms1 and ANKZF1 peptidyl-tRNA hydrolases release nascent chains from stalled ribosomes. *Nature*. 2018;557(7705):446-451. doi:10.1038/s41586-018-0022-5

103. Schüle T, Rose M, Entian KD, Thumm M, Wolf DH. Ubc8p functions in catabolite degradation of fructose-1, 6-bisphosphatase in yeast. *EMBO J*. 2000;19(10):2161-2167. doi:10.1093/emboj/19.10.2161

104. Regelmann J, Schüle T, Josupeit FS, et al. Catabolite degradation of fructose-1,6-bisphosphatase in the yeast Saccharomyces cerevisiae: a genome-wide screen identifies eight novel GID genes and indicates the existence of two degradation pathways. *Mol Biol Cell*. 2003;14(4):1652-1663. doi:10.1091/mbc.e02-08-0456

105. Santt O, Pfirrmann T, Braun B, et al. The Yeast GID Complex, a Novel Ubiquitin Ligase (E3) Involved in the Regulation of Carbohydrate Metabolism. *Mol Biol Cell*. 2008;19(8):3323-3333. doi:10.1091/mbc.E08-03-0328

106. Melnykov A, Chen SJ, Varshavsky A. Gid10 as an alternative N-recognin of the Pro/N-degron pathway. *Proc Natl Acad Sci U S A*. 2019;116(32):15914-15923. doi:10.1073/pnas.1908304116

107. Chen SJ, Wu X, Wadas B, Oh JH, Varshavsky A. An N-end rule pathway that recognizes proline and destroys gluconeogenic enzymes. *Science*. 2017;355(6323):eaal3655. doi:10.1126/science.aal3655

108. Chrustowicz J, Sherpa D, Teyra J, et al. Multifaceted N-Degron Recognition and Ubiquitylation by GID/CTLH E3 Ligases. *J Mol Biol*. 2022;434(2):167347. doi:10.1016/j.jmb.2021.167347

109. Chiang HL, Schekman R. Regulated import and degradation of a cytosolic protein in the yeast vacuole. *Nature*. 1991;350(6316):313-318. doi:10.1038/350313a0

110. Hurt EC, Pesold-Hurt B, Suda K, Oppliger W, Schatz G. The first twelve amino acids (less than half of the pre-sequence) of an imported mitochondrial protein can direct mouse cytosolic dihydrofolate reductase into the yeast mitochondrial matrix. *EMBO J*. 1985;4(8):2061-2068.

111. Rödl S, Hoffman Y, Jung F, et al. A priority code in presequences: mitochondrial targeting signals assign specific import characteristics to precursor proteins. doi:https://doi.org/10.1101/2024.06.27.600981

112. Rödl S, den Brave F, Räschle M, et al. The metabolite-controlled ubiquitin conjugase Ubc8 promotes mitochondrial protein import. *Life Sci Alliance*. 2023;6(1):e202201526. doi:10.26508/lsa.202201526

113. Emanuelsson O, Brunak S, von Heijne G, Nielsen H. Locating proteins in the cell using TargetP, SignalP and related tools. *Nat Protoc*. 2007;2(4):953-971. doi:10.1038/nprot.2007.131

114. van Loon AP, Brändli AW, Schatz G. The presequences of two imported mitochondrial proteins contain information for intracellular and intramitochondrial sorting. *Cell*. 1986;44(5):801-812. doi:10.1016/0092-8674(86)90846-9

115. Funes S, Nargang FE, Neupert W, Herrmann JM. The Oxa2 Protein of Neurospora crassa Plays a Critical Role in the Biogenesis of Cytochrome Oxidase and Defines a Ubiquitous Subbranch of the Oxa1/YidC/Alb3 Protein Family. *Mol Biol Cell*. 2004;15(4):1853-1861. doi:10.1091/mbc.e03-11-0789

116. Rak M, Tetaud E, Duvezin-Caubet S, et al. A yeast model of the neurogenic ataxia retinitis pigmentosa (NARP) T8993G mutation in the mitochondrial ATP synthase-6 gene. *J Biol Chem*. 2007;282(47):34039-34047. doi:10.1074/jbc.M703053200

117. Nicholls SB, Chu J, Abbruzzese G, Tremblay KD, Hardy JA. Mechanism of a Genetically Encoded Dark-to-Bright Reporter for Caspase Activity*. *J Biol Chem*. 2011;286(28):24977-24986. doi:10.1074/jbc.M111.221648

118. Gilon T, Chomsky O, Kulka RG. Degradation signals for ubiquitin system proteolysis in Saccharomyces cerevisiae. *EMBO J*. 1998;17(10):2759-2766. doi:10.1093/emboj/17.10.2759

119. Sanchez MI, Ting AY. Publisher Correction: Directed evolution improves the catalytic efficiency of TEV protease. *Nat Methods*. 2020;17(2):242. doi:10.1038/s41592-019-0729-8

120. Matouschek A, Azem A, Ratliff K, Glick BS, Schmid K, Schatz G. Active unfolding of precursor proteins during mitochondrial protein import. *EMBO J*. 1997;16(22):6727-6736. doi:10.1093/emboj/16.22.6727

121. Backes S, Bykov YS, Flohr T, et al. The chaperone-binding activity of the mitochondrial surface receptor Tom70 protects the cytosol against mitoprotein-induced stress. *Cell Rep*. 2021;35(1):108936. doi:10.1016/j.celrep.2021.108936

122. Opaliński Ł, Song J, Priesnitz C, et al. Recruitment of Cytosolic J-Proteins by TOM Receptors Promotes Mitochondrial Protein Biogenesis. *Cell Rep*. 2018;25(8):2036-2043.e5. doi:10.1016/j.celrep.2018.10.083

123. Brinker A, Scheufler C, Von Der Mulbe F, et al. Ligand discrimination by TPR domains. Relevance and selectivity of EEVD-recognition in Hsp70 x Hop x Hsp90 complexes. *J Biol Chem*. 2002;277(22):19265-19275. doi:10.1074/jbc.M109002200

124. Pettersen EF, Goddard TD, Huang CC, et al. UCSF Chimera--a visualization system for exploratory research and analysis. *J Comput Chem*. 2004;25(13):1605-1612. doi:10.1002/jcc.20084

125. Schopf FH, Huber EM, Dodt C, et al. The Co-chaperone Cns1 and the Recruiter Protein Hgh1 Link Hsp90 to Translation Elongation via Chaperoning Elongation Factor 2. *Mol Cell*. 2019;74(1):73-87.e8. doi:10.1016/j.molcel.2019.02.011

126. Tesic M, Marsh JA, Cullinan SB, Gaber RF. Functional Interactions between Hsp90 and the Co-chaperones Cns1 and Cpr7 in *Saccharomyces cerevisiae**. *J Biol Chem*. 2003;278(35):32692-32701. doi:10.1074/jbc.M304315200

127. Edgar RC. MUSCLE: multiple sequence alignment with high accuracy and high throughput. *Nucleic Acids Res*. 2004;32(5):1792-1797. doi:10.1093/nar/gkh340

128. Chan NC, Likić VA, Waller RF, Mulhern TD, Lithgow T. The C-terminal TPR domain of Tom70 defines a family of mitochondrial protein import receptors found only in animals and fungi. *J Mol Biol*. 2006;358(4):1010-1022. doi:10.1016/j.jmb.2006.02.062

129. Laborenz J, Bykov YS, Knöringer K, et al. The ER protein Ema19 facilitates the degradation of nonimported mitochondrial precursor proteins. *Mol Biol Cell*. 2021;32(8):664-674. doi:10.1091/mbc.E20-11-0748

130. Koch C, Lenhard S, Räschle M, Prescianotto-Baschong C, Spang A, Herrmann JM. The ER-SURF pathway uses ER-mitochondria contact sites for protein targeting to mitochondria. *EMBO Rep*. 2024;25(4):2071-2096. doi:10.1038/s44319-024-00113-w

131. Hämmerle M, Bauer J, Rose M, et al. Proteins of newly isolated mutants and the amino-terminal proline are essential for ubiquitin-proteasome-catalyzed catabolite degradation of fructose-1,6-bisphosphatase of Saccharomyces cerevisiae. *J Biol Chem*. 1998;273(39):25000-25005. doi:10.1074/jbc.273.39.25000

132. Priesnitz C, Pfanner N, Becker T. Chapter 3 - Studying protein import into mitochondria. In: Pon LA, Schon EA, eds. *Methods in Cell Biology*. Vol 155. Mitochondria, 3rd Edition. Academic Press; 2020:45-79. doi:10.1016/bs.mcb.2019.11.006

133. Ellenrieder L, Opaliński Ł, Becker L, et al. Separating mitochondrial protein assembly and endoplasmic reticulum tethering by selective coupling of Mdm10. *Nat Commun*. 2016;7:13021. doi:10.1038/ncomms13021

134. Allison DS, Schatz G. Artificial mitochondrial presequences. *Proc Natl Acad Sci U S A*. 1986;83(23):9011-9015. doi:10.1073/pnas.83.23.9011

135. Vaca Jacome AS, Rabilloud T, Schaeffer-Reiss C, et al. N-terminome analysis of the human mitochondrial proteome. *Proteomics*. 2015;15(14):2519-2524. doi:10.1002/pmic.201400617

136. Schäfer JA, Bozkurt S, Michaelis JB, Klann K, Münch C. Global mitochondrial protein import proteomics reveal distinct regulation by translation and translocation machinery. *Mol Cell*. 2022;82(2):435-446.e7. doi:10.1016/j.molcel.2021.11.004

137. Yamamoto H, Fukui K, Takahashi H, et al. Roles of Tom70 in import of presequence-containing mitochondrial proteins. *J Biol Chem*. 2009;284(46):31635-31646. doi:10.1074/jbc.M109.041756

138. Baysal C, Pérez-González A, Eseverri Á, et al. Recognition motifs rather than phylogenetic origin influence the ability of targeting peptides to import nuclear-encoded recombinant proteins into rice mitochondria. *Transgenic Res*. 2020;29(1):37-52. doi:10.1007/s11248-019-00176-9

139. Nashed S, El Barbry H, Benchouaia M, et al. Functional mapping of N-terminal residues in the yeast proteome uncovers novel determinants for mitochondrial protein import. *PLoS Genet*. 2023;19(8):e1010848. doi:10.1371/journal.pgen.1010848

140. Fünfschilling U, Rospert S. Nascent polypeptide-associated complex stimulates protein import into yeast mitochondria. *Mol Biol Cell*. 1999;10(10):3289-3299. doi:10.1091/mbc.10.10.3289

141. Gautschi M, Lilie H, Fünfschilling U, et al. RAC, a stable ribosome-associated complex in yeast formed by the DnaK-DnaJ homologs Ssz1p and zuotin. *Proc Natl Acad Sci U S A*. 2001;98(7):3762-3767. doi:10.1073/pnas.071057198

142. Komiya T, Hachiya N, Sakaguchi M, Omura T, Mihara K. Recognition of mitochondria-targeting signals by a cytosolic import stimulation factor, MSF. *J Biol Chem*. 1994;269(49):30893-30897.

143. Döring K, Ahmed N, Riemer T, et al. Profiling Ssb-Nascent Chain Interactions Reveals Principles of Hsp70-Assisted Folding. *Cell*. 2017;170(2):298-311.e20. doi:10.1016/j.cell.2017.06.038

144. Trcka F, Durech M, Man P, Hernychova L, Muller P, Vojtesek B. The assembly and intermolecular properties of the Hsp70-Tomm34-Hsp90 molecular chaperone complex. *J Biol Chem*. 2014;289(14):9887-9901. doi:10.1074/jbc.M113.526046

145. Allan RK, Ratajczak T. Versatile TPR domains accommodate different modes of target protein recognition and function. *Cell Stress Chaperones*. 2011;16(4):353-367. doi:10.1007/s12192-010-0248-0

146. Nuttall SD, Hanson BJ, Mori M, Hoogenraad NJ. hTom34: a novel translocase for the import of proteins into human mitochondria. *DNA Cell Biol*. 1997;16(9):1067-1074. doi:10.1089/dna.1997.16.1067

147. Chewawiwat N, Yano M, Terada K, Hoogenraad NJ, Mori M. Characterization of the novel mitochondrial protein import component, Tom34, in mammalian cells. *J Biochem (Tokyo)*. 1999;125(4):721-727. doi:10.1093/oxfordjournals.jbchem.a022342

148. Morgenstern M, Peikert CD, Lübbert P, et al. Quantitative high-confidence human mitochondrial proteome and its dynamics in cellular context. *Cell Metab*. 2021;33(12):2464-2483.e18. doi:10.1016/j.cmet.2021.11.001

149. Mukhopadhyay A, Avramova LV, Weiner H. Tom34 unlike Tom20 does not interact with the leader sequences of mitochondrial precursor proteins. *Arch Biochem Biophys*. 2002;400(1):97-104. doi:10.1006/abbi.2002.2777

150. Su J, Tian X, Wang Z, Yang J, Sun S, Sui SF. Structure of the intact Tom20 receptor in the human translocase of the outer membrane complex. *PNAS Nexus*. 2024;3(7):pgae269. doi:10.1093/pnasnexus/pgae269

151. Wegele H, Haslbeck M, Reinstein J, Buchner J. Sti1 is a novel activator of the Ssa proteins. *J Biol Chem*. 2003;278(28):25970-25976. doi:10.1074/jbc.M301548200

152. Nicolet CM, Craig EA. Isolation and characterization of STI1, a stress-inducible gene from Saccharomyces cerevisiae. *Mol Cell Biol*. 1989;9(9):3638-3646. doi:10.1128/mcb.9.9.3638-3646.1989

153. Dolinski KJ, Cardenas ME, Heitman J. CNS1 encodes an essential p60/Sti1 homolog in Saccharomyces cerevisiae that suppresses cyclophilin 40 mutations and interacts with Hsp90. *Mol Cell Biol*. 1998;18(12):7344-7352. doi:10.1128/MCB.18.12.7344

154. Jores T, Lawatscheck J, Beke V, et al. Cytosolic Hsp70 and Hsp40 chaperones enable the biogenesis of mitochondrial β-barrel proteins. *J Cell Biol*. 2018;217(9):3091-3108. doi:10.1083/jcb.201712029

155. Cohen N, Aviram N, Schuldiner M. A systematic proximity ligation approach to studying protein-substrate specificity identifies the substrate spectrum of the Ssh1 translocon. *EMBO J*. 2023;42(11):e113385. doi:10.15252/embj.2022113385

156. Romei MG, Boxer SG. Split Green Fluorescent Proteins: Scope, Limitations, and Outlook. *Annu Rev Biophys*. 2019;48:19-44. doi:10.1146/annurev-biophys-051013-022846

157. Efficient proximity labeling in living cells and organisms with TurboID - PubMed. Accessed August 6, 2024. https://pubmed.ncbi.nlm.nih.gov/30125270/

158. Catlett MG, Kaplan KB. Sgt1p is a unique co-chaperone that acts as a client adaptor to link Hsp90 to Skp1p. *J Biol Chem*. 2006;281(44):33739-33748. doi:10.1074/jbc.M603847200

159. Lenhard S, Gerlich S, Khan A, et al. The Orf9b protein of SARS-CoV-2 modulates mitochondrial protein biogenesis. *J Cell Biol*. 2023;222(10):e202303002. doi:10.1083/jcb.202303002

160. Neikirk K, Marshall AG, Kula B, Smith N, LeBlanc S, Hinton A. MitoTracker: A useful tool in need of better alternatives. *Eur J Cell Biol*. 2023;102(4):151371. doi:10.1016/j.ejcb.2023.151371

161. Alconada A, Kübrich M, Moczko M, Hönlinger A, Pfanner N. The mitochondrial receptor complex: the small subunit Mom8b/Isp6 supports association of receptors with the general insertion pore and transfer of preproteins. *Mol Cell Biol*. 1995;15(11):6196-6205. doi:10.1128/MCB.15.11.6196

162. Hönlinger A, Bömer U, Alconada A, et al. Tom7 modulates the dynamics of the mitochondrial outer membrane translocase and plays a pathway-related role in protein import. *EMBO J*. 1996;15(9):2125-2137.

163. Dietmeier K, Hönlinger A, Bömer U, et al. Tom5 functionally links mitochondrial preprotein receptors to the general import pore. *Nature*. 1997;388(6638):195-200. doi:10.1038/40663

164. Hill K, Model K, Ryan MT, et al. Tom40 forms the hydrophilic channel of the mitochondrial import pore for preproteins [see comment]. *Nature*. 1998;395(6701):516-521. doi:10.1038/26780

165. van Wilpe S, Ryan MT, Hill K, et al. Tom22 is a multifunctional organizer of the mitochondrial preprotein translocase. *Nature*. 1999;401(6752):485-489. doi:10.1038/46802

166. Shiota T, Imai K, Qiu J, et al. Molecular architecture of the active mitochondrial protein gate. *Science*. 2015;349(6255):1544-1548. doi:10.1126/science.aac6428

167. Araiso Y, Endo T. Structural overview of the translocase of the mitochondrial outer membrane complex. *Biophys Physicobiology*. 2022;19:e190022. doi:10.2142/biophysico.bppb-v19.0022

168. Gerbeth C, Schmidt O, Rao S, et al. Glucose-induced regulation of protein import receptor Tom22 by cytosolic and mitochondria-bound kinases. *Cell Metab*. 2013;18(4):578-587. doi:10.1016/j.cmet.2013.09.006

169. Schmidt O, Harbauer AB, Rao S, et al. Regulation of mitochondrial protein import by cytosolic kinases. *Cell*. 2011;144(2):227-239. doi:10.1016/j.cell.2010.12.015

170. Zaman S, Lippman SI, Zhao X, Broach JR. How Saccharomyces responds to nutrients. *Annu Rev Genet*. 2008;42:27-81. doi:10.1146/annurev.genet.41.110306.130206

171. Rao S, Gerbeth C, Harbauer A, Mikropoulou D, Meisinger C, Schmidt O. Signaling at the gate: phosphorylation of the mitochondrial protein import machinery. *Cell Cycle Georget Tex*. 2011;10(13):2083-2090. doi:10.4161/cc.10.13.16054

172. Sakaue H, Shiota T, Ishizaka N, et al. Porin Associates with Tom22 to Regulate the Mitochondrial Protein Gate Assembly. *Mol Cell*. 2019;73(5):1044-1055.e8. doi:10.1016/j.molcel.2019.01.003

173. Rinaldi L, Senatore E, Iannucci R, Chiuso F, Feliciello A. Control of Mitochondrial Activity by the Ubiquitin Code in Health and Cancer. *Cells*. 2023;12(2):234. doi:10.3390/cells12020234

174. Yamano K, Tanaka-Yamano S, Endo T. Mdm10 as a dynamic constituent of the TOB/SAM complex directs coordinated assembly of Tom40. *EMBO Rep*. 2010;11(3):187-193. doi:10.1038/embor.2009.283

175. Stojanovski D, Guiard B, Kozjak-Pavlovic V, Pfanner N, Meisinger C. Alternative function for the mitochondrial SAM complex in biogenesis of α-helical TOM proteins. *J Cell Biol*. 2007;179(5):881-893. doi:10.1083/jcb.200706043

176. Harbauer AB, Zahedi RP, Sickmann A, Pfanner N, Meisinger C. The protein import machinery of mitochondria-a regulatory hub in metabolism, stress, and disease. *Cell Metab*. 2014;19(3):357-372. doi:10.1016/j.cmet.2014.01.010

177. Lathrop JT, Timko MP. Regulation by heme of mitochondrial protein transport through a conserved amino acid motif. *Science*. 1993;259(5094):522-525. doi:10.1126/science.8424176

178. Boopathi E, Srinivasan S, Fang JK, Avadhani NG. Bimodal protein targeting through activation of cryptic mitochondrial targeting signals by an inducible cytosolic endoprotease. *Mol Cell*. 2008;32(1):32-42. doi:10.1016/j.molcel.2008.09.008

179. Vongsamphanh R, Fortier PK, Ramotar D. Pir1p mediates translocation of the yeast Apn1p endonuclease into the mitochondria to maintain genomic stability. *Mol Cell Biol*. 2001;21(5):1647-1655. doi:10.1128/MCB.21.5.1647-1655.2001

180. De Rasmo D, Panelli D, Sardanelli AM, Papa S. cAMP-dependent protein kinase regulates the mitochondrial import of the nuclear encoded NDUFS4 subunit of complex I. *Cell Signal*. 2008;20(5):989-997. doi:10.1016/j.cellsig.2008.01.017

181. Strobel G, Zollner A, Angermayr M, Bandlow W. Competition of spontaneous protein folding and mitochondrial import causes dual subcellular location of major adenylate kinase. *Mol Biol Cell*. 2002;13(5):1439-1448. doi:10.1091/mbc.01-08-0396

182. Tripodi F, Cirulli C, Reghellin V, et al. CK2 activity is modulated by growth rate in Saccharomyces cerevisiae. *Biochem Biophys Res Commun*. 2010;398(1):44-50. doi:10.1016/j.bbrc.2010.06.028

183. Laborenz J, Hansen K, Prescianotto-Baschong C, Spang A, Herrmann JM. In vitro import experiments with semi-intact cells suggest a role of the Sec61 paralog Ssh1 in mitochondrial biogenesis. *Biol Chem*. 2019;400(9):1229-1240. doi:10.1515/hsz-2019-0196

184. Ford HC, Allen WJ, Pereira GC, Liu X, Dillingham MS, Collinson I. Towards a molecular mechanism underlying mitochondrial protein import through the TOM and TIM23 complexes. *eLife*. 2022;11:e75426. doi:10.7554/eLife.75426

185. Liu W, Duan X, Fang X, Shang W, Tong C. Mitochondrial protein import regulates cytosolic protein homeostasis and neuronal integrity. *Autophagy*. 2018;14(8):1293-1309. doi:10.1080/15548627.2018.1474991

186. Yofe I, Weill U, Meurer M, et al. One library to make them all: streamlining the creation of yeast libraries via a SWAp-Tag strategy. *Nat Methods*. 2016;13(4):371-378. doi:10.1038/nmeth.3795

187. Cruz-Zaragoza LD, Dennerlein S, Linden A, et al. An in vitro system to silence mitochondrial gene expression. *Cell*. 2021;184(23):5824-5837.e15. doi:10.1016/j.cell.2021.09.033

188. Casadaban MJ, Cohen SN. Analysis of gene control signals by DNA fusion and cloning in Escherichia coli. *J Mol Biol*. 1980;138(2):179-207. doi:10.1016/0022-2836(80)90283-1

189. Meselson M, Yuan R. DNA restriction enzyme from E. coli. *Nature*. 1968;217(5134):1110-1114. doi:10.1038/2171110a0

190. Winston F, Dollard C, Ricupero-Hovasse SL. Construction of a set of convenient Saccharomyces cerevisiae strains that are isogenic to S288C. *Yeast Chichester Engl*. 1995;11(1):53-55. doi:10.1002/yea.320110107

191. Giaever G, Chu AM, Ni L, et al. Functional profiling of the Saccharomyces cerevisiae genome. *Nature*. 2002;418(6896):387-391. doi:10.1038/nature00935

192. Sikorski RS, Hieter P. A system of shuttle vectors and yeast host strains designed for efficient manipulation of DNA in Saccharomyces cerevisiae. *Genetics*. 1989;122(1):19-27. doi:10.1093/genetics/122.1.19

193. Woellhaf MW, Sommer F, Schroda M, Herrmann JM. Proteomic profiling of the mitochondrial ribosome identifies Atp25 as a composite mitochondrial precursor protein. *Mol Biol Cell*. 2016;27(20):3031-3039. doi:10.1091/mbc.E16-07-0513

194. Ralser M, Kuhl H, Ralser M, et al. The Saccharomyces cerevisiae W303-K6001 cross-platform genome sequence: insights into ancestry and physiology of a laboratory mutt. *Open Biol*. 2012;2(8):120093. doi:10.1098/rsob.120093

195. Brachmann CB, Davies A, Cost GJ, et al. Designer deletion strains derived from Saccharomyces cerevisiae S288C: a useful set of strains and plasmids for PCR-mediated gene disruption and other applications. *Yeast Chichester Engl*. 1998;14(2):115-132. doi:10.1002/(SICI)1097-0061(19980130)14:2<115::AID-YEA204>3.0.CO;2-2

196. Janke C, Magiera MM, Rathfelder N, et al. A versatile toolbox for PCR-based tagging of yeast genes: new fluorescent proteins, more markers and promoter substitution cassettes. *Yeast Chichester Engl*. 2004;21(11):947-962. doi:10.1002/yea.1142

197. Westermann B, Neupert W. Mitochondria-targeted green fluorescent proteins: convenient tools for the study of organelle biogenesis in Saccharomyces cerevisiae. *Yeast Chichester Engl*. 2000;16(15):1421-1427. doi:10.1002/1097-0061(200011)16:15<1421::AID-YEA624>3.0.CO;2-U

198. Livak KJ, Schmittgen TD. Analysis of relative gene expression data using real-time quantitative PCR and the 2(-Delta Delta C(T)) Method. *Methods San Diego Calif*. 2001;25(4):402-408. doi:10.1006/meth.2001.1262

199. Kyhse-Andersen J. Electroblotting of multiple gels: a simple apparatus without buffer tank for rapid transfer of proteins from polyacrylamide to nitrocellulose. *J Biochem Biophys Methods*. 1984;10(3-4):203-209. doi:10.1016/0165-022x(84)90040-x

200. Rappsilber J, Mann M, Ishihama Y. Protocol for micro-purification, enrichment, pre-fractionation and storage of peptides for proteomics using StageTips. *Nat Protoc*. 2007;2(8):1896-1906. doi:10.1038/nprot.2007.261

201. Kulak NA, Pichler G, Paron I, Nagaraj N, Mann M. Minimal, encapsulated proteomic-sample processing applied to copy-number estimation in eukaryotic cells. *Nat Methods*. 2014;11(3):319-324. doi:10.1038/nmeth.2834

202. Cox J, Mann M. MaxQuant enables high peptide identification rates, individualized p.p.b.-range mass accuracies and proteome-wide protein quantification. *Nat Biotechnol*. 2008;26(12):1367-1372. doi:10.1038/nbt.1511

203. Cox J, Neuhauser N, Michalski A, Scheltema RA, Olsen JV, Mann M. Andromeda: a peptide search engine integrated into the MaxQuant environment. *J Proteome Res*. 2011;10(4):1794-1805. doi:10.1021/pr101065j

204. Tyanova S, Temu T, Cox J. The MaxQuant computational platform for mass spectrometry-based shotgun proteomics. *Nat Protoc*. 2016;11(12):2301-2319. doi:10.1038/nprot.2016.136

205. Ritchie ME, Phipson B, Wu D, et al. limma powers differential expression analyses for RNA-sequencing and microarray studies. *Nucleic Acids Res*. 2015;43(7):e47. doi:10.1093/nar/gkv007

206. Huber W, von Heydebreck A, Sültmann H, Poustka A, Vingron M. Variance stabilization applied to microarray data calibration and to the quantification of differential expression. *Bioinforma Oxf Engl*. 2002;18 Suppl 1:S96-104. doi:10.1093/bioinformatics/18.suppl_1.s96

207. Controlling the False Discovery Rate: A Practical and Powerful Approach to Multiple Testing - Benjamini - 1995 - Journal of the Royal Statistical Society: Series B (Methodological) - Wiley Online Library. Accessed July 16, 2024. https://rss.onlinelibrary.wiley.com/doi/abs/10.1111/j.2517-6161.1995.tb02031.x

208. Stacklies W, Redestig H, Scholz M, Walther D, Selbig J. pcaMethods--a bioconductor package providing PCA methods for incomplete data. *Bioinforma Oxf Engl*. 2007;23(9):1164-1167. doi:10.1093/bioinformatics/btm069

8. ABBREVIATIONS

Abbreviation	Explanation
°C	Grade Celsius
Φ/Hy	Hydrophobic
Δψ	Membrane potential
µg	Microgram
µl	Microliter
µM	Micromolar
AAA+	ATPase Associated with diverse cellular Activities
aa	Amino acid
Amp	Ampicillin
AS	Ammonium sulfate
ATP	Adenosine triphosphate
BN-PAGE	Blue native polyacrylamide gel electrophoresis
BSA	Bovine serum albumine
CAM	Chloramphenicol
CAT	Carboxy-terminal Alanine and Threonine (tails)
CCCP	Carbonylcyanid-m-chlorphenylhydrazon
CK	Casein kinase
D	Degron
DAmP	Decreased abundance by mRNA perturbation
ddH2O	Double-distilled water
DHFR	Dihydrofolate reductase
DMSO	Dimethyl sulfoxide
DNA	Deoxyribonucleic acid
dNTP	Deoxynucleotide triphosphate
DOX	Doxycycline
DTT	Dithiothreitol
DUB	Deubiquitinase
E. coli	*Escherichia coli*
ECL	Enhanced chemiluminescence
EDTA	Ethylene diamine tetraacetate
ER	Endoplasmic reticulum
ERAD	ER-associated degradation
EtOH	Ethanol
ev	Empty vector
FACS	Fluorescence-activated cell sorting
for/fwd	Forward

g	Gravity of earth
GFP	Green fluorescent protein
GFP-Q-D	Green fluorescent protein-Quencher-Degron
GID	Glucose-induced-degradation-deficient
h	Hours
HA	Hemagglutinin
HCl	Hydrochloric acid
HEPES	4-(2-hydroxyethyl)-1-piperazine-ethane sulfonic acid
HF	High fidelity
HOP	Hsp70-Hsp90 organizing protein
Hsp	Heat shock protein
IM	Inner membrane
IMP	Inner membrane protease
IMS	Intermembrane space
iMTS	Internal mitochondrial targeting sequence
ITS	Intermembrane space targeting signal
IQ-Compete	Import and De-Quenching Competition assay
KAN	Kanamycin
kbp	Kilo base pair
kDa	Kilodalton
l	Liter
LB	Lysogeny broth media
LFQ	Label-free quantitation
m	Mature
M	Molarity
mA	Milliampere
MAD	Mitochondria-associated degradation
mg	Milligram
MIA	Mitochondrial intermembrane space assembly
MIM	Mitochondrial import (complex)
min	Minute
MISS	Mitochondrial intermembrane space sorting
MitCOM	Mitochondrial complexome
mitoCPR	Mitochondrial compromised protein import response
mitoRQC	Mitochondrial ribosomal quality control
mitoTAD	Mitochondrial protein translocation-associated degradation
ml	Milliliter
mM	Millimolar
MPP	Matrix processing peptidase
mRNA	Messenger ribonucleic acid

ms	Millisecond
MS	Mass spectrometry
MSF	Mitochondrial import stimulation factor
MTS	Mitochondrial targeting signal
NAC	Nascent-polypeptide-associated complex
NADH	Nicotinamide adenine dinucleotide
NaOH	Sodium hydroxide
ng	Nanogram
nm	Nanometer
ns	Not significant
OD_{600}	Optical density at 600 nm
OM	Outer membrane
p	Precursor
PACE	Proteasome associated control element
PAGE	Polyacrylamide gel electrophoresis
PAM	Presequence translocase-associated motor
PBS	Phosphate-buffered saline
PCA	Principal component analysis
PCR	Polymerase chain reaction
PEG	Polyethylene glycol
PK	Proteinase K
PKA	Protein kinase A
PMSF	Phenylmethylsulfonyl fluoride
Po	Polar
Q	Quencher
qRT-PCR	Real-time quantitative polymerase chain reaction
RAC	Ribosome-associated complex
RNA	Ribonucleic acid
rev	Reverse
rpm	Revolutions per minute
RT	Room temperature
s	Seconds
SA	Signal-anchored
SAM	Sorting and assembly machinery
S. cerevisiae	*Saccharomyces cerevisiae*
SDS	Sodium dodecyl sulfate
SDS-PAGE	Sodium dodecyl sulfate polyacrylamide agarose gel electrophoresis
SILAC	Stable isotope labeling by amino acids in cell culture
ssDNA	Salmon sperm DNA
SWAT	SWAp-Tag

TA	Tail-anchored
TBS	Tris buffered saline
TIM	Translocase of the inner membrane
TMD	Transmembrane domain
TOM	Translocase of the outer membrane
TPR	Tetratricopeptide repeat
Tris	Tris-(hydroxymethyl)-aminomethane
tRNA	Transfer RNA
U	Unit
Ub	Ubiquitin
UBX	Ubiquitin regulatory X
UPS	Ubiquitin-proteasome system
uTEV	Yeast-optimized variant of the Tabacco Etch virus protease
v/v	Volume per volume
w/v	Weight per volume
w/w	Weight per weight
WT	Wild type
YFP	Yellow fluorescent protein

9. APPENDIX

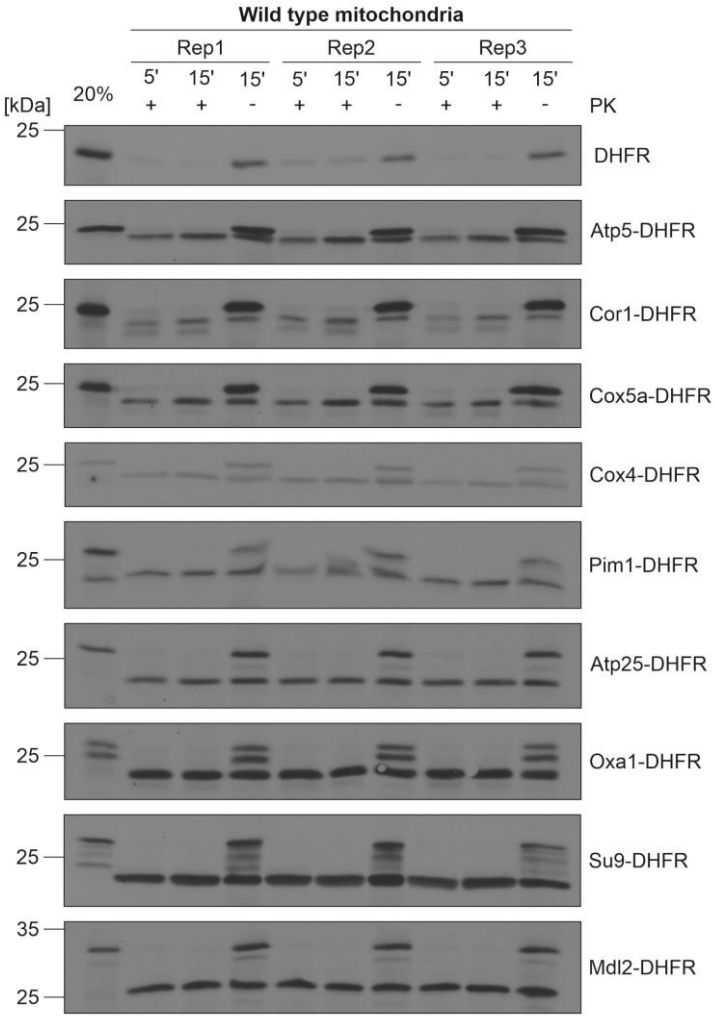

Figure S1: The *in vitro* import efficiency of precursors into WT mitochondria depends on the presequence. Radiolabeled precursors of the indicated fusion proteins (presequences of the designated proteins fused to DHFR) were incubated with mitochondria isolated from WT cells grown in galactose medium. Import was performed in biological triplicates as described for Figure 10A. Adopted from [111].

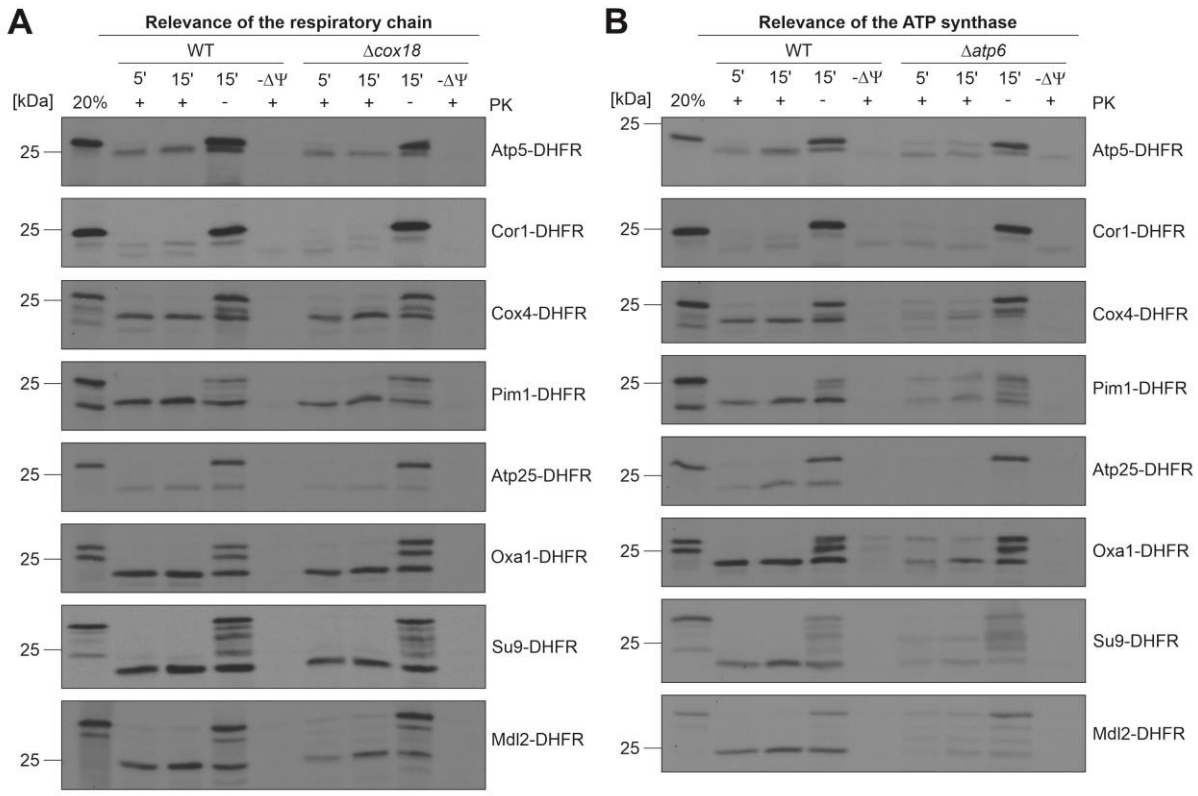

Figure S2: The import of all tested presequences depends on the membrane potential and ATP hydrolysis. Radiolabeled precursors of the indicated fusion proteins (presequences of the designated proteins fused to DHFR) were incubated with mitochondria isolated from *Δcox18* (for **(A)**) and *Δatp6* (for **(B)**) mutant cells grown in galactose medium. Import was performed in biological triplicates as described for Figure 10E and F. Adopted from [111].

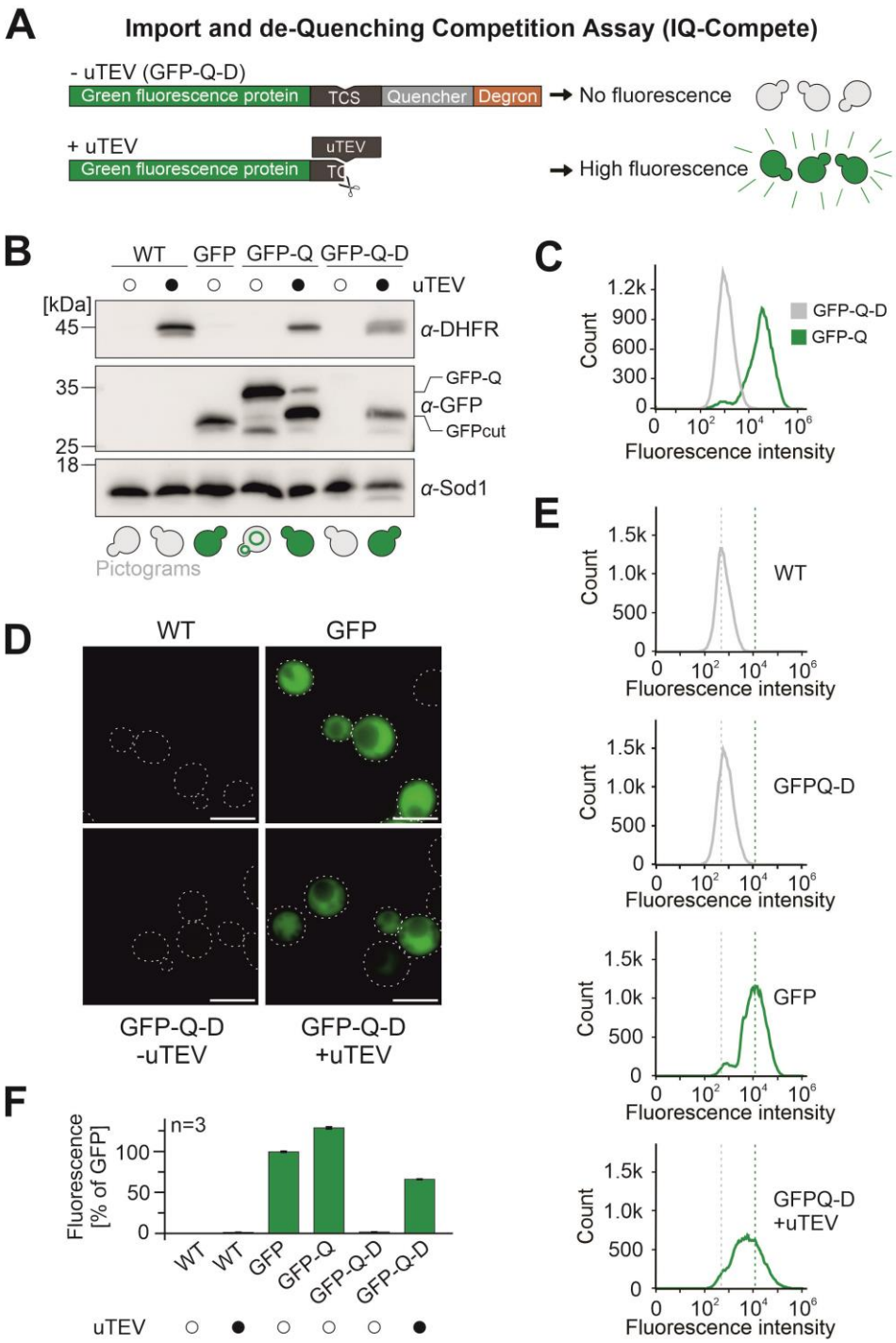

Figure S3: Fluorescence de-quenching of GFP as an efficient strategy to monitor protease levels in the cytosol. (A) Schematic representation of the reporter construct used in the IQ-Compete assay. TCS, TEV cleavage site. **(B)** WT cells carrying plasmids for the expression of uTEV-DHFR as well as of GFP, GFP-Q or GFP-Q-D. Cells were grown to mid-log phase in lactate + 0.2% glucose medium and analyzed via Western blot. The pictograms schematically illustrate the distribution of the GFP signal in these cells. **(C)** WT cells expressing GFP-Q and GFP-Q-D were grown to mid-log phase in lactate + 0.2% glucose medium and the fluorescence intensities were analyzed by flow cytometry. 100,000 cells were analyzed for each sample. **(D)** The indicated strains were analyzed by fluorescence microscopy. Cells were grown to mid-log phase in lactate + 0.2% glucose medium. Scale bar represents 5 µm. **(E)** WT cells expressing the indicated constructs were grown to mid-log phase in lactate + 0.2% glucose medium and the fluorescence intensities were analyzed by flow cytometry. 100,000 cells were analyzed for each sample. The dashed grey line marks the minimal fluorescence intensity of WT cells. The dashed green line indicates maximal fluorescence intensity referring to cells expressing a cytosolic uTEV protease. **(F)** Quantification of the fluorescence intensities shown in F in three independent samples. Shown are mean values and standard deviations of three biological replicates (n=3). Adopted from [111].

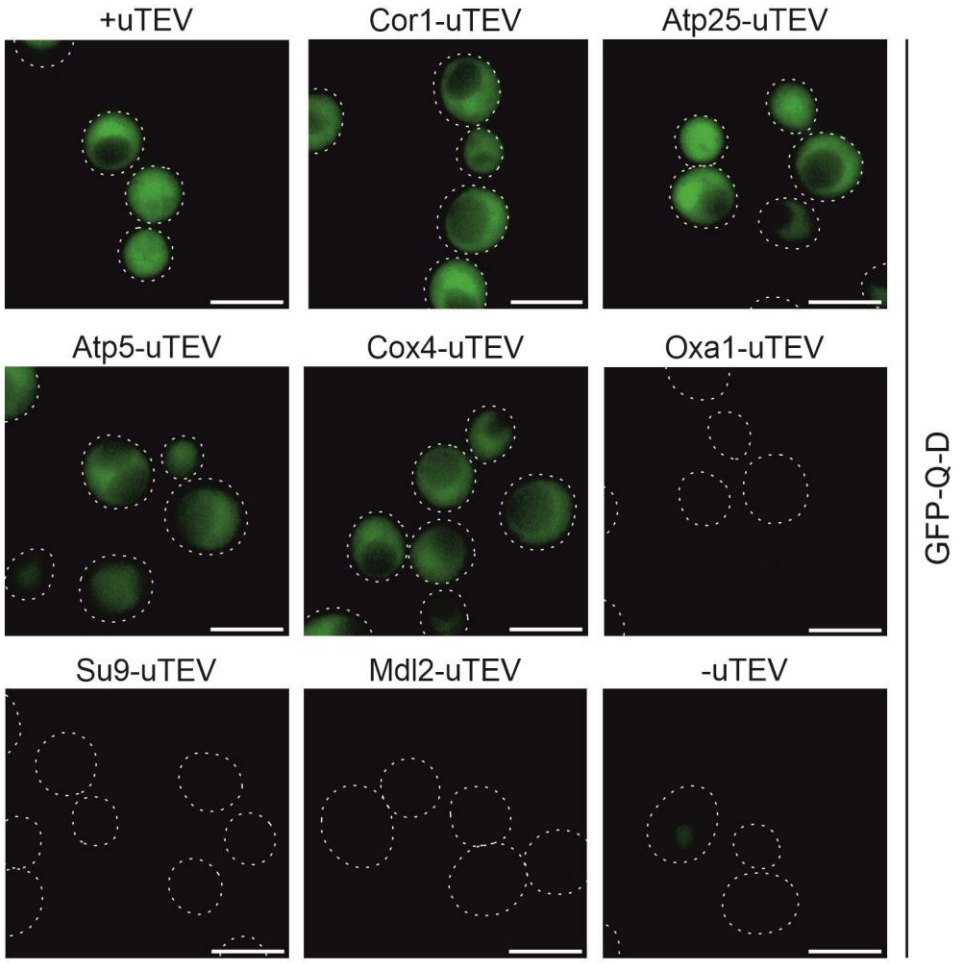

Figure S4: Fluorescence microscopy images of cells analyzed with IQ-Compete. WT cells expressing the GFP-Q-D reporter and the indicated uTEV constructs were grown in glucose medium to mid-log phase and analyzed by fluorescence microscopy. Scale bar represents 5 µm. Adopted from [111].

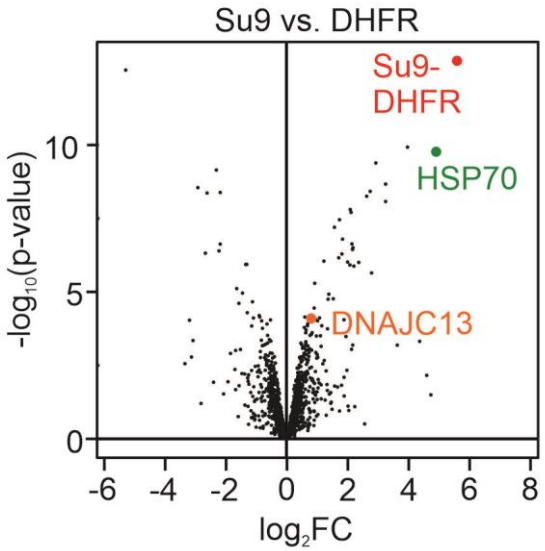

Figure S5: The presequence of Su9 binds to Hsp70 in reticulocyte lysate. Volcano plot showing the interactome comparison of the indicated samples (see Figure 16A and C for details). Adopted from [111].

```
sp|Q15785|TOM34_HUMAN      ------------------------------------------------------------ 0
sp|P33313|CNS1_YEAST       MSSVNANGGYTKPQKYVPGPGDPELPPQLSEFKDKTSDEILKEMNRMPFFMTKLDETDGA 60


sp|Q15785|TOM34_HUMAN      --------------MAPKFPDSVEELRAAGNESFRNGQYAEASALYGRALRVLQAQGSSD 46
sp|P33313|CNS1_YEAST       GGENVELEALKALAYEGEPHEIAENFKKQGNELYKAKRFKDARELYSKGLAVEC----ED 116
                                         :  : .*:::  *** ::  :: :*  **.:.* *      .*


sp|Q15785|TOM34_HUMAN      PEEESVLYSNRAACHLKDGNCRDCIKDCTSALALVPFSIKPLLRRASAYEALEKYPMAYV 106
sp|P33313|CNS1_YEAST       KSINESLYANRAACELELKNYRRCIEDCSKALTINPKNVKCYYRTSKAFFQLNKLEEAKS 176
                            . :. **:*****.*:  * * **:**:.**:: * .:*   * :.*:  *:*   *


sp|Q15785|TOM34_HUMAN      DYKTVLQIDDNVTSAVEGINRMTRALMDSLGPEWRLKLPSIPLVPVSAQK--------RW 158
sp|P33313|CNS1_YEAST       AAT----------FANQR-----------IDPENKSILNMLSVIDRKEQELKAKEEKQQR 215
                              .          * :            :.** :  *  : ::  . *:       :


sp|Q15785|TOM34_HUMAN      NSLPSENHKEMAKSKSKETTATKNRVPSAGDVEKARVLKEEGNELVKKGNHKKAIEKYSE 218
sp|P33313|CNS1_YEAST       EAQERENKKIMLESAMT-----LRNITN--------IKTHSPVELLNEGKIRL------- 255
                           ::   **:* * :*  .      ..: .        : ...  **:::*: :


sp|Q15785|TOM34_HUMAN      SLLCSNLESATYSNRALCYLVLKQYTE--------AVKDCT---E--ALKLDGKNVKAFY 265
sp|P33313|CNS1_YEAST       -------EDPMDFESQLIYPALIMYPTQDEFDFVGEVSELTTVQELVDLVLEGPQE-RF- 306
                                  *.    :  * * .*  *          *.: *   *   * *:* :   *


sp|Q15785|TOM34_HUMAN      RRAQAHKALKDYKSSFADISNLLQIEPRNGPAQKLRQEVKQNLH---------------- 309
sp|P33313|CNS1_YEAST       --------KKEGKENFTPKKVLVFMETKAGGLIKAG--KKLTFHDILKKESPDVPLFDNA 356
                                    *: *..*:  . *: :* : *   *     * .:*


sp|Q15785|TOM34_HUMAN      ------------------------------        309
sp|P33313|CNS1_YEAST       LKIYIVPKVESEGWISKWDKQKALERRSV        385
```

Figure S6: Sequence alignment of human TOMM34 and yeast Cns1. Sequences were analyzed with the Clustal Omega 1.2.4 multiple sequence alignment program using the following sequences: TOMM34 (*Homo sapiens* Q15785 and *S. cerevisiae* Cns1)

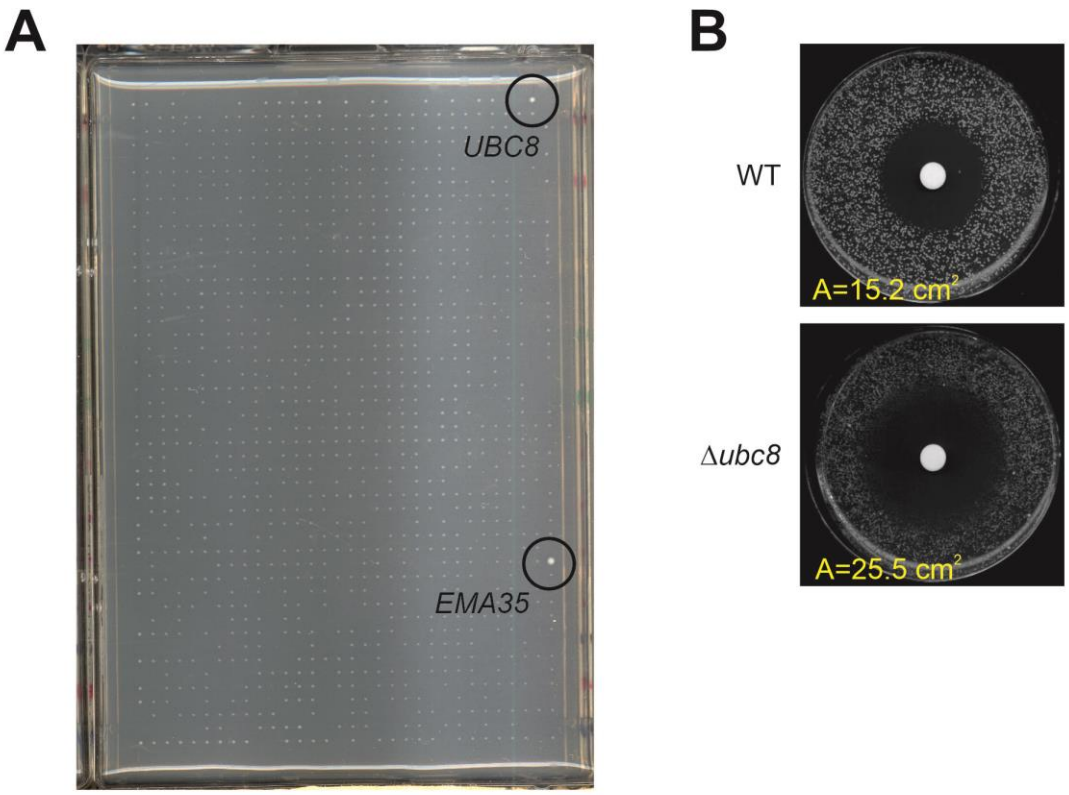

Figure S7: (A) Shown is the entire uracil-deficient plate from which a part was shown in Figure 19B after 1 day of incubation. The colonies for Δ*ubc8* and Δ*ema35* are indicated. Result was obtained by Dr. Katja Hansen. **(B)** Indicated strains were distributed on glycerol plates and a filter disc was placed in the center of the plate. 10 µl of 10 mM CCCP was added to the filter disk. The plates were incubated for 1 day at 30°C and the inhibition area (A) was measured. Modified from [112].

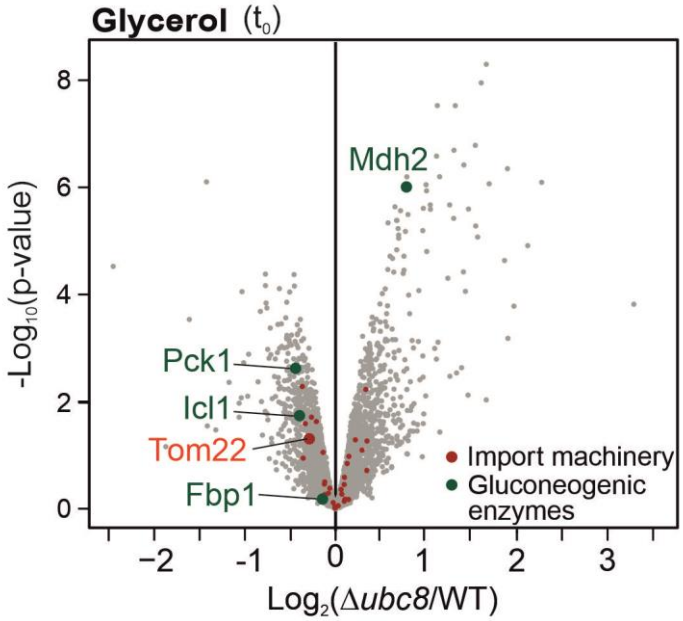

Figure S8: Volcano plot showing the proteome comparison of Δ*ubc8* and WT cells. Cells were continuously grown in glycerol medium. Data points of gluconeogenic enzymes are labeled in green and components of the import machinery are highlighted in red. Adopted from [112].

ACKNOWLEDGMENTS

Als erstes möchte ich dir, **Hannes**, danken. Vielen Dank, dass ich meine Doktorarbeit in deiner Arbeitsgruppe schreiben durfte. Danke für deine Unterstützung in jeglicher Hinsicht, deine motivierenden Worte und deine zahlreichen einfallsreichen Ideen. Und ja, ich muss zugeben, dass ich dir auch dafür danke, dass du mich im Laufe der Zeit bis zu meinem Limit und darüber hinaus gefordert und gefördert hast und mich so aus meiner Komfortzone gelockt hast. Auch wenn mir das nicht immer sofort bewusst war, kann ich rückblickend sagen, dass ich mich dadurch nicht nur fachlich, sondern auch persönlich, weiterentwickelt habe und in beiderlei Hinsicht extrem viel gelernt habe. Danke, dass du es mir ermöglicht hast meine Stärken zu entdecken und dass du diese immer weiter gefördert hast. Die unbezahlbaren Erfahrungen und Eindrücke auf den Konferenzen weltweit und die super Arbeitsgruppe werden mich immer auf eine tolle Zeit zurückblicken lassen.

Ein großes Dankeschön geht auch an dich **Ekkehard Neuhaus**. Danke für die TAC meetings mit den vielen Ideen und neuen Denkanstößen, die mich besonders am Ende meines Projektes auf die richtige Fährte gebracht haben. Danke auch für die Übernahme des Zweitgutachtens meiner Doktorarbeit.

Danke **Tanja Maritzen** für die Übernahme des Vorsitzes meiner Prüfungskommission.

Außerdem möchte ich mich bei dir, **Markus** bedanken. Diese Arbeit lebt nur so von Proteomics-Experimenten. Ohne dich wäre das nicht möglich gewesen. Ich danke dir für deine unermüdliche Unterstützung bei allen Messungen, die ausführlichen Gespräche bezüglich der Planung und der Auswertung und ich danke dir, dass wir zusammen das Beste aus allen Messungen herausgeholt haben.

Liebe **Gabi**, dir danke ich für die super Koordination des Graduiertenkollegs. Mit deiner herzlichen Art stehst du uns jederzeit mit Rat und Tat zur Seite. Danke für die klasse Organisation der Workshops, der Vorträge und der Retreats und dafür, dass du uns so viel ermöglichst.

Ich möchte mich ganz herzlich bei allen meinen Kooperationspartnern für die tolle Zusammenarbeit bedanken.

Ein besonders großer Dank geht an meine gesamte Labor-Familie! **Simone**, danke, dass wir jederzeit mit all unseren Fragen zu dir kommen können. Ohne deine Hilfe hätte ich so manchen

Antrag nicht richtig ausfüllen können. Danke für deine herzliche Art und für alles, was du für uns tust. **Connie**, vielen Dank dafür, dass du mit deiner guten Laune stets dafür sorgst, dass wir problemlos im Labor arbeiten können. **Andrea**, **Sabine** und **Vera**, vielen Dank für alles. Auf euch ist einfach immer Verlass! **Andrea**, danke, dass du mir in schwierigen Zeiten geholfen und mir Mut zugesprochen hast. Du hast von Anfang an an mich geglaubt und ich danke dir für jegliche Unterstützung in den letzten Jahren. **Sabine**, wo soll ich anfangen. Danke, dass du mich in dein Labor aufgenommen hast und wir eine unglaublich tolle Zeit in 13-455 hatten. Danke dafür, dass du mir direkt an meinem Gesichtsausdruck angesehen hast, wenn ich mal wieder maximal gestresst war und du mir jederzeit ohne Zögern geholfen hast. Danke für die vielen Gespräche über Pflanzen, Tiere und auch tiefgründige Themen und danke für jedes Gelächter das wir zusammen hatten! Mit den Essensvorlieben werden wir uns wohl nie einig werden. **Vera**, auch bei dir möchte ich mich für deine zuverlässige Hilfe in allen Situationen bedanken.

Büsra, diese paar Zeilen reichen definitiv nicht aus, um alles runterzuschreiben, wofür ich dir danke. Du bist die beste Laborpartnerin, die ich mir je hätte wünschen können und ich bin sehr froh, dich als Freundin gewonnen zu haben. Ich kann mich immer zu 100% auf dich verlassen, ganz egal um was geht. Ich danke dir dafür, dass du mir immer mit Rat und Tat zur Seite standest und wir uns gegenseitig in allen Situationen unterstützt haben. Du hast all meine Tiefen der letzten Jahre hautnah miterlebt und mir immer geholfen diese durchzustehen. Ebenso hast du dich bei meinen Erfolgen mindestens genauso gefreut wie ich und mit mir gefeiert. Ich danke dir für die zahlreichen Gespräche, das viele Lachen, die wortlose Kommunikation und dafür, dass wir genau wussten, was der andere wann gebraucht hat. Vielen Dank, dass du diese Arbeit Korrektur gelesen hast. Danke!

Ein riesengroßes Dankeschön geht an dich **Svenja**. Ich bin froh, dass ich dich als Studentin betreuen durfte und bin stolz auf dich, dass du es selbst jetzt schon so weit geschafft hast. Auch wenn du dadurch, manchmal wahrscheinlich zu deinem Leid, in mehreren Hinsichten in meine Fußstapfen getreten bist. Gemeinsam haben wir schon viele Endgegner besiegt, Ubc8, Orf9b und SILAC nur mal so als Beispiele zu nennen. Danke, dass du jederzeit ein offenes Ohr für mich hattest und mich immer unterstützt hast. Auch dir danke ich für das Korrekturlesen meiner Arbeit. **Jannik**, dir danke ich für jeden Austausch und jede Unterstützung in den letzten Jahren. Danke euch beiden für die witzigen Spikeball-Sessions, die wir gemeinsam hatten. Jedes bisschen an Muskelkater und jedes offene Knie haben sich gelohnt.

Lea, dir möchte ich für dein offenes Ohr und deine Unterstützung danken. Bei Fragen konnte ich immer zu dir kommen und mit dir reden. Deine Entwicklung und dein Kämpfergeist haben mich sehr inspiriert. Danke für die schöne Fahrradtour und wenn du jemals eine Einschätzung zur Peperonischärfe benötigst, darfst du mich gerne als Testerin einladen. Ich verspreche dir, ich werde die schärfste finden.

Tamara, ich freue mich sehr, dass wir es beide geschafft haben und an unserem Ziel angekommen sind. Deine stets positive und gelassene Art waren eine Bereicherung für das ganze Labor. Danke, dass wir bei Fragen jederzeit auf den anderen zu gehen konnten. Dir helfe ich selbstverständlich auch gerne, die schärfste Peperoni zu finden, falls du damit mal Probleme haben solltest.

Was kann mehr verbinden als die Liebe zu Katzen? **Anna-Lena**, danke, dass du mir mit deinen witzigen Katzenbildern und -geschichten die Zeit ohne eine eigene Katze versüßt hast. Deine Liebe zum Detail, deine Ehrlichkeit und dein Durchhaltevermögen haben mich stark beeindruckt. Danke für deine Zuverlässigkeit und dafür, dass ich jederzeit mit dir sprechen konnte.

Annika, ohne dich wäre ich wohl immer noch mit meinen R-Problemen beschäftigt. Danke für deine große Hilfe bei der Auswertung und für dein offenes Ohr.

Ein riesiger Dank geht auch an dich **Yasmin**. Ich habe mich sehr gefreut, dich als Studentin betreuen dürfen. Du hast einen wesentlichen Beitrag zu meinem Projekt beigetragen und eine super Arbeit geleistet. Ich danke dir dafür, dass wir ein so tolles Team waren und dafür, dass wir uns gegenseitig oft zum Lachen gebracht haben.

Ich möchte mich auch bei euch, **Lorenz** und **Christian** bedanken. Ich bin froh, euch als Teil der Labor-Familie kennengelernt zu haben. Danke, dass wir uns immer gegenseitig geholfen haben.

Katja und **Janina**, ihr zwei wart meine Betreuerinnen, als ich selbst noch eine Studentin war. Ich danke euch dafür, dass ich von euch beiden so viel lernen konnte, so dass ich jetzt hier sitze und die letzten Sätze meiner Doktorarbeit schreibe.

Yura, I am glad that you joined our lab and that I had the opportunity to chat with you about my research.

Pavel, **Nikita** and **Aleks**, it was always fun coming into your lab. I always enjoyed following your extensive discussions about a wide variety of topics. Thank you for always supporting me in case of questions.

Ein ganz großes Dankeschön geht an meine **Familie**. Mama, Papa, ohne euch wäre das alles hier gar nicht erst möglich geworden. Ich danke euch von ganzem Herzen, dass ihr mich in allen Lebenslagen unermüdlich unterstützt und mir alles, was ich machen wollte, ermöglicht habt. Ihr habt nie an mir gezweifelt und mich so weit gebracht, dass ich voller Dankbarkeit und Stolz diese Zeilen hier schreiben kann. Danke!

Mein letzter Dank geht an dich **Alex**. Ohne dich hätte mir Word dieses Dokument wahrscheinlich schon mehrfach zerschossen und ich wäre schon unzählige Male am Rad gedreht. Aber gemeinsam haben wir es geschafft! Du hast mich immer wieder beruhigt, mir Mut zugesprochen und mir den nötigen Rückhalt gegeben, wenn nicht mehr weiterwusste. Danke für die unermüdliche Korrektur dieser Arbeit. Danke, dass du immer an mich glaubst und mich bei allem unterstützt!

CURRICULUM VITAE

Saskia Rödl, *Master of Science*

Place of Birth:	Speyer, Germany

Education

Since 08/2020	**PhD Studies** Rheinland-Pfälzische Technische Universität Kaiserslautern-Landau Cell Biology Supervisor: Prof. Dr. Johannes Herrmann "Mitochondrial protein import is under surveillance of cytosolic factors: specific roles of TOMM34 and Ubc8"
10/2018 – 06/2020	**Master of Science, Molecular Cell Biology** Rheinland-Pfälzische Technische Universität Kaiserslautern-Landau Cell Biology Supervisor: Prof. Dr. Johannes Herrmann "Proteomanalyse zur Untersuchung des Glukose-induzierten Proteinabbaus in *S. cerevisiae*"
10/2015 – 09/2018	**Bachelor of Science, Biowissenschaften** Rheinland-Pfälzische Technische Universität Kaiserslautern-Landau Human Biology and Human Genetics Supervisor: Prof. Dr. Stefan Kins "Influence of the glypican family on trans-dimerization of APP"
2006 – 2015	**Allgemeine Hochschulreife** Heinrich-Böll-Gymnasium, Ludwigshafen-Mundenheim

Grants and Funding

Since 06/2022	**Associated member of the Research Training Group RTG 2737 "STRESSistance"** Deutsche Forschungsgemeinschaft (DFG)"
2019	**Erasmus+ Fellowship** "Deutscher Akademischer Austauschdienst (DAAD)"
2017 - 2020	**Scholarship** "Deutschlandstipendium University of Kaiserslautern"